

**Interference-Assisted Techniques for Transmission
and Multiple Access in Optical Communications**

GUAN, Xun

A Thesis Submitted in Partial Fulfillment
of the Requirements for the Degree of
Doctor of Philosophy
in
Information Engineering

The Chinese University of Hong Kong

January 2017

ProQuest Number:10663734

All rights reserved

INFORMATION TO ALL USERS

The quality of this reproduction is dependent upon the quality of the copy submitted.

In the unlikely event that the author did not send a complete manuscript and there are missing pages, these will be noted. Also, if material had to be removed, a note will indicate the deletion.



ProQuest 10663734

Published by ProQuest LLC (2017). Copyright of the Dissertation is held by the Author.

All rights reserved.

This work is protected against unauthorized copying under Title 17, United States Code
Microform Edition © ProQuest LLC.

ProQuest LLC.
789 East Eisenhower Parkway
P.O. Box 1346
Ann Arbor, MI 48106 – 1346

Acknowledgement

With all my heart, I would like to thank all those people who have made this thesis possible.

Foremost, I would like to express my deepest gratitude to my supervisor Prof. Calvin Chun-Kit Chan. If it was not him, I would not be so fortunate to appreciate the delight of optical communication. His guidance has always been a beacon to me. My personal growth, my enjoyment of research, my academic works, all the things that may have been achieved during the past four years, I owe them to Prof. Chan, to his support without reservation, to his readiness to listen and suggest, to his valuable advices and criticism, and to his foresight and sagacity in research.

I also take the chance to express my sincere thanks to Prof. Lian-Kuan Chen, for his attention, suggestions and discussions. His pursuit of perfection has always set me a perfect model, both academically and morally.

It is my great honor and pleasure to work with my labmates in Lightwave Communication Laboratory. I would like to give my thanks to Tianwai Bo, Zheyu Fan, Shuang Gao, Chao Xiang, Yajun Wu, Qianmei Yang, Yang Hong, Tesi Wu, Hugo Mak, Dr. Hon Tung Luk, Dr. Jin Tang, Dr. Zhixin Liu, Dr. Wei Jia, Dr. Dicky Tse, and Dr. Ming Li, for their help and accompany. We went through the ups and downs together. Your friendship will be cherished for my lifetime.

Last but not least, I would like to say a heartfelt thank you to my beloved family, my grandmother, grandfather, mother and father, for their faith in me and support to my personal ambition. I would be nothing without your unconditional love, care, tolerance and encouragement.

Abstract

Optical communications can be in wired or wireless form. Fiber optics communication (FOC) connects transmitters and receivers with optical fiber. Benefitting from its high bandwidth, low cost per volume and stability, it gains a significant market share in long-haul networks, access networks and data centers. Meanwhile, optical wireless communication (OWC) is also emerging as a crucial player in the communication market. In OWC, free-space optical communication (FSO) and visible light communication (VLC) are being studied and commercially deployed extensively.

Interference is a common phenomenon in multi-user communication systems. In both FOC and OWC, interference has long been treated as a detrimental effect. However, it could also be beneficial to system applications. The effort of harnessing interference has spurred numerous innovations. Interesting examples are physical-layer network coding (PNC) and non-orthogonal multiple access (NOMA).

The first part of this thesis is on the topic of PNC. PNC was firstly proposed in wireless communication to improve the throughput of a two-way relay network (TWRN). As a variation of network coding (NC), PNC turns the common channel interference (CCI) as a natural network coding operation. In this thesis, PNC is introduced into optical communication. Three schemes are proposed in different scenarios. Firstly, PNC is applied to a coherent optical orthogonal frequency division multiplexing (CO-OFDM) system so as to improve the throughput of the multicast network. The optical signal to noise ratio (OSNR) penalty is quite low. Secondly, we

investigate the application of PNC in an OFDM passive optical network (OFDM-PON) supporting heterogeneous services. It is found that only minor receiver power penalties are observed to realize PNC-based virtual private networks (VPN), both in the wired service part and the wireless service part in an OFDM-PON with heterogeneous services. Thirdly, we innovate relay-based visible light communication (VLC) by adopting PNC, with a newly proposed phase-aligning method. PNC could improve the throughput at the bottlenecking relay node in a VLC system, and the proposed phase aligning method can improve the BER performance.

The second part of this thesis discusses another interference-assisted technology in communication, that is, non-orthogonal multiple access (NOMA). NOMA multiplexes signals from multiple users in another dimension: power domain, with a non-orthogonal multiplexing in other dimensions such as time, frequency and code. Three schemes are proposed in this part. The first and the second schemes both realize NOMA in VLC, with different multiuser detection (MUD) techniques and a proposed phase pre-distortion method. Although both can decrease the system BER compared to conventional NOMA, the scheme using joint detection (JD) outperforms the one using successive interference cancellation (SIC). The third scheme investigated in this part is a combination of NOMA and a multicarrier precoding (MP) technology based on an orthogonal circulant transform matrix (OCT). This combination can avoid the complicated adaptive bit loading or electronic equalization, making NOMA more attractive in a practical system.

摘要

光通信技術的連接方式分為有線和無線方式。光纖通信技術使用有線的光纖連接發射機和接收機。受益於其高帶寬、低單位成本和穩定性，光纖通信技術在長距傳輸、接入網和數據中心市場上佔據了極大的份額。另一方面，光無線通信技術也正在成為通信市場的重要成員；其中的自由空間光通信和可見光通信正獲得大量的研究和廣泛的商用化。

干擾是來自於其它用戶的影響。長期以來，在光通信系統內，干擾被認為是有害的。然而，干擾也可以被利用。這一點引發了各式各樣的創新。本文關注其中的兩點：物理層網絡編碼和非正交多址接入。

本文的第一部分內容有關光物理層網絡編碼。物理層網絡編碼最初用於無線通信中提升雙向中繼網絡的容量。作為網絡編碼的一種變體，物理層網絡編碼將共信道干涉轉化為一種天然的網絡編碼操作。本文將物理層網絡編碼用於三種光通信系統中。首先，我們將物理層網絡編碼應用到相干光正交頻分複用中，來提升多播網絡的容量；而僅帶來有限的光噪比損失。其次，我們研究了物理層網絡編碼在多樣服務的正交頻分複用無源光接入網中的應用。研究發現，物理層網絡編碼可在僅有少量功率代價的條件下同時實現有線和無線服務的虛擬專用網絡。再次，我們在基於中繼的可見光通信中加入了物理層網絡編碼，並提出了一種新的共相方案。物理層網絡編碼可以提升中繼處的容量瓶頸，而新提出的共相方法可以提升系統的誤碼率性能。

本文的第二部分討論了另一種干擾利用技術：非正交多址接入。非正交多

址接入在功率域上複用信號，而在時域、頻域、和碼域上混疊信號。在此我們提出了三種方案。第一種和第二種方案都將非正交多址接入應用於可見光通信中，惟使用了不同的多用戶檢測方案與不同的相位預失真方法。第三種方案是非正交多址接入與一種基於正交循環變換矩陣的多載波預編碼方案的聯合。這一聯合可以免去正交頻分複用系統中複雜的動態加載或者電域均衡，使得非正交多址接入技術在實際系統中更具可行性。

Table of contents

Acknowledgement.....	i
Abstract	iii
摘要.....	v
List of figures and tables	xi
Chapter 1 Introduction	1
1.1 Optical communication.....	1
1.1.1 Fiber optics communication.....	1
1.1.2 Optical wireless communication	7
1.2 OFDM in optical communications	9
1.2.1 Fundamentals of OFDM	9
1.2.2 OFDM in fiber optics communication	13
1.2.3 OFDM in optical wireless communication	15
1.3 Contributions of this thesis	16
1.3.1 Physical-layer network coding in optical communication.....	16
1.3.2 Non-orthogonal multiple access in optical communication.....	18
1.4 Outline of this thesis	18
Chapter 2 Background: Interference-Assisted Techniques in Optical Communication	20
2.1 Introduction	20
2.2 Physical-layer network coding (PNC).....	22

2.2.1	General concept.....	22
2.2.2	Classification of PNC.....	26
2.2.3	PNC studies and implementations	29
2.3	Non-Orthogonal Multiple Access.....	31
2.3.1	General concept.....	31
2.3.2	Balancing throughput and fairness: an example	34
2.3.3	Channel capacity of NOMA.....	38
2.3.4	NOMA studies.....	45
Chapter 3	Physical-Layer Network Coding in Optical Communication	48
3.1	Physical-layer network coding in CO-OFDM.....	48
3.1.1	Introduction	48
3.1.2	Principle of operation.....	49
3.1.3	Experiments and simulations	55
3.1.4	Conclusion	60
3.2	Physical-layer network coding for VPN in OFDM-PON supporting heterogeneous services.....	60
3.2.1	Introduction	60
3.2.2	Principle of operation.....	62
3.2.3	Experimental setup.....	65
3.2.4	Experimental results and discussions.....	69
3.2.5	Conclusion	69
3.3	Physical-layer network coding in visible light communication	70

3.3.1	Introduction	70
3.3.2	System model	72
3.3.3	Decoding algorithm of physical-layer network coding.....	78
3.3.4	Phase-aligned physical-layer network coding.....	81
3.3.5	Experiments.....	83
3.3.6	Conclusion	86
Chapter 4	Non-Orthogonal Multiple Access in Optical Communications	87
4.1	Introduction	87
4.1.1	Background	87
4.1.2	MUD methods.....	88
4.2	Non-orthogonal multiple access in visible light communication with successive interference cancellation and phase pre-distortion.....	89
4.2.1	Introduction	89
4.2.2	System model	90
4.2.3	SIC-based NOMA with phase pre-distortion in NOMA.....	93
4.2.4	Experiment	98
4.2.5	Conclusion	104
4.3	Joint detection of visible light communication signals under non- orthogonal multiple access.....	105
4.3.1	Introduction	105
4.3.2	System model	106
4.3.3	Multiuser detection algorithms for NOMA.....	107

4.3.4	Experiments.....	113
4.3.5	Conclusion	116
4.4	Non-orthogonal multiple access with multicarrier precoding in visible light communications	116
4.4.1	Introduction.....	116
4.4.2	Principles.....	118
4.4.3	Numerical simulations	119
4.4.4	Summary	124
Chapter 5	Summary and Future work.....	125
5.1	Summary.....	125
5.2	Future work.....	127
	List of publications.....	130
	Journals	130
	Conferences.....	130
	List of abbreviations.....	132
	Bibliography	139

List of figures and tables

Figure 1-1 Changes in number of broadband subscribers.....	3
Figure 1-2 FSAN evolution roadmap.....	4
Figure 1-3 A typical 3-Tier data center topology.	6
Figure 1-4 A Li+WiFi heterogeneous network.	9
Figure 1-5 Schematic view of an OFDM system.....	10
Figure 1-6 Spectrum of an OFDM symbol.	10
Figure 1-7 The time domain depiction of CP.....	13
Figure 2-1 CCI in a cellular network.	21
Figure 2-2 A two-way relay network	23
Figure 2-3 Non-network-coded scheme.....	23
Figure 2-4 Network-coded scheme	24
Figure 2-5 Physical-layer-network-coded scheme.....	25
Figure 2-6 A multiple access system with two transmitters (T_1 and T_2) and one receiver (R).....	34
Figure 2-7 (a)-(c) Spectrum allocation in OFDMA: (a) the whole spectrum assigned to T_1 ; (b) half of the spectrum assigned to T_1 , the other half to T_2 ; (c) 1/3 of the spectrum assigned to T_1 , 2/3 to T_2 ; (d) NOMA.....	36
Figure 2-8 J and R with regard to the spectrum ratio assigned to T_1 in OFDMA.	37
Figure 2-9 Transmission process of downlink NOMA.....	39
Figure 2-10 Rate region of the two-user downlink OFDMA and NOMA.....	42

Figure 2-11 Transmission process of uplink NOMA.	43
Figure 2-12 Rate region of the two-user uplink OFDMA and NOMA.	45
Figure 3-1 Optical multicast topology: (a) wavelength division multiplexing, (b) timing division multiplexing, (c) OPNC.	49
Figure 3-2 (a) OFDM model, (b) OPNC model, (c) Frames alignment of OPNC (d) OPNC spectrum.	51
Figure 3-3 (a) Experimental setup (b) DSP process.	55
Figure 3-4 Experimental results showing the BER-OSNR relationships with and without OPNC.	57
Figure 3-5 Simulation results: (a) System performance as a function of the misalignment between two signals represented by the number of samples (b) System performance as a function of the synchronization error of decoded arm between two signals represented by the number of samples.	58
Figure 3-6 Schematic view of a RoF-PON supporting PNC-based VPN; (b) ONU configuration; (c) non-PNC VPN data streams; (d) PNC VPN data streams.	62
Figure 3-7 (a) Symbol-level synchronization, (b) frame structure.	65
Figure 3-8 (a) Experimental setup, (b) Digital spectrum of the transmitted signal, (c) DSP procedures.	66
Figure 3-9 Experimental results: (a) Wired, (b) Wireless.	68
Figure 3-10 A two-way relay VLC network	73
Figure 3-11 Two end nodes exchange a pair of packets via the relay node in the	

visible light communication network: (a) the conventional VLC bi-directional relay takes four time slots; (b) the PNC-VLC only takes two time slots	74
Figure 3-12 The media access control (MAC) procedure of the PNC-VLC	77
Figure 3-13 (a) Experimental Setup; (b) Frame structure	83
Figure 3-14 SNR and power ratio (PR) of the two users, AWG sampling rate at 400 MSa/s	84
Figure 3-15 Experimental results: (a) BER vs. single user data rate; (b) BER vs. SNR. PA: phase align.	85
Figure 4-1 Successive interference cancellation process of a two-user NOMA.	88
Figure 4-2 (a) System model for the non-orthogonal multiple access in visible light communication; (b) power levels of S and W; (c) asynchrony in NOMA.	90
Figure 4-3 The symbol error rate (P_{e1}) in step (1) of successive interference cancellation decoding versus the phase difference φ between the two users. (a) P_{e1} vs S(QPSK)-W(QPSK) relative phase φ ; (b) P_{e1} vs S(QPSK)-W(BPSK) relative phase φ	94
Figure 4-4 (a) Experimental Setup to evaluate the proposed phase pre-distortion method, AWG: arbitrary waveform generator, AMP: amplifier, DC: direct current, LED: lighting emitted diode, PD: photodiode, TIA: trans-impedance amplifier, DSO: digital storage oscilloscope; (b) frame format for the NOMA	

users.	98
Figure 4-5 Bit error rate (BER) versus the SNR of the strong signal, for strong signal (S) in QPSK and weak signal (W) in QPSK: (a) $r_{dB}=1.2$ dB, (b) $r_{dB}=4.2$ dB, (c) $r_{dB}=6.9$ dB.	100
Figure 4-6 Measured BER versus the relative power ratio r_{dB} between the strong signal S (in QPSK) and the weak signal W (in QPSK), with the SNR of S is fixed as 20.5 dB.	101
Figure 4-7 Measured BER versus the SNR of the strong signal S , under the scenario of signal S was in QPSK modulation and W was in BPSK modulation, and the relative power ratios r_{dB} were (a) 2.0 dB, (b) 4.8 dB, and (c) 8.2 dB, respectively.....	102
Figure 4-8 Measured BER versus the relative power ratio r_{dB} between the strong signal S (in QPSK) and the weak signal W (in BPSK), with the SNR of S is fixed as 20.5 dB.	103
Figure 4-9 System model for the NOMA in visible light communications. LED: lighting emitted diode; PD: photo diode, S and W are the transmitted signals from LED ₁ and LED ₂ , respectively; (b) an example of the three Euclidean distances at $r=1.43$, where $d_1=1/r$; $d_2 = 1-(1+j)/re^{j\varphi} $; $d_3 = 1-1/re^{j\varphi} $	106
Figure 4-10 Distances comparison of the three terms in four cases: (a) $r=2.5$; (b) $r=2.2$; (c) $r=1.98$; (d) $r=1.43$	112
Figure 4-11 (a) Experimental setup to evaluate the proposed joint detection	

method with phase pre-distortion; (b) frame format for the NOMA users.	113
Figure 4-12 Bit error rate (BER) versus the SNR of the strong signal: (a) $r_{dB}=1.2$ dB, (b) $r_{dB}=4.2$ dB, (c) $r_{dB}=6.9$ dB.	115
Figure 4-13 (a) System Model (b) DSP of W in three cases.....	117
Figure 4-14 Simulation setup.....	119
Figure 4-15 SNR of OFDM data subcarriers: (a) LED power=2W, PD at P ₂ , (b) LED power=2W, PD at P ₄	121
Figure 4-16 BER comparisons: (a) LED power=1.5W, (b) LED power=2W .	122
Figure 4-17 BER comparisons: (a) PD at P ₂ , (b) PD at P ₄	123
Table 2-1 Mapping table of BPSK PNC	27
Table 4-1 Simulation Parameters	120

Chapter 1 Introduction

1.1 Optical communication

With the drastic increasing demand of higher communication capacity, optical communication is garnering an unprecedented market today. One main contributor to this bloom is fiber optical communication (FOC), which dominates the market of backbone networks and gains a great share in the market of access networks. Meanwhile, optical communication technologies beyond the medium of fiber, or more accurately, optical wireless communication (OWC), is also promising. In this section, we briefly review these two forms of optical communications.

1.1.1 Fiber optics communication

The rise of modern optical communication is initiated by the proposal of using optical fiber as a medium of communication [1]. In the early stage of such development, several commercial FOC connections were built up, between Long Beach and Artesia in California by GTE, and in downtown Chicago by AT&T. Both links were designed for the live transmission of telephone traffic. Since then, FOC has long been considered as a key player in the arena of communications, beyond its initial application of voice interconnection.

After decades of rapid development, FOC has entered its mature age. A brief introduction classifies different variants of FOC into several categories [2], according to the scale of operation, namely, long haul networks, optical access networks and

optical data centers.

1.1.1.1 Long haul networks

With the extremely low loss in optics fiber (less than 0.2 dB/km today [3]), FOC is more than suitable for the transmission over a long distance. Long-haul optical fiber telecommunication is now the main force for ultra-long distance communication. The intercontinental and transoceanic networks, the domestic backbone networks such as US-NET, and the regional backbone networks, are examples of long haul networks. These networks are regarded as core networks. They connect core nodes that provide international, domestic and regional services.

Long haul networks aim at long distance, high throughput, and easy add and drop. These requirements are enabled by many key technologies including erbium doped fiber amplifier (EDFA) [4], wavelength division multiplexing (WDM) [5], reconfigurable optical add-drop multiplexer [6], and so on.

However, the continuous growing of bandwidth demand has evoked the demand of more advanced technologies. Today, researchers keep reforming the area of long haul networks with novel technologies, such as software defined networks (SDN) [7], advanced signal modulation formats [8], flexible sliceable bandwidth variable transponder [9], flexible optical switch [10], adaptive spectrum allocation [11], and more other exciting innovations.

1.1.1.2 Optical access networks

Nowadays, the demand of access data rate continually increases, driven by the blooming of new media, high resolution videos, online games and peer-to-peer (P2P) services [12]. It is a universal trend that optical access network (OAN) is replacing digital subscriber line (DSL) in connecting end users into the Internet, defined as fiber to the home (FTTH) in ‘the last mile’ [13]. Figure 1-1 depicts the changes of the number of broadband subscribers in Japan, showing a notable trend that FTTH is seizing a huge market share from conventional DSL.

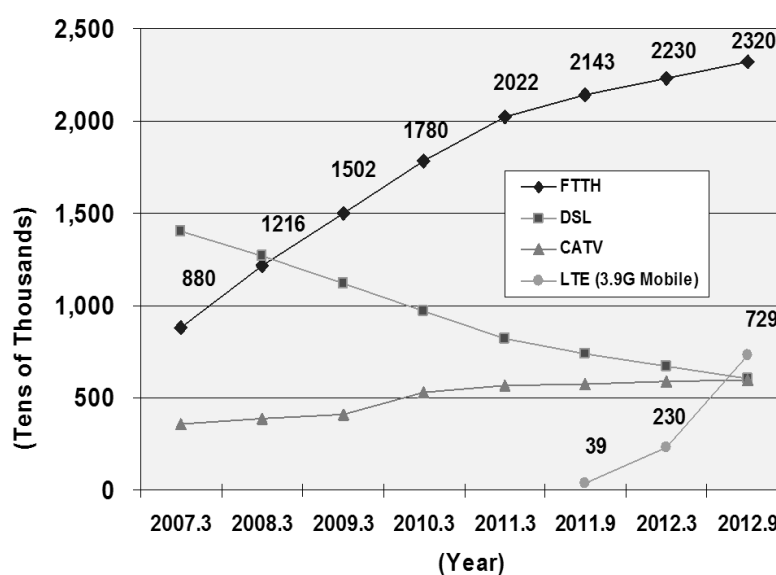


Figure 1-1 Changes in number of broadband subscribers [14].

There are mainly two types of OAN, active optical network (AON) and passive optical network (PON) [15]. Though AON has also been considered as a potential candidate for OAN, PON has been widely preferred, considering its low-cost, power-efficiency and reliability. International Telegraph Union Telecommunication Standardization Sector (ITU-T) has proposed a roadmap for the development of PON,

with the evaluation to gigabit PON (GPON) [16], as shown in Figure 1-2, while elastic PON (EPON) defined by IEEE is also a powerful competitor [17]. This standardization process, as well as the commercialization of PON, has driven the development of numerous novel technologies, upgrading the performance of today's OAN.

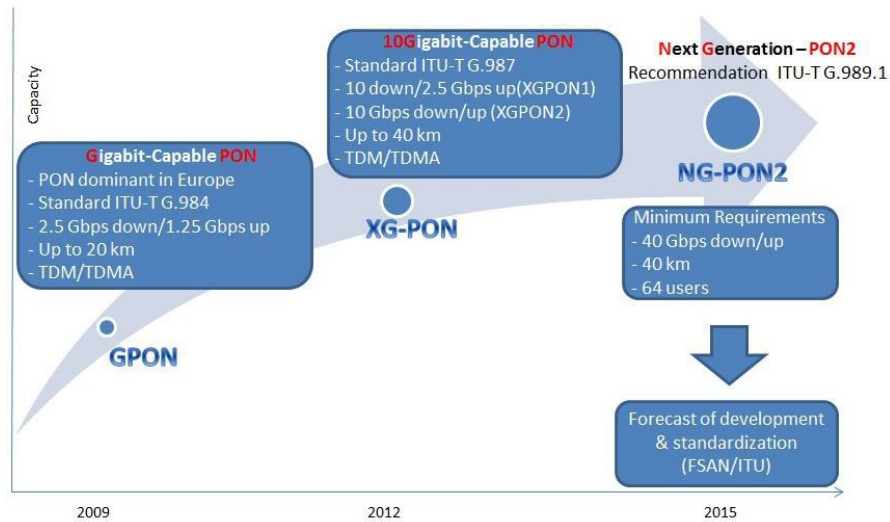


Figure 1-2 FSAN evolution roadmap [18].

However, there are still many challenges. The bandwidth demand in the access networks keeps increasing. Moreover, the unit cost of capacity should be reduced, as OAN is quite sensitive to cost. Furthermore, the possible technology innovation should be better based on the deployed infrastructure, considering the large investment that has been made by the network operators. Besides, more users and further reach distances are yet to be supported. In addition, adaptive bandwidth allocation should be allowed to provide more flexible services to users. Finally, higher resilience and security are also necessary in future OAN.

These requirements have stimulated the emergence of many new technologies.

For example, in order to reduce the cost of PON, self-seeded PONs are being widely studied today [19], since the removal of local oscillators at the optical network users (ONU) reduces the cost of OAN. Moreover, the adoption of orthogonal frequency division multiplexing (OFDM) enables more flexible bandwidth allocation, both at optical line terminal (OLT) and ONU [20]. Furthermore, advanced modulation formats and high baud rate transceivers increase the capacity and performance of OAN [21]. Besides, ultra-dense WDM is providing higher data rates to ONU [22]. All these technologies, as well as more innovations, are renovating our old knowledge of OAN.

1.1.1.3 Optical datacenters

Cloud computing provides shared computation and storage resources at centralized stations, known as data centers (DC). The extensive storage and computation resources of the servers at DC do not only motivate the development of high performance computation facilities, but also arouse the demand of high performance interconnection. A DC is usually a centralized warehouse residing numerous servers, each of which should have a large I/O bandwidth far beyond the capability of electrical interconnection. Therefore, optical DC is being considered as a better solution today.

Figure 1-3 shows an example of a typical 3-Tier data center topology [23]. Edge layer includes the ‘Top of Rack (ToR) switches’. A ToR switch interconnects the servers within one rack, usually in the order of tens. The racks are connected by the aggregation layer, and are also connected to Internet by the core switches in the core layer.

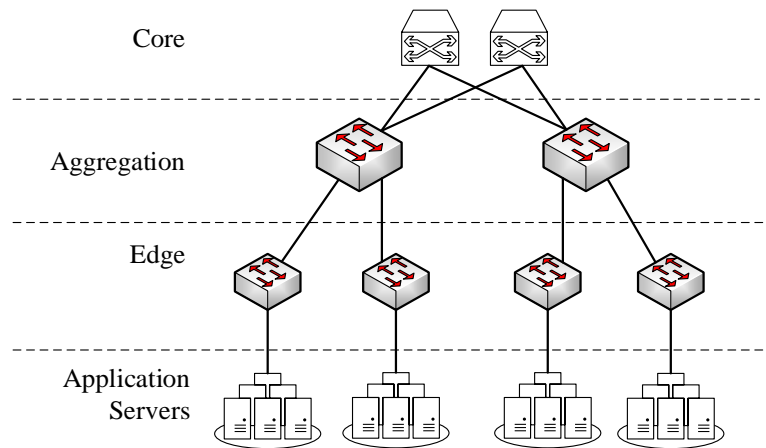


Figure 1-3 A typical 3-Tier data center topology.

Despite the fast development of FOC data center networking, there are also many challenges facing ahead. The interconnection throughput of DC is yet to be improved, considering the successive increase of DC data volumes. Similar to OAN, the cost is also another important issue in DC. Due to the nature of DC, the transmission latency at DC should be very low, thus calling for the necessity of latency reduction technologies.

To address these problems, many novel FOC technologies are emerging recently. For example, advanced modulation formats and novel multiplexing technologies are being adopted in DC, such as pulse amplitude modulation 4 (PAM4) [24] and orthogonal frequency division multiplexing (OFDM) [25]. Besides, low-cost solutions based on vertical-cavity surface-emitting lasers (VCSEL) are being studied [26]. Low-cost silicon photonic chips will play a crucial role in DC [27].

In conclusion, regardless the working scale, FOC is always fast developing to meet the demands nowadays. These advances are based on the basis of the mature

technologies that have been achieved in the past few decades, as well as the fantastic innovations to take place in the future.

1.1.2 Optical wireless communication

In contrary to the ‘wire-connected’ FOC, another branch of optical communication without wired medium, namely OWC, is also fast developing. Actually, the very early commencement of OWC is initiated by the invention of “photophone” by Alexander Graham Bell [28]. Bell’s invention is the prototype of FSO, one form of OWC. In the following century, FSO has experienced continuous development, owing to its advantages in many aspects [29]. For example, the distance of transmission is extended to several kilometers and the data rate of FSO can be as much as tens of Gbps. Moreover, FSO is free from electromagnetic interference as it’s free from other RF bands. Besides, FSO is also free from license and the eye safety can be guaranteed if FSO is within the regulation power level. Besides, the setup can be deployed efficiently and swiftly.

FSO takes the advantages of the high carrier frequency, hence high modulation bandwidth of lightwave, as FOC does. Also, being free from optical fiber, OWC can be deployed free from many physical restrictions. A good example is deep space communication, such as the lunar laser communication demonstration (LLCD) installed by National Aeronautics and Space Administration (NASA) [30]. LLCD supports a data connection up to 622-Mbps between a spacecraft at the orbit of Moon and a ground station by FSO.

Besides FSO, researchers have also proposed a new communication technology named as visible light communications (VLC) [31]. VLC employs the light emitting diodes (LED) which are primarily for illumination, for the optical transmitting source.

As an eye-catching technology today, VLC enjoys a lot of advantages over conventional radio-frequency-based (RF-based) wireless communications [32]. On one hand, VLC works in the license-free band. The utilization of visible light unlocks an unused broad band, which can alleviate the congestion in the RF band. On the other hand, VLC can provide data service to venues which are electromagnetism prohibited, for example, hospitals and laboratories. What's more, due to its line-of-sight (LoS) nature, VLC can enjoy a high spatial diversity and freedom, as multiple connections can be set up in a small space with less interference from each other. Moreover, VLC employs low cost components and equipment, making it quite economical.

Meanwhile, there are also some limitations in VLC [32]. First, the service coverage of VLC is quite limited due to the large path loss of visible light. Second, VLC is quite vulnerable to the shot and thermal noises of photodiodes. Third, for data communication in VLC, LED has to be powered on during the whole transmission period. Forth, although improving the diversity and freedom, LOS is also a problem in practical systems as the loss of LOS would largely affect the performance of the VLC systems.

From the foregoing analyses, it can be concluded that VLC cannot fully replace the functionality of RF-based communication technologies. In contrast, it can work

well as a complement of RF communications in future communication systems [33].

Figure 1-4 shows a combination of Li-Fi (light fidelity) and Wi-Fi (wireless fidelity), named as Li+WiFi heterogeneous network [34].

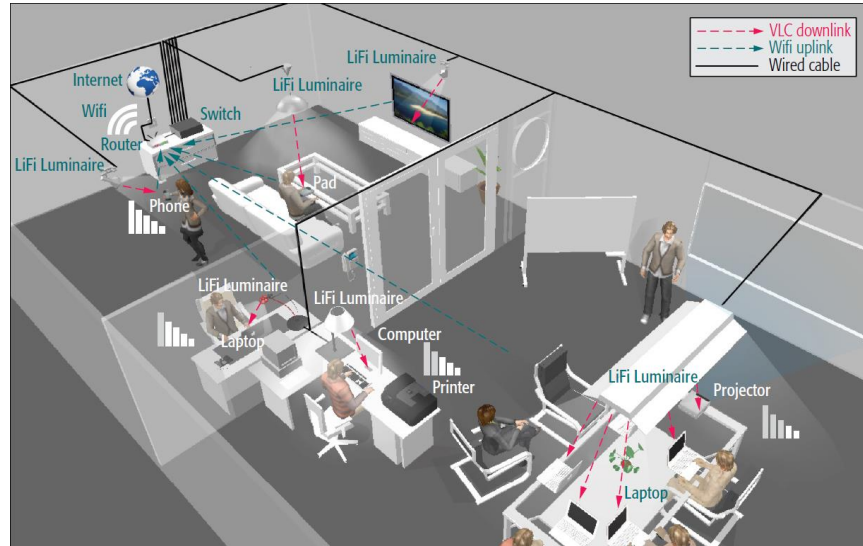


Figure 1-4 A Li+WiFi heterogeneous network [34].

1.2 OFDM in optical communications

As most systems discussed in this thesis are in orthogonal frequency division multiplexing (OFDM), we will briefly introduce the basics of OFDM in this section.

The applications of OFDM in optical communications will also be reviewed.

1.2.1 Fundamentals of OFDM

OFDM is a multicarrier modulation technology. Firstly proposed in [35], it is now among the most promising multicarrier technologies, with wide implementations in various communication systems such as DSL, Wi-Fi and long term evolution (LTE).

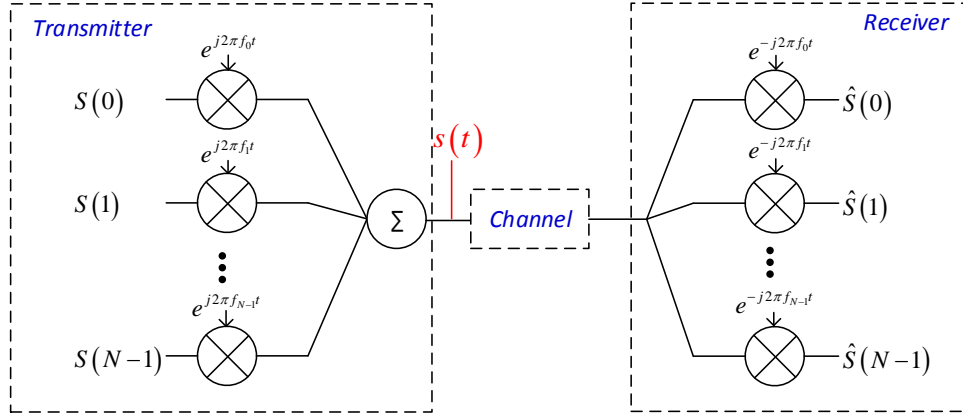


Figure 1-5 Schematic view of an OFDM system.

An OFDM transmitter modulates its symbols onto multiple frequency component, which are called subcarriers. Figure 1-5 gives an illustration of an OFDM system.

Let $S(k) (k \in [0, N-1])$ denote the symbols to be modulated, the transmitted signal sent from the OFDM transmitter in the time domain is

$$s(t) = \sum_{k=0}^{N-1} S(k) e^{j2\pi f_k t}, \text{ for } t \in [0, T_s] \quad (1.1)$$

$$f_k = f_{DC} + k\Delta f$$

where f_{DC} denotes the frequency of the main carrier; f_k is the frequency of the k^{th} subcarrier; Δf is the subcarrier spacing; T_s is the duration of one OFDM symbol.

The relationship of Δf and T_s is $T_s \cdot \Delta f = 1$.

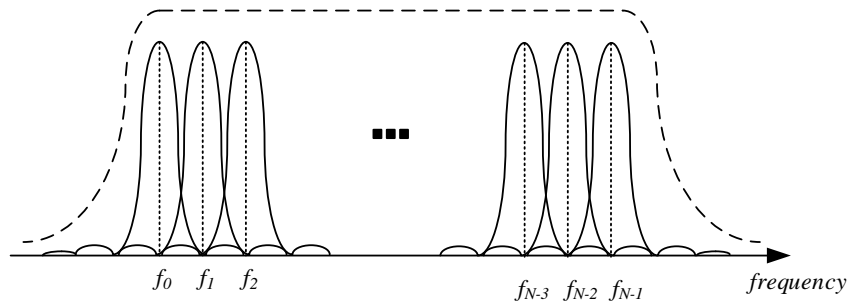


Figure 1-6 Spectrum of an OFDM symbol.

The signal represented in (1.1) is a summation of multiple signals on different subcarriers in different frequencies, contributing to a non-regular time domain waveform. The spectrum of an OFDM signal can be depicted as in Figure 1-6.

The following orthogonality holds

$$\frac{1}{T_s} \int_0^{T_s} e^{j2\pi f_m t} e^{-j2\pi f_n t} dt = \frac{1}{T_s} \int_0^{T_s} e^{j2\pi(f_m - f_n)t} dt = \frac{1}{T_s} \int_0^{T_s} e^{j2\pi(m-n)\Delta f t} dt = \delta(m-n) \quad (1.2)$$

where $\delta(m-n)$ is the Kronecker delta function which is defined as

$$\delta(m-n) = \begin{cases} 1 & \text{if } m = n \\ 0 & \text{if } m \neq n \end{cases} \quad (1.3)$$

The demodulation process at the OFDM receiver can be expressed as

$$\begin{aligned} \hat{S}(k) &= \frac{1}{T_s} \int_0^{T_s} s(t) e^{-j2\pi f_k t} dt \\ &= \frac{1}{T_s} \int_0^{T_s} \left(\sum_{p=0}^{N-1} s(p) e^{j2\pi f_p t} \right) e^{-j2\pi f_k t} dt \\ &= \sum_{k=0}^{N-1} s_k \delta(p-k) \\ &= S(k) \end{aligned} \quad (1.4)$$

Therefore, the symbols on different subcarriers can be demodulated individually without interference among each other.

In practice, the transmitter and the receiver both work in digital domain. The transmitting and the receiving processes can be expressed in digital form, as follows

$$\begin{aligned} s(n) &= \sum_{k=0}^{N-1} S(k) e^{j2\pi f_k n} = iDFT \{S(k)\} \\ \hat{S}(k) &= \sum_{n=0}^{N-1} s(n) e^{-j2\pi f_k n} = DFT \{s(n)\} \end{aligned} \quad (1.5)$$

Equation (1.5) gives the definitions of these two digital processes as *inverse discrete Fourier transform (iDFT)* and *discrete Fourier transform (DFT)*. It is unveiled in [36] that these *IDFT* and *DFT* can be simplified mathematically to *inverse fast Fourier transform (IFFT)* and *fast Fourier transform (FFT)* [37]. In this simplification process, the number of multiplication operation decreases from N^2 to $\frac{N}{2} \log_2 N$, that is, from quadratic to linear, to the number of subcarriers [].

Widely adopted in wireless communications, OFDM addresses the problem of channel fading [37]. The detrimental effect induced by channel fading includes the crosstalk from a neighboring symbol (inter-symbol interference) and incomplete symbol window (orthogonality disruption, thus inter-carrier interference) [38]. The key technology to combat the channel fading in wireless communications is the insertion of cyclic prefix (CP) [39]. By cutting off a last portion of the transmitted OFDM symbol and inserting it to the start of the same symbol, OFDM can eliminate the aforementioned detrimental effects caused by channel fading. The insertion can be at the end of an OFDM symbol, named as cyclic suffix; or be at both the start and the end of an OFDM symbol. An example of CP is depicted in Figure 1-7, in which the last part of the original OFDM symbol are truncated and inserted as the prefix.

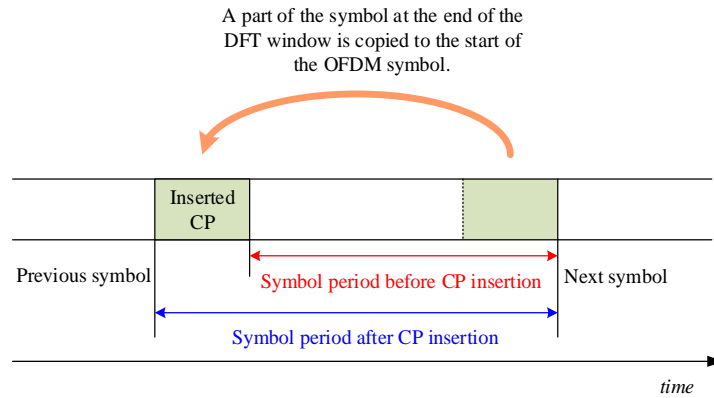


Figure 1-7 The time domain depiction of CP.

1.2.2 OFDM in fiber optics communication

The introduction of OFDM in FOC dates back to the publication by Pan and Green in 1996 [40]. However, it did not arouse great attention due to its large computation complexity, and its lack of advantages known at that time.

In the last decade, OFDM in FOC redrew researchers' attention with some key publications [41]. The reborn technology have then generated numerous publications and implementations [42,43]. The revival of OFDM in FOC should be largely attributed to the recent improvement of computation capability in digital signal processor (DSP).

On the other hand, the merits of OFDM in FOC have been widely recognized. There are a lot of advantages in optical OFDM, compared to the case of single carrier.

1. **Dispersion tolerance:** The problem of dispersion in long-reach FOC seriously deteriorates the system performance, raising the necessity of complex chromatic compensation in single carrier system. However, the

introduction of cyclic extension in OFDM can efficiently combat dispersion, including chromatic dispersion (CD) [37], polarization mode dispersion (PMD) (which could be treated as beneficial as claimed in [38]), and modal dispersion in multimode fiber [41]. Compared to single carrier system which combat the CD and PMD with complicated DSP such as equalization, OFDM can relieve these effects with no DSP cost.

2. **DSP:** DSP in conventional single carrier optical communication systems involves quite complicated operations such as channel state information (CSI) estimation, carrier frequency offset (CFO) estimation, and carrier phase estimation. These operations may be quite unstable and complex. However, these estimations can be simply conducted by inserting training sequences and pilot tones, hence greatly enhance its robustness. For instance, constant modulus algorithm (CMA), which is usually adopted to estimate CSI in a conventional single carrier system, is vulnerable to error propagation [38]. However, in OFDM, the estimation of CSI can be done easily with training sequences. The DSP complexity of OFDM may outperform the single carrier systems in some cases [38].
3. **Flexibility and scalability in modulation formats:** In conventional single carrier system, the upgrade of modulation format requires hardware replacement, for example, the upgrade of digital-analog-converter (DAC) [38]. In OFDM, the upgrade only involves software-defined reconfiguration.

This makes OFDM quite attractive in the system throughput enhancement in the future.

4. **Oversample rate:** In a traditional single carrier system, the sampling rate should be twice the baud rate of the signal for timing synchronization. In OFDM, oversampling can be realized by zero-padding at the subcarriers at the edge of the OFDM spectrum. Twice oversampling is not necessary. The oversampling rate is usually 10%-20%, which is quite flexible.
5. **Adaptive bit and power loading:** OFDM divides the spectrum into multiple subcarriers. Based on the channel states, the modulation format on each subcarrier can be adaptive adjusted according to the channel condition [44]. Meanwhile, the power on each subcarrier can also be adaptively loaded [45]. This feature helps optimize the performance of OFDM in FOC.

The aforementioned merits, as well as other advantages, increases the attractiveness of OFDM in FOC.

1.2.3 OFDM in optical wireless communication

Unlike the case of FOC, in OWC, OFDM has always been considered as a key technology. In practice, the performance of OWC is influenced by many detrimental effects. Fortunately, OFDM can play a positive role in resisting many of them.

For example, in a FSO terrestrial link, the system performance is seriously affected by the atmosphere turbulence. The system performance degradation should

be mitigated by advanced technologies. It has been demonstrated in [38] that in an atmosphere turbulence channel, a low-density parity check (LDPC) channel-coded OFDM FSO system outperforms a LDPC channel-coded on-off-keying (OOK) FSO system. This should be attributed to the extended symbol duration in association with channel coding, which increases the system tolerance to the deep fades induced by the atmosphere turbulence.

In VLC, OFDM also shows advantages compared to conventional single carrier system. For example, the reflected light beams from different surfaces may arrive at the receiver at different times. This phenomenon, called as multipath effect, leads to inter-symbol interference in a VLC system. However, by inserting cyclic extension, OFDM in VLC can efficiently eliminate the impairment of multipath fading [46].

1.3 Contributions of this thesis

This thesis focus on harnessing the interference in optical communications. By making use of the interference caused by the simultaneous arrivals of multiple signals at a common receiver, the system throughput can be improved, or a novel multiple access dimension can be achieved. The main efforts can be generalized into two parts: physical-layer network coding (PNC) and non-orthogonal multiple access (NOMA).

1.3.1 Physical-layer network coding in optical communication

In this thesis, we investigate the applications of PNC in different optical communications scenarios, including coherent optical orthogonal frequency division

multiplexing (CO-OFDM), orthogonal frequency division multiplexing passive optical networks (OFDM-PON), and visible light communications (VLC).

We firstly applies PNC in CO-OFDM to increase the system throughput of a multicast topology. In a specific multicast network that two multicast streams share a common path, the throughput is bottlenecked at the shared path. By applying PNC in this scenario, the throughput can be significantly improved, with a reasonable optical signal to noise ratio (OSNR) penalty. The problem of different CFO and different common phase errors (CPE) of two signals are solved by specially designed training sequences and pilot tones.

OFDM-PON has been considered as a promising access technology to support the access services of multiple users, with the potential of supporting heterogeneous services including wireless services over RF spectra. In another study, we demonstrate the virtual private network (VPN) services in an OFDM-PON on different services, including baseband wired service, and Wi-Fi service with a carrier frequency of 2.5 GHz. Experimental demonstration has been conducted to verify the feasibility of the proposed scheme.

In another work, we study PNC in VLC. Different from the previous two schemes, this PNC scheme involves the decoding at the relay node. This can be categorized into another class of PNC, called as finite-set PNC (PNCF), which will be introduced in details in Section 2.2.2.2. With the property of VLC, we also propose a phase-matching method in this scenario. It is shown that our newly proposed phase-matched PNC can

significantly improve the system performance.

1.3.2 Non-orthogonal multiple access in optical communication

NOMA is a novel multiple access technology in which multiple users are multiplexed in the power domain. After the commencement in information theory and wireless communications, it has been introduced to various different scenarios. In this thesis, we focus on the application of NOMA in VLC.

Different multiuser detection (MUD) methods can be adopted in the detection of NOMA in VLC, namely, successive interference cancellation (SIC) and joint detection (JD). We study both MUD methods in VLC NOMA and propose novel phase pre-distortion methods in both detections. In a following study, we introduce a novel multicarrier precoding algorithm to equalize the frequency responses of OFDM subcarriers. The precoding algorithm works well in combination with the proposed VLC as well as the phase pre-distortion method.

1.4 Outline of this thesis

The rest of this thesis is organized as follows:

Chapter 2 reviews the basic concepts of PNC and NOMA. In the PNC part, the fundamentals of PNC are reviewed, followed by the introduction of different types of PNC, including infinite-set PNC (PNCI) and finite-set PNC (PNCF). Both of them have been considered in our studies. Then, we briefly summarize some previous

studies of PNC. In the NOMA part, the general concepts of NOMA are briefly introduced. Then, an example is given to elaborate the advantage of NOMA in balancing the system throughput and fairness. The channel capacities of NOMA in downlink and uplink are later discussed. Then, we briefly discuss the past studies of NOMA in different scenarios. The challenges encountered in these studies are then given, as a motivation of our studies.

Chapter 3 describes our studies of PNC in different optical communications, namely, CO-OFDM, OFDM-PON and VLC. The theoretical and experimental results are given in details, respectively.

Chapter 4 introduces our researches in NOMA in VLC. SIC and joint detection (JD) are adopted separately, in combination with the newly proposed phase pre-distortion method. Then, we discuss a multicarrier precoding method in cooperation with the previous VLC NOMA and phase precoding method.

Chapter 5 summarizes the thesis and gives suggestions for possible future works.

Chapter 2 Background: Interference-Assisted Techniques in Optical Communication

2.1 Introduction

Conventionally, noise is the main contributor to the performance deterioration in a communication system, since noise exists everywhere and dominates the destructive effect to a signal. Scientists and engineers have made great efforts to recover the right information against the ubiquitous noise.

Meanwhile, interference is also another important issue in communication. Interference refers to the contribution from other unwanted signals, which is different from noise that originates from a noise source. There are many types of interference such as inter-carrier interference (ICI), inter-symbol interference (ISI), multiple access interference (MAI), co-channel interference (CCI), etc.

ICI is the interference induced by other subcarriers in an OFDM system [47]. It can be attributed to many factors, including CFO [48], local oscillator phase noise (PN) [49], or imperfect symbol window synchronization (which destroys the orthogonal condition and introduces ICI) [50]. The aforementioned imperfections may bring interference from other subcarriers when demodulating the information on a subcarrier.

ISI in a system does not obey Nyquist ISI criterion [51]. Typical conditions that destroy Nyquist ISI criterion include the band-limited system, and the multipath

effect. ISI introduces interference from other symbols to the target symbol.

In a multiple access (MA) system such as a WiFi system, multiple users are connected to the same access point. Orthogonal conditions should be obeyed to eliminate the crosstalk from other users, which, however, cannot be guaranteed all the time. The interference induced by other users connected to the same access point is called as MAI. This is a common interference in code division multiple access (CDMA) system [52].

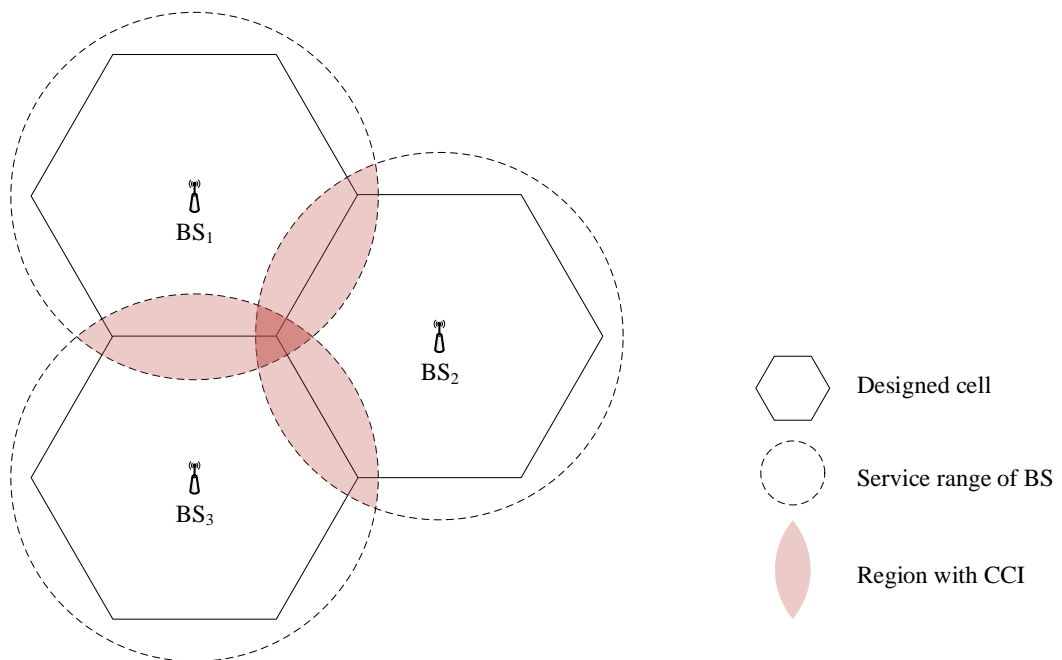


Figure 2-1 CCI in a cellular network.

In a broadcasting communication system, the receiver may receive signal from other transmitters. For example, in a cellular wireless communication system, the broadcasting from a neighboring cell cannot be always ideally avoided. This effect is depicted in Figure 2-1. The leakages from other cells lead to CCI, or crosstalk [53].

Generally speaking, interference is ‘bad’, and ‘undesired’. Therefore, tremendous

efforts have been made to reduce the negativity of interference. For instance, the ICI induced by CFO in an OFDM system can be alleviated by CFO compensation [54] or ICI cancellation [47]. To reduce the MAI in a CDMA system, orthogonal code words have to be designed to guarantee the orthogonality among different MA users [55]. The ISI can be combated by equalizers at the receiver or pre-distortion at the transmitter [51]. In summary, the successful reduction of interference is usually beneficial for a communication system, thus cost a lot of efforts for communication engineers.

Nevertheless, interference can also be useful at a second look. Significant benefit can be brought by taking advantages of the interference in communication systems. Different schemes have been proposed to take advantages of different types of interference. The major objective of this thesis is to harness the interference so as to benefit the optical communication systems. Here, we introduce two methods to harness the interference, such that the conventionally ‘harmful’ interference turns useful and helpful.

2.2 Physical-layer network coding (PNC)

2.2.1 General concept

The concept of PNC was originated from the scenario of two-way relay channel (TWRC) in wireless communications. Figure 2-2(a) depicts a typical TWRC, with two source nodes A and B, as well as a relay node R.

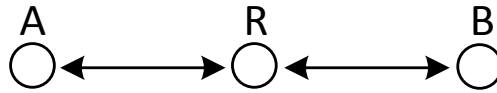


Figure 2-2 A two-way relay network

A-R-B is a three node network while nodes A and B exchange their packets P_A and P_B . Due to the lack of direct link between A and B, a relay node R is necessary to pass P_A to B and P_B to A.

2.2.1.1 Non-network-coded scheme

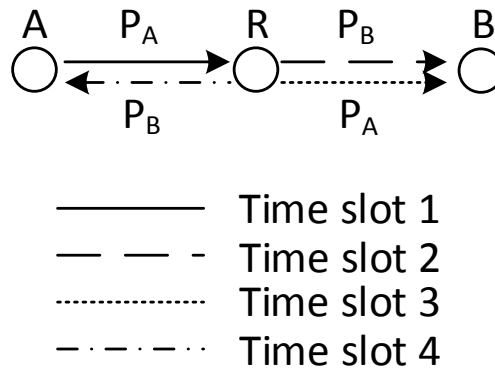


Figure 2-3 Non-network-coded scheme

The intuitive way for A and B to exchange their packets in the TWRC is depicted in Figure 2-3, which is regarded as the conventional scheme. The conventional scheme takes four time slots, consisting of two phases. In the first phase, A and B transmit P_A and P_B to R, respectively. Due to the broadcasting nature of the channel, P_A and P_B cannot be transmitted and received simultaneously without interference. Therefore, the first phase takes two time slots. In the second phase, R transmits P_A and P_B to B and A, respectively. Similarly, R cannot send P_A and P_B simultaneously, so the second

phase also takes two time slots. Overall, it takes four time slots for A and B to exchange one packet with each other.

2.2.1.2 Network-coded scheme (NC)

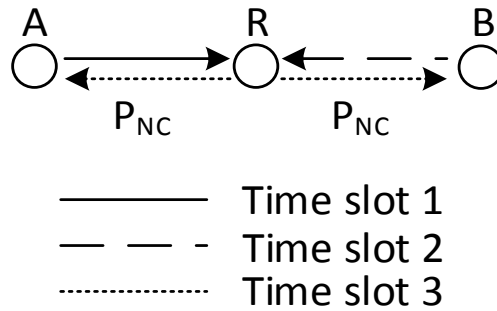


Figure 2-4 Network-coded scheme

Network coding (NC) [56] can help reduce the required number of time slots in the preceding transmission process in TWRC. Figure 2-4 depicts the schematic diagram of this scenario. Similarly, NC-based TWRC transmission also comprises two phases. The first phase resembles that of the conventional scheme. Two time slots are needed, during which A and B transmit P_A and P_B to R. Nevertheless, the second phase of NC-based scheme is different from that of the conventional scheme. In NC-based process, node R receives P_A and P_B and forms the interference of them into P_{NC} . Instead of sending P_A and P_B to B and A respectively, R broadcasts P_{NC} to A and B simultaneously. Note that only one packet is to be sent to both A and B in the second phase of NC-based scheme, which only occupies one time slot. Hence, it realizes a reduction of 25% in the required number of time slots, as compared with the conventional scheme. This leads to 33% improvement in throughput.

In NC, P_A and P_B should be encoded into a function of them. A frequently used function is logic exclusive OR (XOR), which can be expressed as

$$P_{NC} = P_A \oplus P_B \quad (2.1)$$

Note that although P_A and P_B are packets, the XOR should be bitwise, based on the bits of P_A and P_B .

After receiving P_{NC} , B and A recover P_A and P_B by another XOR operation, respectively, as follows,

$$\begin{aligned} P_A &= P_{NC} \oplus P_B \quad \text{for node B} \\ P_B &= P_{NC} \oplus P_A \quad \text{for node A} \end{aligned} \quad (2.2)$$

2.2.1.3 Physical-layer-network-coded scheme (PNC)

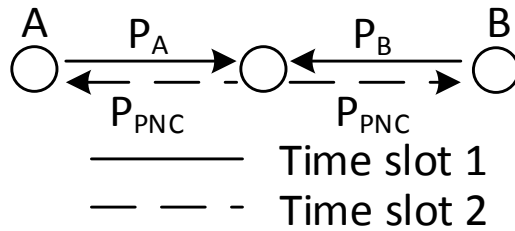


Figure 2-5 Physical-layer-network-coded scheme

PNC further reduces the number of slots needed for the preceding mission. In PNC, the natural interference of electromagnetic waves are exploited. Figure 2-5 depicts the process of PNC realizing TWRC.

PNC differs from the aforementioned two schemes even in the first phase. In the first phase of PNC, A and B respectively transmit P_A and P_B simultaneously to R. P_A and P_B interfere at R, with the electromagnetic (EM) waves of P_A and P_B combined

into a composite EM wave. It turns out that this kind of interference, however, incorporates the information of P_A and P_B . Therefore, it works as a coding process by nature. The coded packet is P_{PNC} . In the second phase, R broadcasts packet P_{PNC} to A and B, while P_B and P_A were recovered at A and B, respectively.

From Figure 2-5, it can be observed that by adopting PNC, both two phases occupy only one time slot. Hence, only two time slots are needed compared to four in the conventional scheme and three in NC. A 50% reduction in time or a 100% improvement in throughput is achieved, compared to the conventional scheme.

Another very important feature is the benefit brought by channel coding. During the operation at the relay node, channel decoding and recoding can be done. Hence, the possible errors introduced in the first phase of PNC can be corrected. Therefore, the gain brought by PNC is not limited to the erasure of the noise term, but also the error correction brought by channel coding.

2.2.2 Classification of PNC

The interfered EM wave at R incorporating the information of P_A and P_B are retransmitted to B and A, respectively. The output signal could be treated as a mapping of the input signals. Depending on the operation taken at R, PNC can be generalized into two types: infinite-set PNC (PNCI) and finite-set PNC (PNCF).

2.2.2.1 PNCI

In PNCI, R takes an operation to re-map P_A and P_B into an infinite set, as in analog

network coding (ANC) [57]. In ANC, the naturally interfered signal as the addition of A and B is not decoded. Relay R simply amplifies the interfered signal, then forwards to A and B. This process is called as amplify-and-forward (AF). This AF process could be seen as a remapping from two signals to an analog signal, which is infinite.

2.2.2.2 PNCF

Oppositely, PNCF maps the received interfered signal to a finite set. A good example of PNCF is the XOR mapping operation. We consider one symbol period in the interfered signal.

Table 2-1 Mapping table of BPSK PNC

Bits of x_A^I, x_B^I	BPSK symbol of x_A^I, x_B^I	Received symbol of x_{PNC}^I	Mapped BPSK symbol of x_{PNC}^I, y_{PNC}^I	Mapped bits for x_{PNC}^I, y_{PNC}^I
0,0	1,1	2	1	0
0,1	1,-1	0	-1	1
1,1	-1,-1	-2	1	0
1,0	-1,1	0	-1	1

Denote the signal of the symbol x_A with RF modulation as s_A in the packet P_A , while x_B and s_B regarding P_B , and the carrier frequency as ω . Assume QPSK modulation is adopted, then $x_A, x_B \in (1+i, -1+i, -1-i, 1-i)$. By neglecting the carrier

frequency offset (CFO), the phase noise (PN), the asynchrony between the carriers of P_A and P_B , the background noise, the symbol misalignment between s_A and s_B , and other defective conditions, the interfered signal, combined by s_A and s_B , that is, s_{PNC} , is given as

$$\begin{aligned}
s_{PNC} &= s_A + s_B \\
&= x_A^I \cos(\omega t) + x_A^Q \sin(\omega t) + x_B^I \cos(\omega t) + x_B^Q \sin(\omega t) \\
&= (x_A^I + x_B^I) \cos(\omega t) + (x_A^Q + x_B^Q) \sin(\omega t)
\end{aligned} \tag{2.3}$$

where the superscripts I and Q denote the components of the in-phase and the quadrature-phase, respectively; $x_A^I, x_A^Q, x_B^I, x_B^Q \in \{-1, +1\}$. One dimension of quadrature phase shift keying (QPSK) is binary phase shift keying (BPSK) modulation. For each phase, -1 corresponds to bit 0, while +1 corresponds to bit 1. Define the symbol of s_{PNC} as x_{PNC} . We can get the in-phase and quadrature-phase of x_{PNC} as

$$\begin{aligned}
x_{PNC}^I &= x_A^I + x_B^I \\
x_{PNC}^Q &= x_A^Q + x_B^Q
\end{aligned} \tag{2.4}$$

Take the in-phase as an example. Depending on the values of x_A^I, x_B^I , Table 2-1 lists the four cases. Despite the four possible combinations of x_A^I, x_B^I , x_{PNC}^I only takes three possible values. Therefore, x_{PNC}^I can be mapped to the two-value system of BPSK as

$$y_{PNC}^I = \begin{cases} -1 & \text{if } x_{PNC}^I = 0 \\ 1 & \text{if } x_{PNC}^I \in \{-2, 2\} \end{cases} \tag{2.5}$$

After BPSK de-mapping, the bit obtained is just the XOR of the original bits, as can be seen in the last column of Table 2-1. Therefore, this mapping is named as XOR mapping. Practically, the signal output from the transmitter of relay R does not take

the BPSK de-mapping, but only takes the signal representation in the BPSK form, just as it does at the transmitter A or B. After receiving the relayed signal and with BPSK de-mapping, A and B can easily recover the information bits that belong to P_B and P_A by another XOR operation, respectively. The case of the quadrature-phase component is performed in the same manner.

Generally, it could be concluded PNC aims at producing a discrete output at the relay node, which is different from the analog output in PNCI.

2.2.3 PNC studies and implementations

PNC was first proposed in 2006 by Zhang, as a variation of NC in information theory [58]. This topic has drawn great research interests and led to numerous publications. In [58], the basic concept of PNC was introduced. Meanwhile, the concept of ANC, a form of PNCI was also proposed in the same year in [57].

In the analysis in Section 2.2.2.2, an ideal condition is assumed that there exists no CFO, no PN, and no noise. However, this is not practical. In a theoretical study on PNC in a wireless system reported in [59], it was found that when the modulation format of P_A and P_B increased beyond BPSK to, for example, QPSK, the phase offset between the two signals seriously degraded the performance of PNC. Specifically, when P_A and P_B were QPSK-modulated, a special 16-quadrature-amplitude-modulation (16QAM) would be formed. Then BER of PNC would vary with respect to the relative phase difference, φ , between the symbols of P_A and P_B . The best case was $\varphi=0$ while the worst case was $\varphi=\pi/4$. The penalty could be as large as 6 dB at

$BER=10^{-2}$, as reported in [59]. Although it was found that this phase asynchrony dropped when there also existed symbol offset [59], these two conditions were difficult to meet simultaneously. This issue largely hindered the practicality of PNC in wireless communications, as phase offset was ubiquitous in wireless communications due to CFO and PN.

A practical implementation of PNC is later demonstrated in [60], in which experiments based on universal software radio peripheral (USRP) were carried out. In this implementation, the PNC was in the frequency domain, so as to be called frequency PNC (FPNC). In other words, P_A and P_B are in orthogonal frequency division multiplexing (OFDM), while PNC is between each subcarrier of the OFDM symbols of P_A and P_B .

As has been pointed out in Section 2.2.1, the benefit brought by channel coding in PNC is a very important issue in PNC. There are numerous works studying channel coded PNC, leading to many publications, such as [61,62], and many others.

The study of PNC was initiated by a TWRN. However, PNC should not be limited to this form. In [63], the authors put forth nine PNC atoms as the basic forms of PNC application, in which TWRN was included as a special form. This paper has paved the way for a wider application of PNC in more general scenarios in communication systems.

PNC was later introduced into optical communications. In [64], researchers applied PNC into passive optical networks (PON) to realize virtual private networking

(VPN). By employing PNC-based bi-directional VPN between optical network users (ONU) could work in full-duplex mode by bypassing optical line terminal (OLT). Compared to the traditional VPN in which optical line terminal was involved, a 100% percent VPN throughput gain was achieved. Here, PNC was applied into a time division multiplexing PON (TDM-PON). The wavelengths of the two ONU should be different to avoid optical beating noise (OBN). Similarly, another optical PNC (OPNC) structure have tried to avoid OBN by aligning the two PNC component signals onto orthogonal polarizations [65].

Another OPNC scheme was proposed in [66]. This scheme was based on a coherent optical communication system. Unlike the preceding two OPNC systems, coherent optical communication systems could eliminate the effect of OBN. Therefore, the system was a common-channel OPNC system in which no polarization or frequency difference was needed.

PNC was also applied in the combination of optical communication and wireless communication, or more specifically, fiber-wireless (Fi-Wi) communication. In [67], a Fi-Wi network with PNC was proposed. The implementation doubled the system throughput in a star-topology Fi-Wi system.

2.3 Non-Orthogonal Multiple Access

2.3.1 General concept

Multiple access (MA) is a classical topic in communication systems, or more

specifically, in multiuser communication systems. When multiple transmitters share a common link to transmit their respective messages to a common receiver, a MA system is built up. It should also be noted that there are also other types of multiuser communication systems, for example, broadcast networks. Contrary to a MA system, a single transmitter transmits information to multiple users in a broadcast network [68].

There are several MA strategies working in different principles. Time division multiple access (TDMA) divides the time duration into multiple subintervals, and allocates them to multiple users. In frequency division multiple access (FDMA), the whole spectrum is divided into subchannels to be assigned to multiple users. A specific variation of FDMA is orthogonal frequency division multiple access (OFDMA), in which the spectrum is naturally divided into multiple subcarriers by fast Fourier transform (FFT). One user can be assigned to one or more subcarriers for information transmission [69].

An alternative way is to use code division multiple access (CDMA). In CDMA, each user is assigned a unique code sequence, or signature sequence. The transmitter spreads its signal over the whole band by multiplexing the signature sequence. At the receiver, signals from different users are recovered by correlation with different signature sequences. The code sequences are designed to be zero-cross-correlation, for example, Walsh codes [70]. Therefore, when recovering the signal from one specific transmitter, the crosstalk from other users can be minimized [71].

Non-orthogonal multiple access (NOMA) is a novel MA technique [72]. For

example, the combination of NOMA with OFDMA assigns one subcarrier to multiple users simultaneously, while signals of different users are in different power levels [73]. Unlike TDMA, FDMA and CDMA, different NOMA signals are overlapped rather than orthogonally multiplexed in the power domain. Hence, NOMA does not orthogonally divide the signals from different users in any domain, which differs from TDMA, FDMA and CDMA.

There are many advantages brought by the adoption of NOMA.

First of all, in a system with extremely high throughput, NOMA can outperform other MA methods such as OFDMA, as it grants concurrent access of multiple users to one subcarrier, or in other words, resource reuse [74].

Moreover, NOMA provides a solution to the dilemma of throughput versus fairness in other MA strategies [75]. The dilemma of throughput versus fairness lies in a MA system in which multiple end users locate randomly. This advantage will be addressed by an instance in Section 2.3.2.

Furthermore, it can be proved that NOMA innately enjoys a higher throughput than OFDMA in some particular conditions [75]. Section 2.3.3 will discuss this issue.

2.3.2 Balancing throughput and fairness: an example

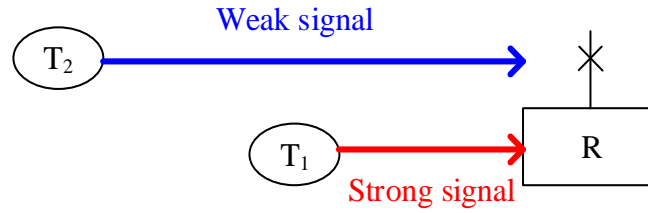


Figure 2-6 A multiple access system with two transmitters (T₁ and T₂) and one receiver (R).

Figure 2-6 shows a multiple access system composed of a receiver, R, and two transmitters, T₁ and T₂. T₁ lies nearer to R, from which T₂ lies farther away. The channel gains of T₁ and T₂ to R are different, due to different losses in the transmission paths. The allocation of resources is a problem in this scenario, with the trade off of throughput and fairness.

We introduce a new index to quantize the fairness, known as Jain's fairness index [76]. Assume there are n connections and x_n is the throughput of the n^{th} connection, then the Raj Jain's equation, is given by

$$J(x_1, x_2, \dots, x_n) = \frac{\left(\sum_{i=1}^n x_i \right)^2}{n \cdot \sum_{i=1}^n x_i^2} \quad (2.6)$$

It gives a measure of the fairness in a multiple access network. The value of Jain's index varies from $\frac{1}{n}$ (worst case) to 1 (best case).

Recall the two-transmitter-one-receiver MA scenario above. Assume both users adopt OFDMA, the MA resource allocation strategy refers to the allocation of spectrum. Assume the available OFDM spectrum is F Hz, and the modulation format by the nearer user T₁ is 16QAM, while 4QAM is adopted by the farther user T₂. We

describe three schemes here in resource allocation in this scenario.

To achieve the largest throughput of the system, we shall assign the spectrum to the user with higher spectrum efficiency. So in the first scheme, the whole band of F Hz is assigned to T_1 while T_2 is allocated nothing. In this scheme, the overall throughput is $4F$, while the Jain's fairness index, according to the definition above, is $1/2$, which is the worst case.

We can also assign half of the spectrum to T_1 while the other half to T_2 . In the second scheme, the OFDM spectrum is equally divided to the user, that is, $F/2$ is occupied by T_1 and $F/2$ is occupied by T_2 . In this scheme, the overall throughput of the system is $3F$, while $2F$ is for T_1 and F is for T_2 . Hence, according to the definition, the Jain's fairness of this scheme is $9/10$. Its fairness is better than that in the first scheme, however its throughput decreases.

In the third scheme. $1/3$ of the whole spectrum is allocated to T_1 , while the other $2/3$ is allocated to T_2 . The throughputs of E_1 and E_2 are both $4F/3$, reaching a overall throughput of $8F/3$. The fairness is 1, which is the best case of Jain's definition. However, the throughput is less than the previous two schemes.

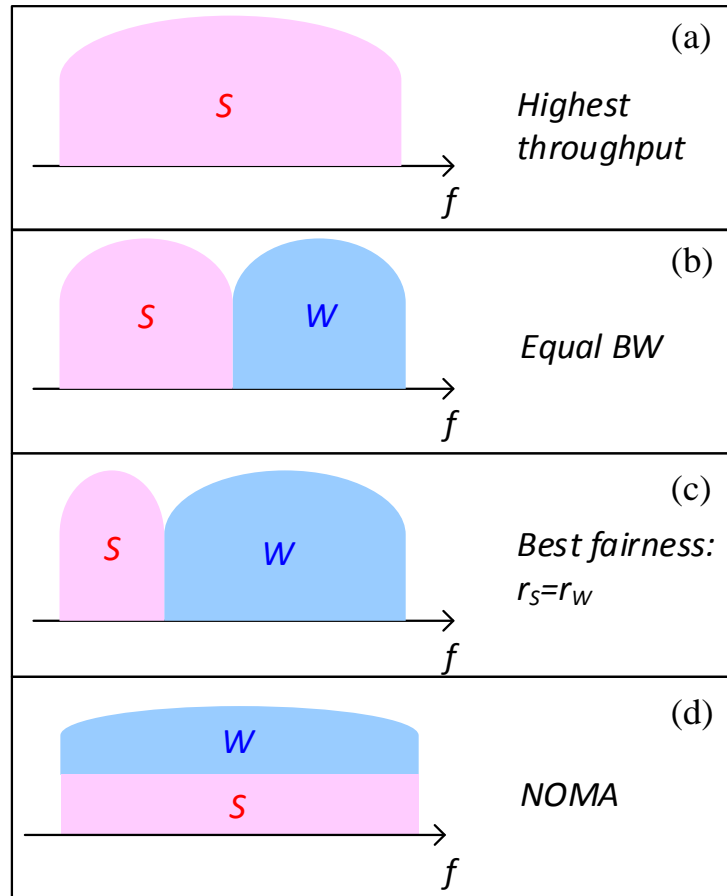


Figure 2-7 (a)-(c) Spectrum allocation in OFDMA: (a) the whole spectrum assigned to T_1 ; (b) half of the spectrum assigned to T_1 , the other half to T_2 ; (c) 1/3 of the spectrum assigned to T_1 , 2/3 to T_2 ; (d) NOMA.

Figure 2-7 (a)-(c) depicts the three spectrum allocation schemes. The three schemes above fail to balance the throughput and the fairness. In the scheme with larger throughput, the fairness is the worst; when the fairness is optimized, the throughput drops. The target is to find a method to achieve better fairness while maintaining the high throughput.

Actually, with regard to the spectrum allocated to T_2 , which is denoted as x , the Jain's fairness factor J and the overall throughput R can be expressed as

$$J = \frac{1}{2 \left(\left(\frac{2x}{4-2x} \right)^2 + \left(\frac{4-4x}{4-2x} \right)^2 \right)} \quad (2.7)$$

$$R = 2x + 4(1-x) = 4 - 2x \quad (2.8)$$

J and R are plotted in Figure 2-8. Obviously, the best throughput and the best fairness could not be achieved simultaneously, putting forward a dilemma on the balance between throughput and fairness.

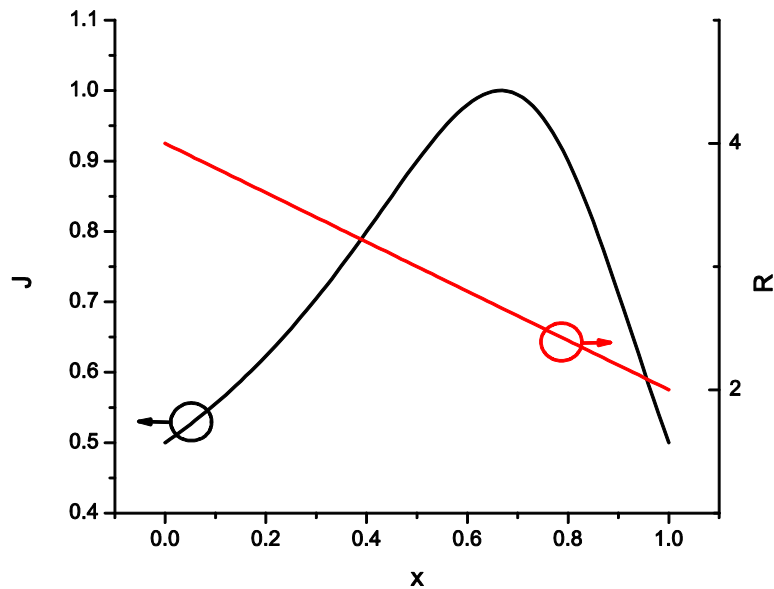


Figure 2-8 J and R with regard to the spectrum ratio assigned to T_1 in OFDMA.

One solution to this dilemma is non-orthogonal multiple access (NOMA). NOMA harnesses the imbalanced channel gains of T_1 and T_2 to multiplex the two signals in the power domain. Figure 2-7(d) depicts the comparison of NOMA to the three schemes in OFDMA. It can be observed that the whole OFDM spectrum is occupied by T_1 and T_2 simultaneously, and both of them are in 4QAM modulation format. Now,

the overall throughput of the system in $4F$, corresponding to the maximum throughput of OFDMA. $2F$ is for T_1 , while the other $2F$ is for T_2 . Hence, the Jain's fairness index here is 1, which is also the best case. In other words, by adopting NOMA, we reaches the best fairness and the best throughput simultaneously, which is impossible in conventional OFDMA. In this sense, NOMA outperforms OFDMA.

2.3.3 Channel capacity of NOMA

In a wireless communication system consisting of one base station and multiple user terminals, the base station is connected to the backbone network via a fixed connection, while the user terminals are connected to the base station wirelessly. The transmissions from the base station to the multiple user terminals are denoted as downlink, otherwise uplink. NOMA is applicable to both downlink and uplink.

In this section, we will demonstrate the system improvement brought by NOMA compared to orthogonal multiple access (OMA), or specifically, OFDMA [75]. Without loss of generality, we discuss a system with two user terminals here.

2.3.3.1 Downlink

The downlink is actually a broadcast channel. However, we still name the proposed scheme as NOMA in accordance with the previous terminology [77].

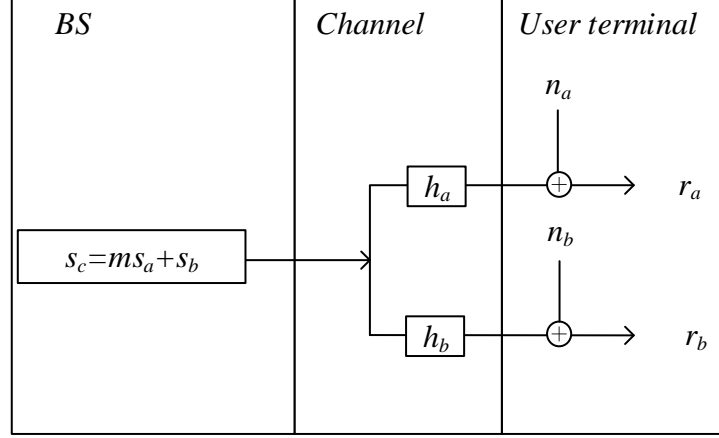


Figure 2-9 Transmission process of downlink NOMA.

In the downlink, the base station (*BS*) simultaneously transmits the signal to two user terminals. Figure 2-9 illustrates the whole transmission process. The transmitted composite signal from the base station is

$$s_c = m s_A + s_B, m = \sqrt{\frac{P_A}{P_B}} \quad (2.9)$$

where s_A and s_B are the normalized transmitted signals destined for user terminal *A* and *B*, respectively. The power of the signal for *A* is P_A , while the power of the signal for *B* is P_B . We assume $P_A < P_B$, which means that the power of signal to *A* is smaller than that to *B*.

The received signals at *A* and *B* are

$$\begin{aligned} r_A &= h_A \left(\sqrt{\frac{P_A}{P_B}} s_A + s_B \right) + n_A \\ r_B &= h_B \left(\sqrt{\frac{P_A}{P_B}} s_A + s_B \right) + n_B \end{aligned} \quad (2.10)$$

where h_A and h_B denote the channel gains from *BS* to *A* and *B*, respectively, while n_A and n_B denote the noise at *A* and *B*, respectively. We assume additive white Gaussian noise (AWGN) channel here. By Shannon's law, the maximum capacities of the two

connections of *BS-A* and *BS-B* can be given as (assume the bandwidth is 1 Hz)

$$\begin{aligned} C_{A-\max} &= \log_2 \left(1 + \frac{P_A |h_A|^2}{N_{0A}} \right) \\ C_{B-\max} &= \log_2 \left(1 + \frac{P_B |h_B|^2}{N_{0B}} \right) \end{aligned} \quad (2.11)$$

$C_{A-\max}$ and $C_{B-\max}$ denote the maximum information rate when *BS* is fully devoted to *A* or *B*, respectively. By applying orthogonal multiple access strategies such as OFDMA, the channel capacity is bounded by these two values. As shown in Figure 2-10, two points on the axes indicate $C_{A-\max}$ and $C_{B-\max}$. The channel capacity pair is

$$\begin{aligned} C_A &= \beta \log_2 \left(1 + \frac{P_A |h_A|^2}{\beta N_{0A}} \right) \\ C_B &= (1-\beta) \log_2 \left(1 + \frac{P_B |h_B|^2}{(1-\beta) N_{0B}} \right) \end{aligned} \quad (2.12)$$

where β is the spectrum assigned to *A*, out of 1 Hz in total; and N_{0A} and N_{0B} denote average power density of the Gaussian noise at *A* and *B*. This capacity pair is below or equal to the dashed line in Figure 2-10 [78], which bounds the available rate pair of OFDMA. Figure 2-10 depicts two cases of the capacity pair. The symmetric pair is for the case when the SNR of *A* equals that of *B*, while the asymmetric pair is for the case when the SNR of the two users are different.

In NOMA, successive interference cancellation (SIC) is adopted to decode the two signals [77]. For *A*, the process takes three steps: (1) decode s_b treating the signal to *A* as interference; (2) recover and subtract the signal to *B* from the composite signal; (3) decode s_a . For *B*, the decoding process just involves step (1). Assume P is the

overall power, the power assigned to user A is αP , and the power assigned to user B is $(1 - \alpha)P$. The capacity pair of NOMA is [75,77]

$$\begin{aligned} C'_A &= \log_2 \left(1 + \frac{(1-\alpha)P|h_A|^2}{\alpha P|h_A|^2 + N_{0A}} \right) \\ C'_B &= \log_2 \left(1 + \frac{\alpha P|h_B|^2}{N_{0B}} \right) \end{aligned} \tag{2.13}$$

In NOMA, the 1 Hz spectrum is not divided to A and B without overlapping, but occupied by A and B simultaneously. Hence, the channel capacity pair is just the one in Equation (2.13). The achievable region is depicted in Figure 2-10, bounded by the colored curve [77]. Clearly, the achievable channel capacity of NOMA is larger than that of OFDMA.

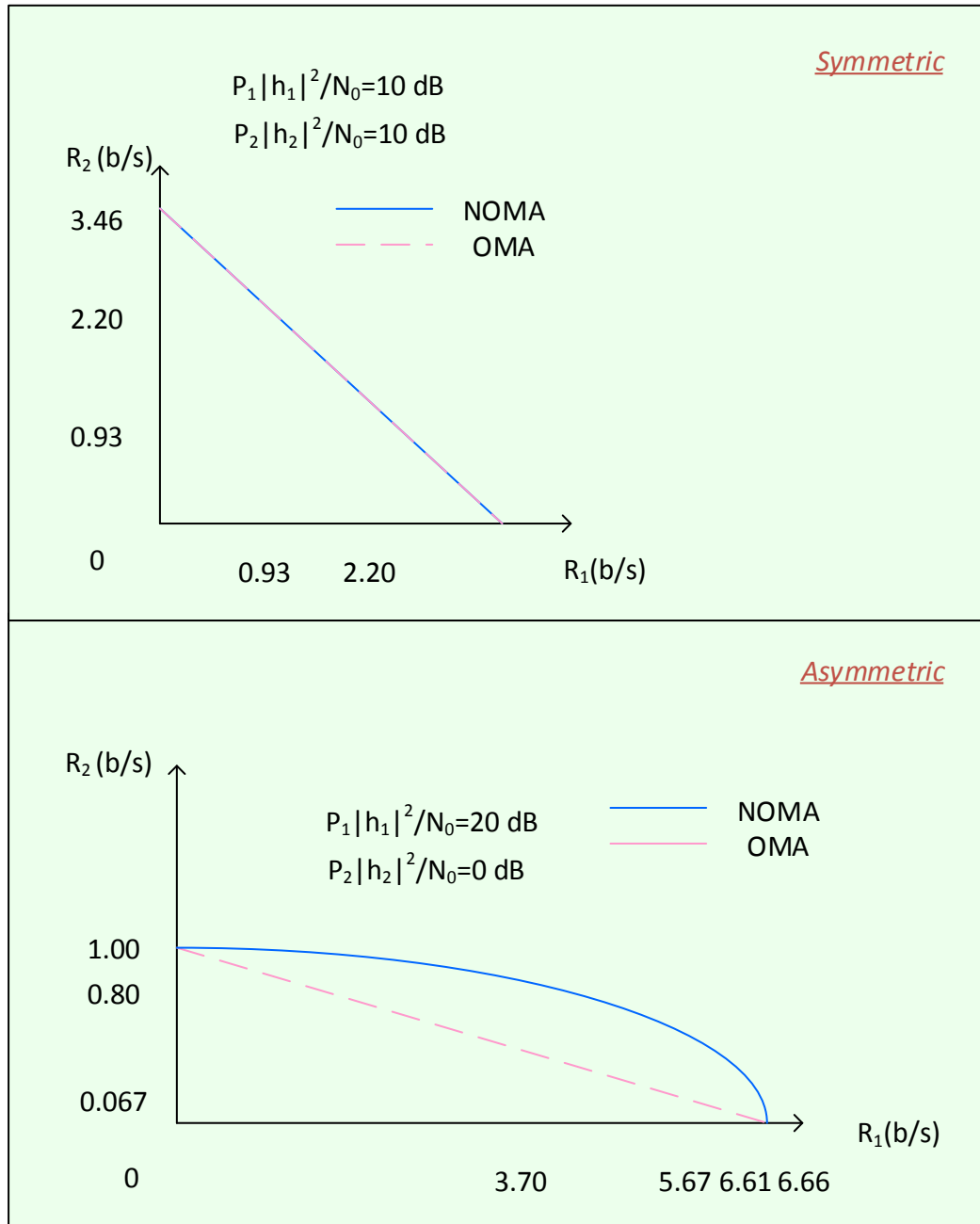


Figure 2-10 Rate region of the two-user downlink OFDMA and NOMA.

2.3.3.2 Uplink

Figure 2-11 shows the NOMA in uplink consisting two user terminals, A and B , as well as one base station (BS). The received signal at BS is

$$r_C = h_A s_A + h_B s_B + n \quad (2.14)$$

where s_A and s_B are the respective normalized transmitted signals originated from user terminal A and B ; h_A and h_B denote the respective channel gains from BS to A and B ; n represents the noise at BS receiver. The transmitting power relationship between the two signals is absorbed into the channel responses h_A and h_B .

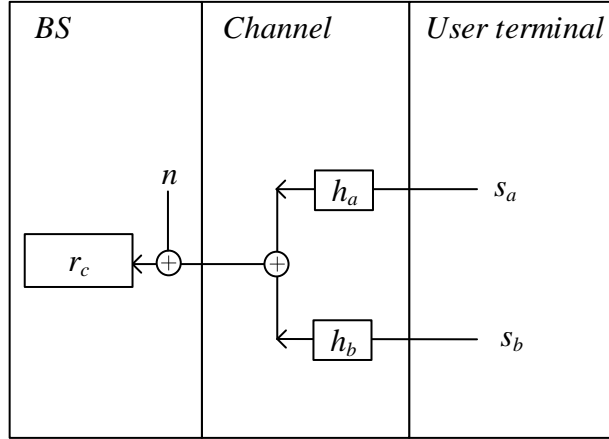


Figure 2-11 Transmission process of uplink NOMA.

Assume the receiving power at BS 's receiver is P . By Shannon's law, the channel capacity pair with the adoption of OFDMA is

$$\begin{aligned}
 C_A &= \beta \log_2 \left(1 + \frac{P|h_A|^2}{\beta N_0} \right) \\
 C_B &= (1-\beta) \log_2 \left(1 + \frac{P|h_B|^2}{(1-\beta)N_0} \right)
 \end{aligned} \tag{2.15}$$

where β is the spectrum assigned to A , out of 1 Hz in total; and N_0 denotes average power density of the Gaussian noise at BS . This channel capacity pair is depicted in Figure 2-12, bounded by the dashed curve [78]. Different SNRs of A and B may result in different regions, shown as symmetric and asymmetric.

On the other hand, the channel pair in NOMA is [75,77]

$$\begin{aligned}
C'_A &= \log_2 \left(1 + \frac{P|h_A|^2}{N_0} \right) \\
C'_B &= \log_2 \left(1 + \frac{P|h_B|^2}{P|h_A|^2 + N_0} \right)
\end{aligned} \tag{2.16}$$

The channel capacity pair in NOMA is different from the one in orthogonal multiple access. Figure 2-12 shows the NOMA channel capacity pair, bounded by the solid line [77]. It could be observed that the achievable channel pair region of NOMA is generally a superset of orthogonal multiple access when the SNRs of two users are different. Therefore, it could be deduced that NOMA enjoys a higher channel capacity than orthogonal multiple access in most cases.

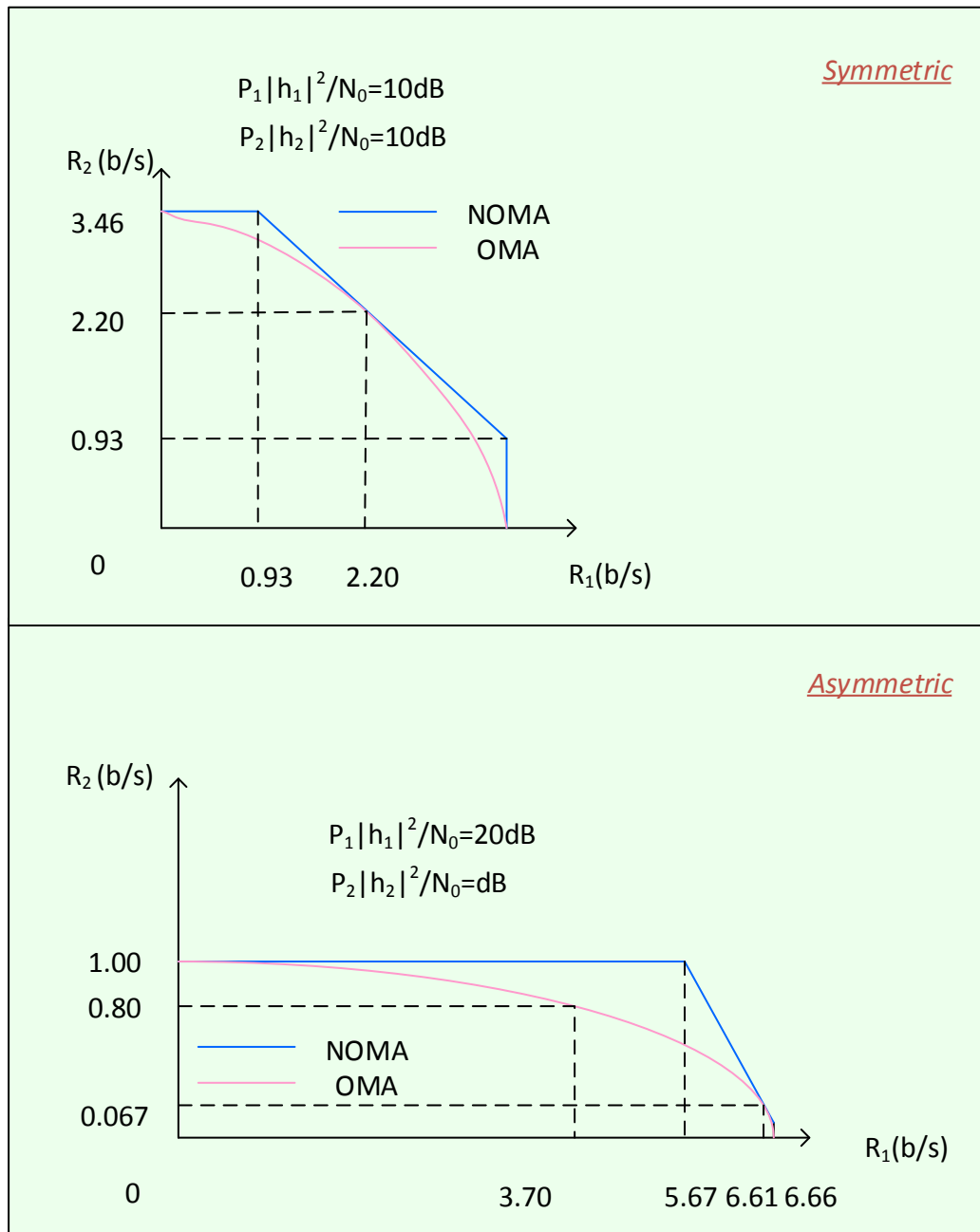


Figure 2-12 Rate region of the two-user uplink OFDMA and NOMA.

2.3.4 NOMA studies

Early studies on NOMA included the studies in information theory as well as the implementation in wireless systems.

In 2009, researchers from Alcatel Lucent Germany theoretically studied the

enhancement of throughput and fairness brought by NOMA in 4G wireless access systems [75]. It is found that NOMA could not only balance the throughput and fairness, but also boost the throughput compared to orthogonal schemes in some cases.

NOMA was later experimentally demonstrated. An experiment showed that NOMA could achieve a 61% throughput improvement in laboratory and 51% improvement in field trial, compared to OFDMA [79]. It was later written into NTT DOCOMO's 5G white paper [80].

The research on NOMA later extended to forms beyond its simplest form and prototype implementation. For example, the combination of NOMA with beamforming was proposed and studied [81]. Some researchers tried to relax the stringent synchronization requirement in NOMA by proposing triangle successive interference cancellation, a new decoding method to solve the asynchrony problem in OFDM based NOMA [82]. The NOMA in cooperation with MIMO was also studied [83]. A novel NOMA-based diversity scheme was proposed in [84]. In the past two to three years, plenty of papers have been published on the topic of NOMA, indicating that it has become a new hot topic among researchers in related fields.

The introduction of NOMA into optical communication was later than wireless communication. In [85], researchers proposed a NOMA scheme in visible light communications. A novel power allocation scheme, called gain ratio power allocation (GRPA) was also proposed. In [86] and [87], researchers reported their studies on NOMA in VLC. In all these works, the performance of NOMA in VLC were

numerically studied, without experimental demonstration.

Chapter 3 Physical-Layer Network

Coding in Optical Communication

3.1 Physical-layer network coding in CO-OFDM

3.1.1 Introduction

As described in Chapter 2, PNC can improve the system throughput in various communication systems. In the past, there have been many efforts made in implementing PNC into different systems, such as wireless communication system, intensity-modulation direct- detection (IM-DD) optical system, and coherent single carrier optical system.

Orthogonal frequency division multiplexing (OFDM) technique has been widely recognized as a promising approach to support high-speed optical fiber transmission, owing to its high and flexible spectrum efficiency in both optical and electronic domains, as well as the robustness in combating chromatic dispersion (CD) and polarization mode dispersion (PMD) in optical fiber.

To date, the application of PNC into CO-OFDM system is still an open question. In this section, we demonstrate the application of PNC in CO-OFDM system. The results show that the two optically combined CO-OFDM frames could be effectively separated and recovered by digital signal processing techniques at the destined node. Both common phase errors, as well as carrier frequency offset, can be effectively compensated by simple pilot-subcarrier-aided approaches.

3.1.2 Principle of operation

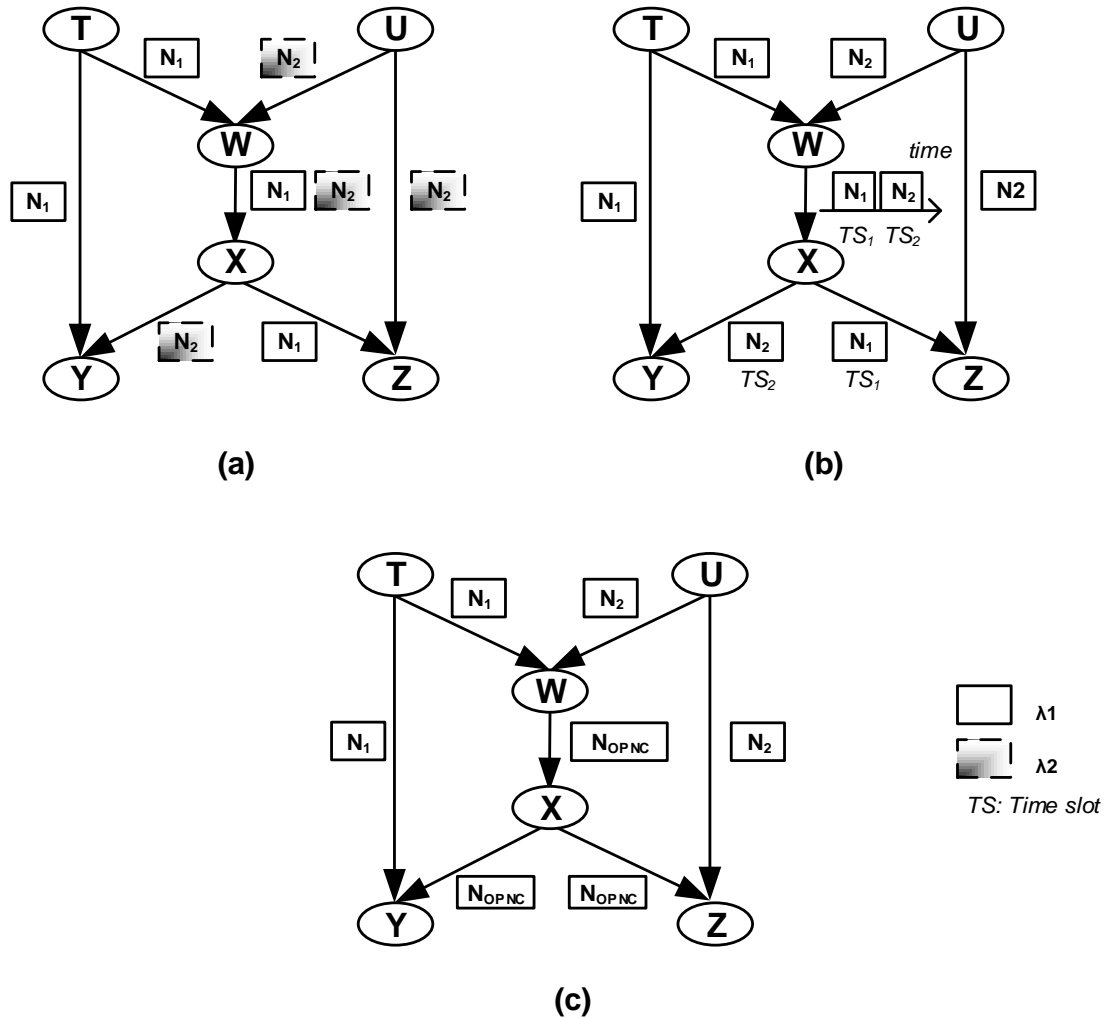


Figure 3-1 Optical multicast topology: (a) wavelength division multiplexing, (b) timing division multiplexing, (c) OPNC.

The basic principle of OPNC can be illustrated by considering an optical multicast topology, as shown in Figure 3-1. Suppose nodes T and U are sending multicast data frames to nodes Y and Z , simultaneously, N_1 is a multicast data frame from node T to nodes Y and Z , while N_2 is another multicast data frame sent from node U to nodes Y and Z . It is assumed that there exists a common link, say W - X , in the network topology. Figure 3-1(a) illustrates a solution in which N_1 and N_2 are occupying two wavelengths to avoid collisions. Figure 3-1(b), on the other hand, depicts the case that time division

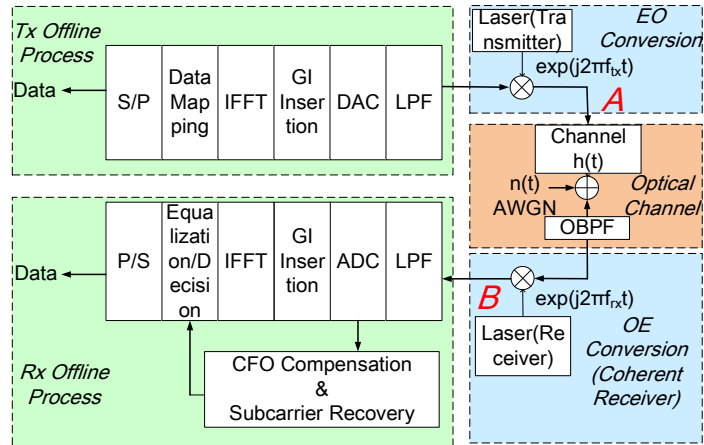
multiplexing is employed to resolve the link contention of the two multicast frames at the expense of requiring two transmission time slots to complete their transmissions. One better approach to save the spectrum or timing resources is to transmit a coded frame, containing the mutual information of N_1 and N_2 , on the common link $W-X$, and each of them are decoded individually at their respective destined nodes, as shown in Figure 3-1(c). N_1 and N_2 from nodes T and U are combined at node W to generate a composite OPNC frame, N_{OPNC} , before it is transmitted to nodes Y and Z , via link $W-X$. In our scheme, the coding at node W is just a simple optical power addition operation. The scheme is limited to combine two source data frames only.

Figure 3-2(a) depicts a simplified model of CO-OFDM [88]. The orthogonal subcarriers are generated by inverse fast Fourier transform (IFFT) manipulations by digital signal processing (DSP) at the transmitter and the receiver. Ignoring other effects such as laser phase noise and white Gaussian noise, for the simplicity of discussion, one symbol of the transmitted signal in the time domain at point A can be written as

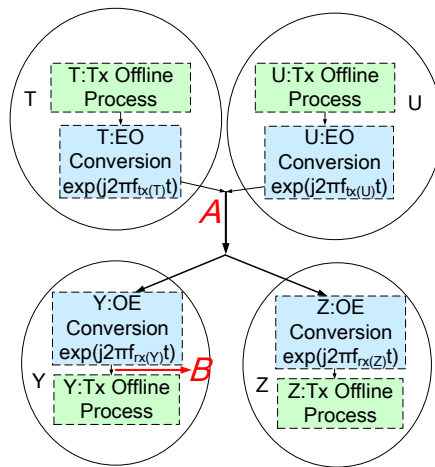
$$x_A(t) = \exp(j2\pi f_{ix}t) \cdot s(t) \quad (3.1)$$

$$s(t) = \sum_{k=0}^{N-1} S(k) \cdot \exp(j2\pi f_k t + \theta) = F^{-1}\{S(k)\} \quad (3.2)$$

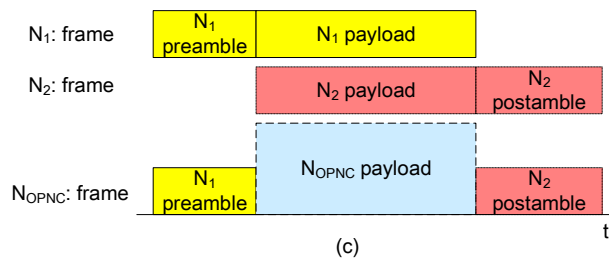
$$\Delta f = f_k - f_{k-1}, \quad k-1, k \in [0, N-1] \quad (3.3)$$



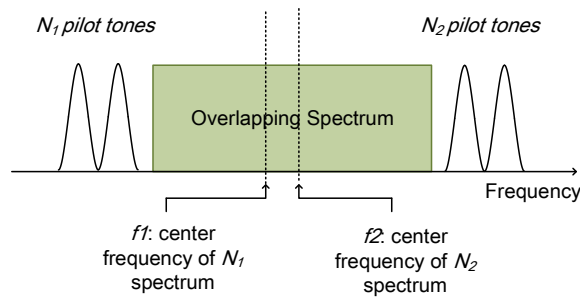
(a)



(b)



(c)



(d)

Figure 3-2 (a) OFDM model, (b) OPNC model, (c) Frames alignment of OPNC (d) OPNC spectrum.

$$x_B(t) = \exp(j2\pi f_{IF}t + \theta) \cdot F^{-1}\{S(k) \cdot H(k)\} \quad (3.4)$$

where $H(k)$ stands for the channel response of the k^{th} subcarrier. f_{IF} is the intermediate frequency f_{IF} determined by the frequency difference between f_{tx} and f_{rx} , that is, $f_{IF} = f_{rx} - f_{tx}$. This component is treated as carrier frequency offset (CFO), which is estimated and compensated by offline DSP at the receiver.

Figure 3-2(b) shows the model of OPNC corresponding to the topology in Figure 3-1. Only the OPNC stream at point Y is depicted. N_1 is sent by T and N_2 is from U .

The signal at point A can be written as

$$x_A(t) = \exp(j2\pi f_{tx(T)}t + \theta_1) \cdot s_{N_1}(t) + \exp(j2\pi f_{tx(U)}t + \theta_2) \cdot s_{N_2}(t) \quad (3.5)$$

$$s_{N_1}(t) = F^{-1}\{S_{N_1}(k)\} \quad (3.6)$$

$$s_{N_2}(t) = F^{-1}\{S_{N_2}(k)\} \quad (3.7)$$

where $S_{N_1}(k)$ and $S_{N_2}(k)$ are the information symbols from T and U , respectively. $s_{N_1}(t)$ and $s_{N_2}(t)$ are their respective baseband signals in the time domain. The OPNC signal at point B becomes:

$$x_B(t) = \exp(j2\pi f_{IF(N_1)}t + \theta_{N_1}) \cdot F^{-1}\{S_{N_1}(k) \cdot H_{N_1}(k)\} \\ + \exp(j2\pi f_{IF(N_2)}t + \theta_{N_2}) \cdot F^{-1}\{S_{N_2}(k) \cdot H_{N_2}(k)\} \quad (3.8)$$

Here, $f_{IF(N_1)} = f_{rx(Y)} - f_{tx(T)}$, $f_{IF(N_2)} = f_{rx(Y)} - f_{tx(U)}$, $H_{N_1}(k)$ and $H_{N_2}(k)$ stands for the channel response of the k^{th} subcarrier of N_1 and N_2 in the coded signal N_{OPNC} . Assume the information symbols from T has been successfully demodulated and decoded at node Y , which is $S_{N_1}(k)$ in this case. To retrieve $S_{N_2}(k)$, the channel responses $H_{N_1}(k)$ and $H_{N_2}(k)$ and the carrier frequency offsets $f_{IF(N_1)}$ and $f_{IF(N_2)}$ are estimated by inserting

training symbols into the OPNC frames. Figure 3-2(c) depicts the original and the OPNC frames in time domain. In the OPNC frame N_{OPNC} , the non-overlapping symbols are the preamble of N_1 and the postamble of N_2 , which will be used for respective carrier frequency offset estimation and channel estimation. Then

$$x_{N_1}(t) = \exp(j2\pi f_{IF(N_1)}t + \theta_{N_1}) \cdot F^{-1}\{S_{N_1}(k) \cdot H_{N_1}(k)\} \quad (3.9)$$

$$x_{N_2}(t) = x_B(t) - x_{N_1}(t) \quad (3.10)$$

$$x_{N_2}(t) = \exp(j2\pi f_{IF(N_2)}t + \theta_{N_2}) \cdot F^{-1}\{S_{N_2}(k) \cdot H_{N_2}(k)\} \quad (3.11)$$

$$S_{N_2}(k) = \frac{F\{x_{N_2}(t) \cdot \exp(-j2\pi f_{IF(N_2)}t - \theta_{N_2})\}}{H_{N_2}(k)}, \quad k = 0, \dots, N-1 \quad (3.12)$$

where F stands for the Fourier transform. Once the channel responses and the CFOs have been estimated, $S_{N_2}(k)$ can be recovered by fast Fourier transform (FFT), together with an one-tap equalizer in offline DSP. In order to ensure the training symbols in one frame (say N_1) is not overlapping with the payload field of the other frame (say N_2), proper synchronization between the two frames have to be performed, via proper scheduling at their source nodes or proper placement of training symbols in the preambles or postambles of the two frames.

Another major consideration raised in Equation (3.9)-(3.12) is θ_{N_1} and θ_{N_2} , which are the common phase error (CPE) mainly caused by the phase noise of the laser and this leads to possible rotation in the CO-OFDM information symbols' constellation. Different from CFO and channel response, CPE should be estimated symbol by symbol. In CO-OFDM, pilot tones are inserted to estimate CPE's angle θ based on the fact that CPE is constant over all the subcarriers [88]. However, this effect is even

aggravated in the OPNC scenario. In an OPNC symbol N_{OPNC} , the frequency components of the two source OFDM symbols (N_1 and N_2) overlap with each other and they are not guaranteed to be orthogonal to each other. This makes the intra-symbol CPE of the OFDM symbols difficult to be estimated, especially considering that the two CPE's θ_1 and θ_2 should be estimated, simultaneously. However, since it is possible to coarsely control the laser frequency, we can specifically assign the pilot tones at the designated subcarrier frequencies. Figure 3-2(d) shows the spectrum of an OPNC symbol N_{OPNC} . The center frequency of N_1 's spectrum, f_1 , and that of N_2 's spectrum, f_2 , are decided by the local oscillator's (LO) laser frequency, $f_{rx(Y)}$, and the two signal's laser carrier frequencies, $f_{tx(T)}$ and $f_{tx(U)}$. We set the three laser frequencies such that $f_{tx(T)}$ is smaller than $f_{tx(U)}$ by Δf_{tx} , and thus we can insert pilot tones at the lower spectral edge of N_1 's spectrum, as well as the upper spectral edge of N_2 's spectrum. Suppose the number of non-overlapped pilot subcarriers in two spectra is m , which is indicated by the subcarrier indices as $k=0$ to $m-1$ of N_1 and $k_2=(N-m)$ to $(N-1)$ of N_2 in (3.6) and (3.7). The non-overlapping relationship can be guaranteed by

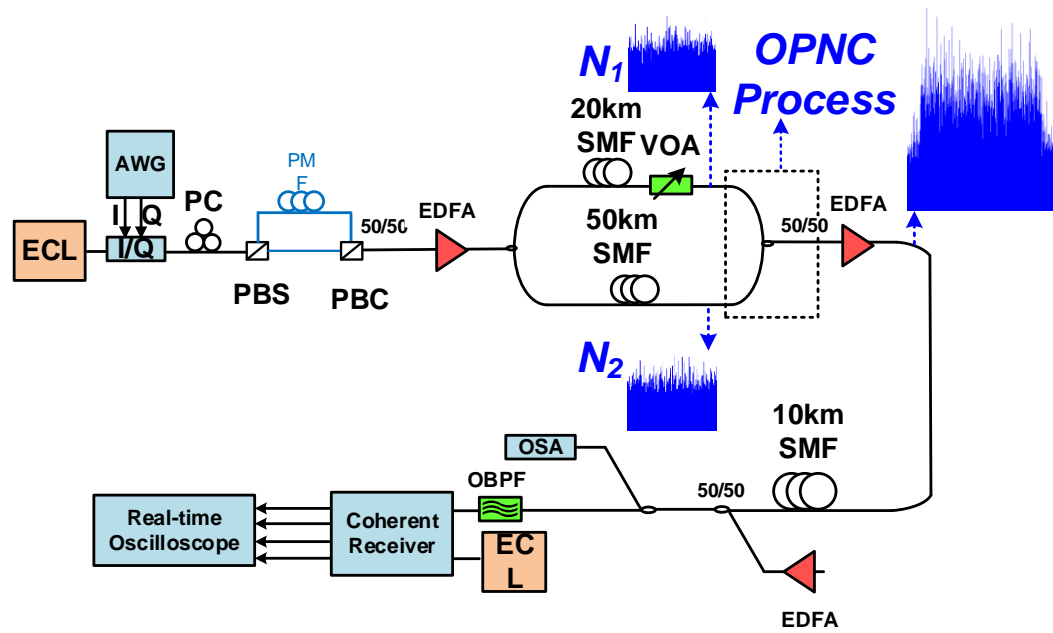
$$\Delta f_{tx} = |f_{tx(T)} - f_{tx(U)}| \quad (3.13)$$

$$\Delta f_{tx} \geq m\Delta f \quad (3.14)$$

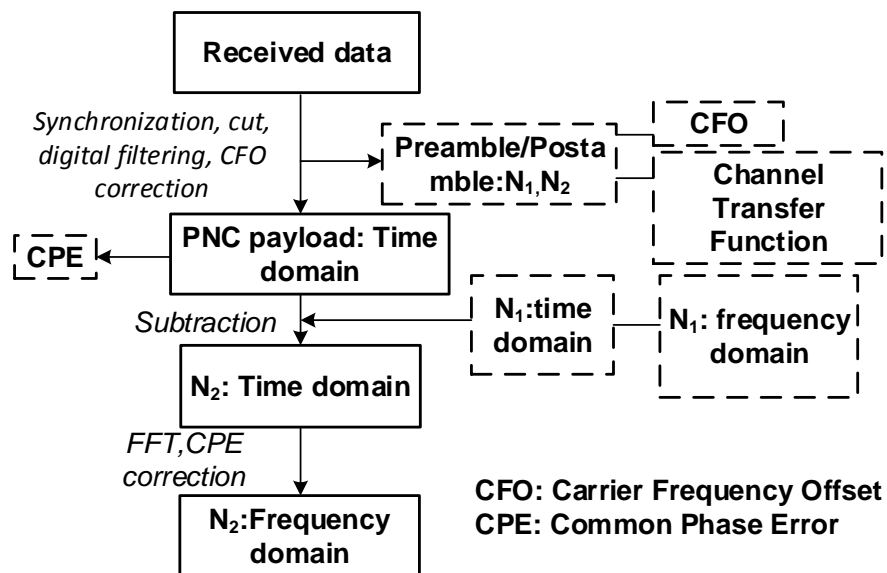
Hence, it is possible to estimate the CPE of the N_1 component in N_{OPNC} (CPE_{N1} for $k=0$ to $(m-1)$), as well as that of the N_2 component in N_{OPNC} (CPE_{N2} for $k=(N-m)$ to $(N-1)$). Note from Equation (3.13) that the frequency relationship between $f_{tx(T)}$ and $f_{tx(U)}$ can also be reversed. These estimations can indicate the CPE of the overlapped data subcarriers of their symbols, since CPE is identical over all the subcarriers. The

insertion of non-overlapping pilot tones enables the estimation of the respective CPE of the two source optical OFDM signals.

3.1.3 Experiments and simulations



(a)



(b)

Figure 3-3 (a) Experimental setup (b) DSP process.

Figure 3-3(a) depicts the experimental setup. The output of an external cavity laser (ECL) was split into two parts, one of which was adopted as the local oscillator of the coherent receiver. The other laser output was modulated by an optical IQ modulator, driven by the electrical signal from a Tektronix arbitrary waveform generator (AWG), operating at 10 Gsample/s. The offline generated OFDM samples were in FFT size of 256, of which 192 subcarriers were used as data subcarriers and 8 for pilot tones for satisfactory performance [89]. With polarization division multiplexing, the transmission baud rate of this system was 7.5 GBaud. A cyclic prefix (CP) of 8 samples was added. The output of the optical IQ modulator was then divided into two arms, the signal emulating N_1 was transmitted over a separate piece of 20-km single mode fiber (SMF), while the SMF emulating N_2 was 50 km in length. The path difference of 30 km was sufficient to reduce the coherency of the two signals and thus they were used to emulate two optical signals from two different optical sources. Each of these two optical signals was then amplified by its Erbium doped fiber amplifier (EDFA), before being polarization-controlled, via a polarization controller (PC), so as to keep the signal in one polarization state at the receiver. The signal power values of the two arms were controlled to be the same, via an optical variable attenuator (VOA) in one arm, so as to assure optimal operation performance and to facilitate evaluation of the penalty of the OPNC. After combining the output from the two arms, the composite OPNC signal was sent over 20-km SMF. Another EDFA was inserted to control the optical signal-to-noise ratio (OSNR). A portion of the OPNC signal was then fed into an optical spectrum analyzer (OSA) to monitor the OSNR, while the rest was fed into a

dual-polarization coherent receiver for detection. An optical bandpass filter (OBPF) with 0.88-nm bandwidth was inserted before the coherent receiver to filter out the out-of-band amplified spontaneous emission noise (ASE), since the coherent receiver was vulnerable to high power. The detected signal was sampled by a Tektronix real-time digital sampling analyzer (DSA). The three insets in Figure 3-3(a) showed the received electrical intensity waveforms after coherent detection of the outputs from the two individual arms, as well as the OPNC signal after transmission, respectively. The received data was decoded by offline digital signal processing (DSP) procedures, which were illustrated in Figure 3-3(b).

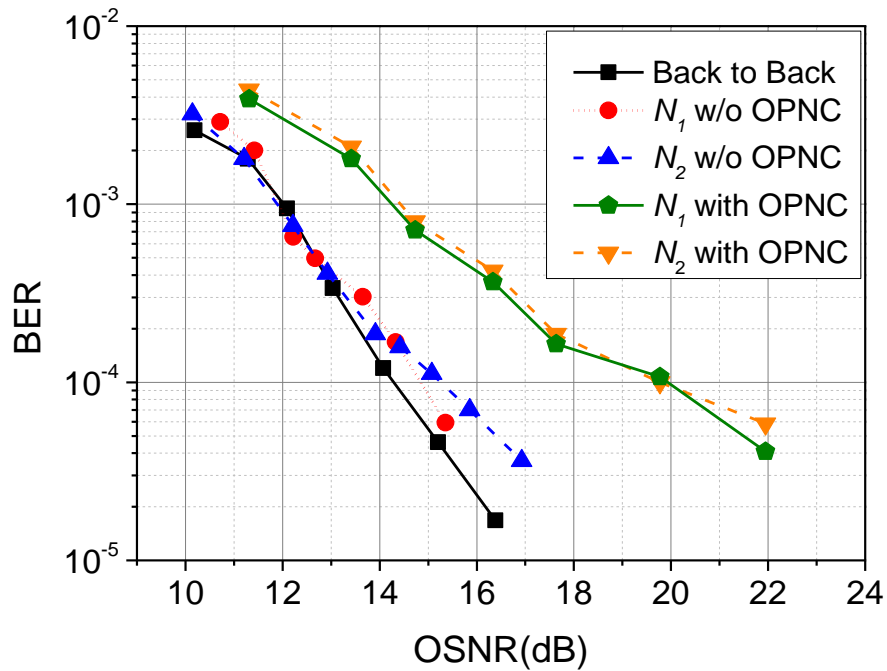
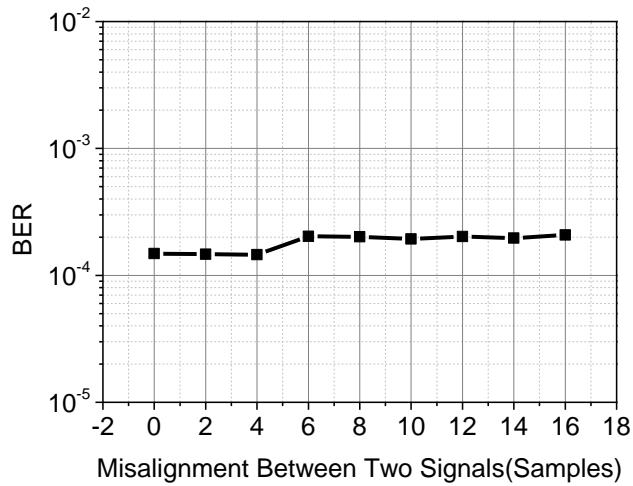
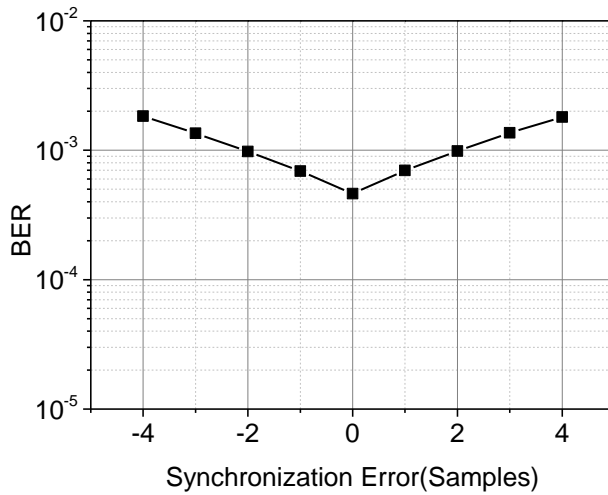


Figure 3-4 Experimental results showing the BER-OSNR relationships with and without OPNC.



(a)



(b)

Figure 3-5 Simulation results: (a) System performance as a function of the misalignment between two signals represented by the number of samples (b) System performance as a function of the synchronization error of decoded arm between two signals represented by the number of samples.

Figure 3-4 depicts the comparisons of the cases with and without OPNC in terms of the measured bit-error-rate (BER) of the OFDM frames versus their respective OSNR. The BER was calculated by counting the number of errors over 50 OFDM frames, each of which consisted of 4 training symbols for CFO estimation, 20 training

symbols for channel estimation and 400 data symbols. In particular, each OFDM data symbol consisted of 192 quadrature phase shift keying (QPSK) data samples. The actual transmission bit rate was 27.4 Gbit/s. It could be noticed that, at the BER around 10^{-3} , both of the OSNR penalties of OPNC at both arms were about 2 dB, which showed good feasibility of the OPNC decoding.

The reconstruction of one of the component signals was the key procedure in this scheme. Exact symbol alignment between the two signals is not necessary during the encoding and decoding process, which means that the system performance did not rely on the relative time shift between the two source signals. We have conducted numerical simulation in MATLAB to study BER performance under the influence of the relative time shift (in number of samples) between the two signals, and the results were depicted in Figure 3-5(a). It could be noticed that the timing misalignment between the two signals brought slight performance degradation to the decoded signal. Therefore, no stringent sample-level alignment between two code sources was mandatory in OPNC. This feature could largely relieve the constraint of the proposed scheme, and enhance its application in practical scenarios. In addition, the synchronization constraint of the OFDM signal was relieved by the insertion of CP. However, the system performance was actually affected by the synchronization error of the reconstructed signal, since possible imperfect reconstruction produced unintended samples acting as noise in the decoding and demodulation of the decoded signal. Another numerical simulation was also conducted to study the effect of synchronization errors, and the results were depicted in Figure 3-5(b). It could be seen

that a slight synchronization error, such as one sample, did not bring great influence to the system performance. When the synchronization error continued to increase, the performance started to degrade. Practically, the adoption of advanced synchronization methods could assure the synchronization error of the reconstructed signal in a moderate range, thus the system performance could be guaranteed. Besides, appropriate labels can be added to the header of the optical frames to identify the frames that have to be decoded.

3.1.4 Conclusion

In this section, we have experimentally demonstrated and characterized the application of OPNC in a CO-OFDM system. Individual OFDM frames are successfully separated and decoded at the destined receiver after the two source OFDM frames are optically combined in the immediate node. In the experiment, the OPNC achieved acceptable OSNR penalty and showed good feasibility of OPNC in coherent optical OFDM systems.

3.2 Physical-layer network coding for VPN in OFDM-PON supporting heterogeneous services

3.2.1 Introduction

Peer-to-peer (P2P) services are getting quite dominant in the broadband access arena. Bidirectional intra-PON P2P transmission, or virtual private network (VPN), are

attracting increasing interests [90]. In [64], a PNC based VPN in passive optical networks (PON) was demonstrated. A 100% improvement in the throughput of VPN was achieved with the adoption of PNC.

What's more, hybrid fiber-wireless (FiWi) technology have attracted much attention [91]. In FiWi systems, fiber communication services and wireless services overlay and inter-operate with each other. Numerous innovative schemes have been proposed to integrate wireless and wired services in access networks. A novel structure that supports both orthogonal frequency division multiplexing-based passive optical network (OFDM-PON) and wireless services has drawn great attention, which is referred as radio-over-fiber PON (RoF-PON) [92].

It has been discussed in 2.2 that PNC is a promising technology to improve system throughput in fiber optics communications. At the same time, PNC also holds the potential to improve system throughput in fiber wireless (Fi-Wi) [67]. This becomes quite important along with the fast development of Fi-Wi technology, which incorporates wired services and wireless services.

In this section, we investigate the application of PNC for simultaneously supporting wired and wireless VPN in a RoF-PON system, therefore paving the way for more flexible VPN configurations. Furthermore, compared to a conventional half-duplex VPN, the proposed PNC-based full-duplex VPN brings a considerable throughput improvement.

3.2.2 Principle of operation

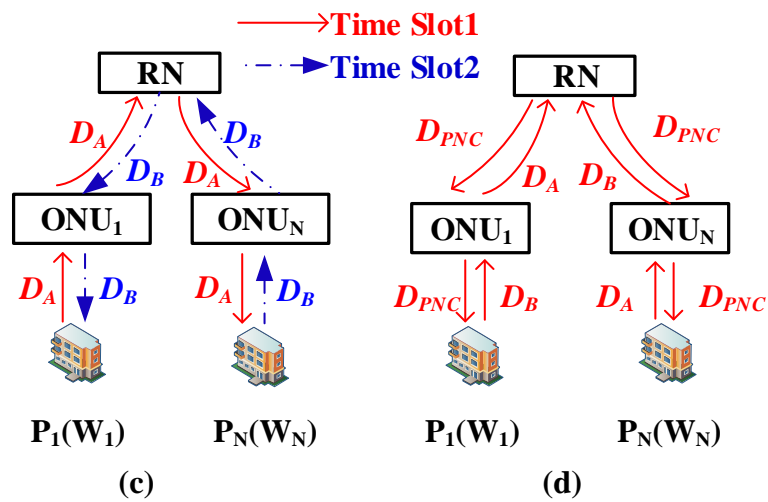
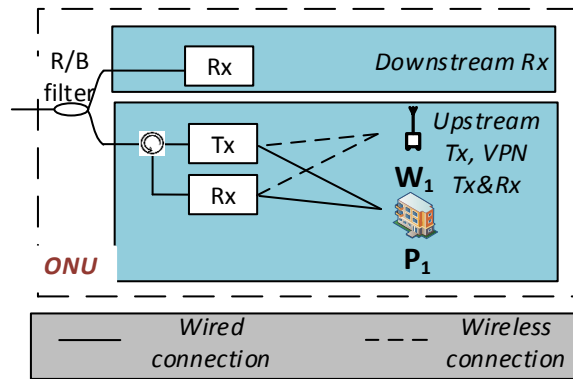
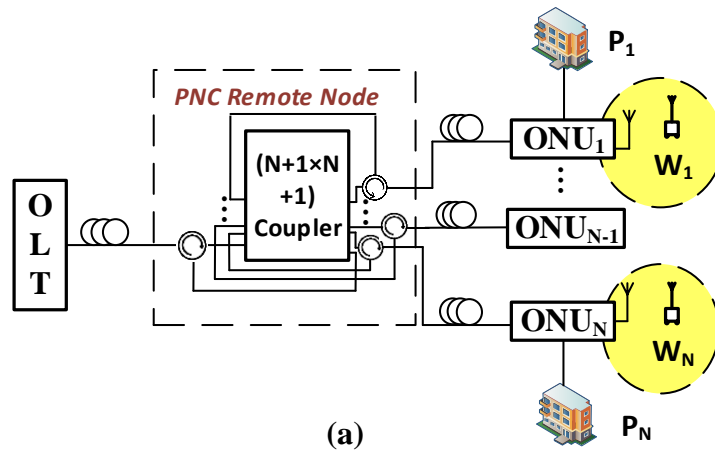


Figure 3-6 Schematic view of a RoF-PON supporting PNC-based VPN; (b) ONU configuration; (c)

non-PNC VPN data streams; (d) PNC VPN data streams.

Figure 3-6(a) shows a simplified architecture of the RoF-PON composed of N optical network units (ONUs). The ONUs as well as optical line terminal (OLT) are connected, via a specially designed remote node (RN), which connects the output ports of an $(N+1)\times(N+1)$ optical coupler to the port 1 of $(N+1)$ optical circulators, respectively. There are two kinds of users in RoF-PON: wired users (denoted by P) having access to the conventional OFDM-PON service and wireless users (denoted by W). For the OFDM-PON wired connections, wired user P_1 and P_n are connected to the ONU₁ and ONU_n, respectively. For the wireless services, the wireless user W_1 was served by ONU₁, and W_n is wirelessly covered by ONU_n.

The configuration of one ONU, ONU₁, is depicted Figure 3-6(b). The upstream and the downstream of the OFDM-PON here are full-duplex by adopting an optical red/blue filter. The wired data is modulated onto the subcarriers in a common OFDM modulation process, while the subcarriers that correspond to the frequencies of wireless services (wireless pipes) are left unoccupied. The wireless signal is received from the W_1 and combined with the OFDM-PON signal by an electric coupler [93].

Consider the wired VPN firstly. As is shown in Figure 3-6(c), a pair of VPN users ONU₁ and ONU_n exchange data in a bi-directional manner. In a conventional VPN setup, ONU₁ sends its data D_A to ONU_n in the first time slot and the transmission of D_B from ONU_n to ONU₁ is in the second time slot. The exchanging process is indeed half-duplex. By employing the proposed PNC scheme, full-duplex VPN is realized to halve the time consumed, as is depicted in Figure 3-6(d). ONU₁ and ONU_n

simultaneously transmit D_A and D_B . The signals are encoded at the RN by a simple combination. The encoded signal are then broadcasted to all ONUs and OLT. For the decoding process at ONU_1 , D_{PNC} is converted back into electrical signal. D_A is then subtracted from the encoded signal D_{OPNC} to retrieve D_B . D_B is similarly decoded at ONU_n . A 100% improvement in VPN throughput is achieved compared to conventional scheme. Compared to NC-based inter-ONU connection [94], the proposed PNC-based VPN bypasses the OLT to avoid the logical encoding operations, the workload and power consumption, and the storage occupation [64]. The PNC-based VPN in the wireless part resembles the wired part only with extra steps of wireless transmission and receiving.

As the PNC VPN data is merged into the upstream data which is broadcasted to all ONUs and OLT, VPN and upstream data can be transmitted simultaneously by allocating different subcarriers to different services. Furthermore, the proposed scheme can also support multiple VPN connections simultaneously. Different VPNs are assigned with different subcarriers, while the pair of users in a VPN load data on the common subcarriers. Hence, the proposed scheme is highly flexible.

3.2.3 Experimental setup

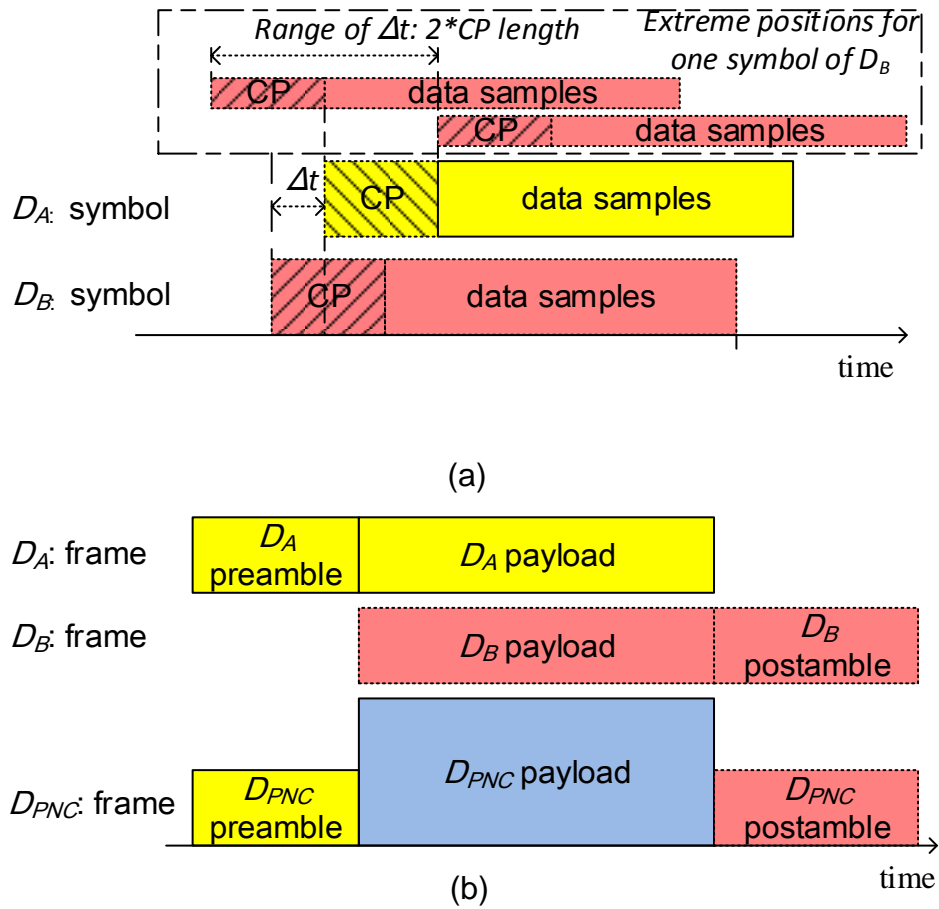


Figure 3-7 (a) Symbol-level synchronization, (b) frame structure.

We experimentally examined the feasibility of the proposed scheme. For OFDM signals, the decoding process is in the frequency domain. The PNC signal should be transformed into frequency domain before decoding. Therefore, the OFDM symbols of the two encoded signals should be synchronized. However, the insertion of cyclic prefix (CP) relieves this synchronization constraint to within-CP constraint [60], which is depicted in Figure 3-7(a). Figure 3-7(b) depicts the frame structure. The preamble and postamble were non-overlapping symbols for the channel estimation of D_A and D_B , respectively.

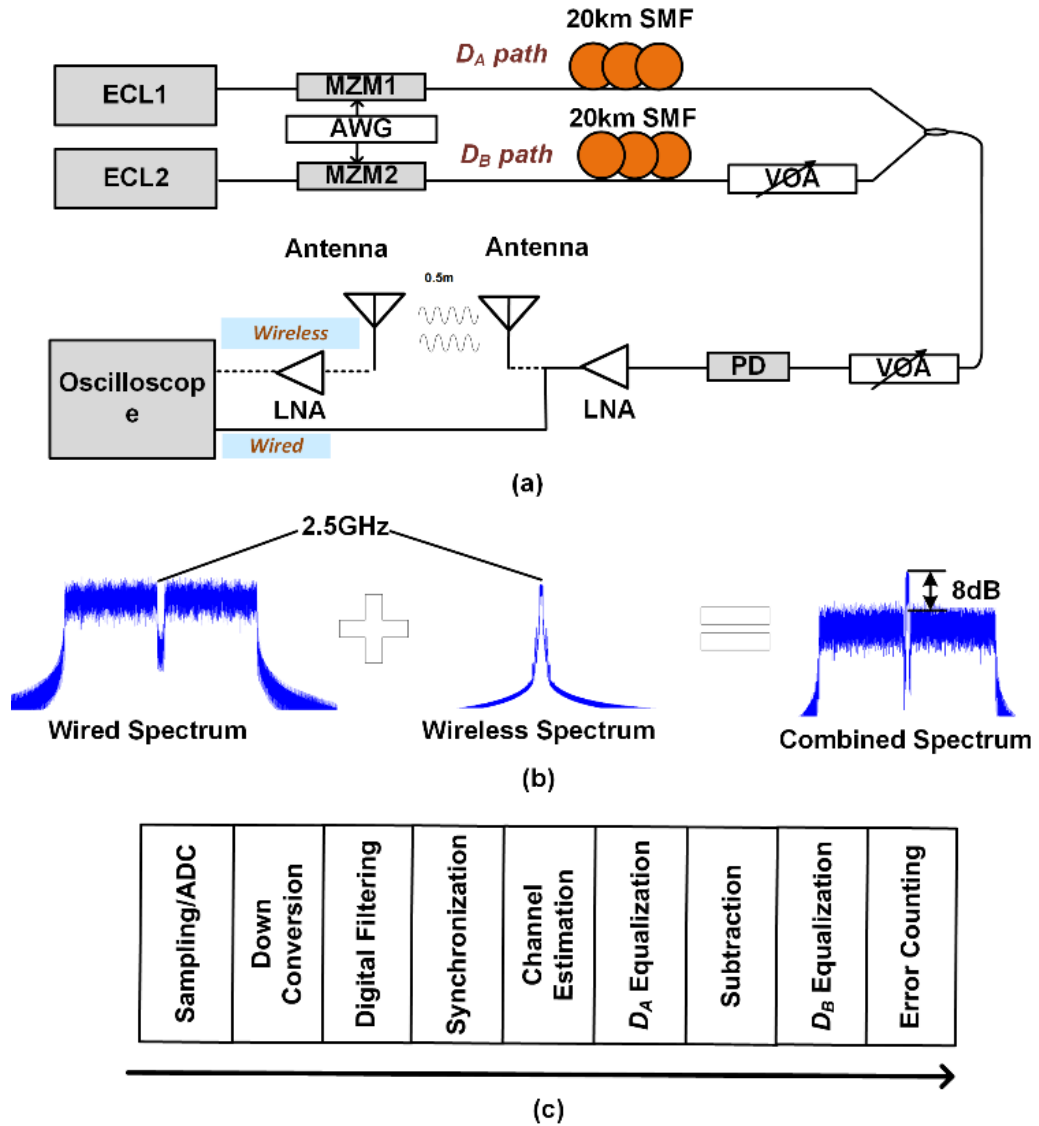
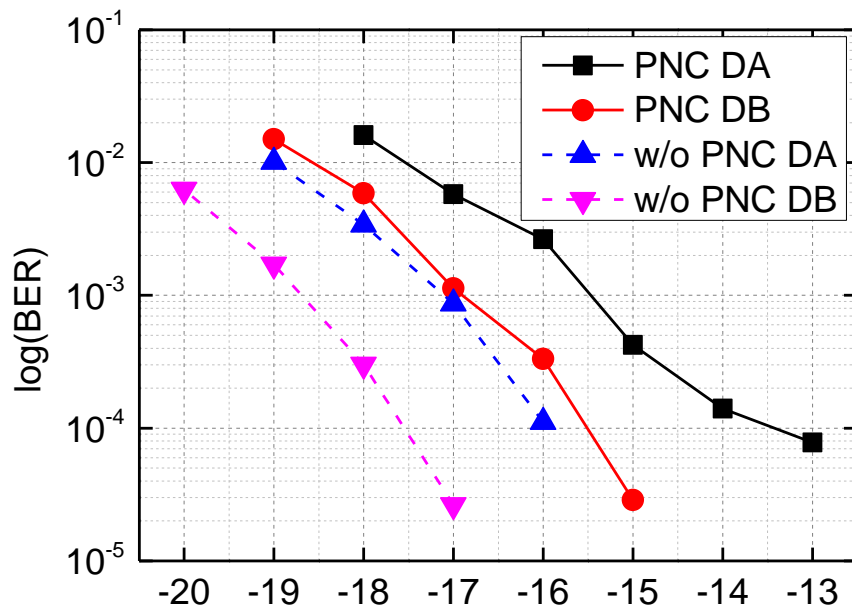


Figure 3-8 (a) Experimental setup, (b) Digital spectrum of the transmitted signal, (c) DSP procedures.

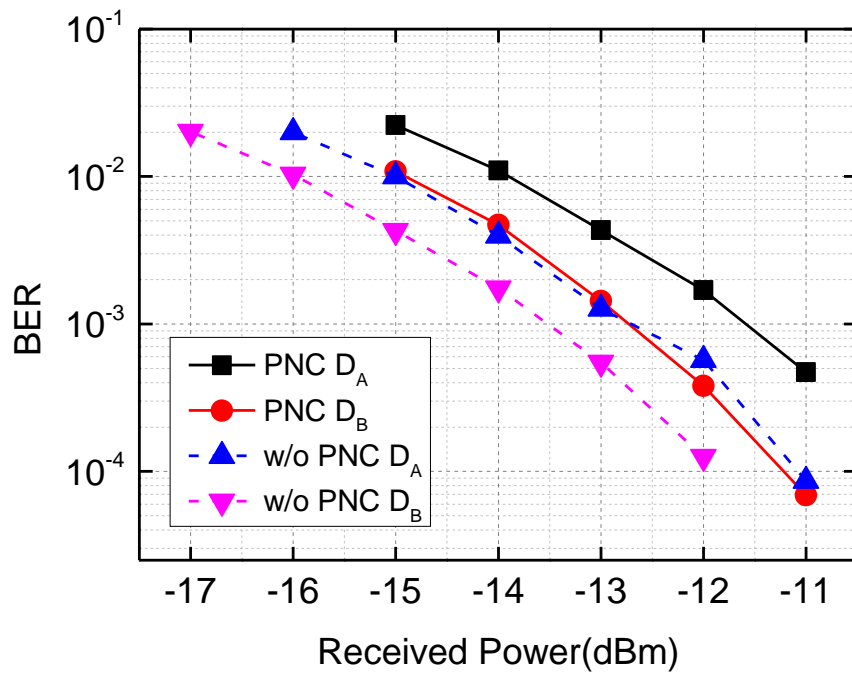
Figure 3-8(a) shows the experimental setup. For simplicity, the transmission process from wireless users to ONUs were omitted. The modulation formats of OFDM subcarriers in wired and wireless portions were both QPSK. The wired and wireless signals were generated and combined in MATLAB to emulate the electrical coupler. The offline generated signal were then output from an arbitrary waveform generator (AWG) working at 10 Gsample/s. For the wired part, the FFT size was 256, of which 128 subcarriers were adopted as data subcarriers. The inverse fast Fourier transform

(IFFT) transforms two ways of 5 Gsample/s QPSK data into two 5Gsample/s baseband complex signals. The complex signal was then digitally IQ-mixed [92] to 2.5 GHz radio frequency (RF) to form a 10 Gsample/s real-value band-pass signal. In each wired OFDM frame there was 500 symbols, including 10 symbols in preamble or postamble as training symbols for channel estimation, and 490 payload symbols. Overall, the wired signal was 2.37 Gbaud QPSK. For the wireless part, the FFT size and data subcarrier numbers were 256 and 128, respectively. Two ways of 50 Msample/s QPSK data were transformed into two time domain signals by IFFT. The baseband signal were then zero-order hold, digitally up-converted to 2.5 GHz and IQ-mixed to be a 10 Gsample/s signal. Each wireless frame contained 2 training symbols and 18 payload symbols. To converge wired and wireless signals, in the spectrum of the wired signals, the 5 subcarriers (one is DC in baseband) around 2.5 GHz were left blank for wireless pipes. The wireless data was 45 Mbaud QPSK. The wired and wireless signals were then combined in MATLAB. Figure 3-8(b) shows the spectrums of the wired, the wireless, and the combined signals.

Two wavelength channels from external cavity lasers (ECL) were individually modulated by two electrical signals from an AWG), via two respective Mach-Zehnder modulators (MZM). The wavelengths of ECL1 and ECL2 were 1550.00 nm and 1549.60nm, respectively, with a 50-GHz frequency difference, to avoid the optical beating interference (OBI). The two optical output signals were then fed into two pieces of single mode fibers (SMF) of lengths 20-km, respectively. A variable optical attenuators (VOA) was inserted to equalize the powers of the two signals. The signals



(a)



(b)

Figure 3-9 Experimental results: (a) Wired, (b) Wireless.

of the two paths were then combined by an optical coupler. A second VOA was then employed to control the input power to the photo diode (PD). The detected signal was then amplified by an electronic linear amplifier (LNA). The two paths with or without

a 0.5-m wireless transmission respectively correspond to the wireless or wired transmission. The received signal was sampled by an oscilloscope at 50 Gsample/s. After offline digital signal processing (DSP) and decoding, the BER was calculated by error counting. Figure 3-8 (c) shows the DSP process.

3.2.4 Experimental results and discussions

Figure 3-9 shows the experimental results. As the powers of D_A and D_B were identical, the received powers of PNC cases were 3-dB larger than those of non-PNC cases. This value has been deducted for fair comparisons. Figure 3-9(a) shows the experimental results of the wired part. It could be learnt from the figure that the power penalties at $\text{BER}=10^{-3}$ introduced by PNC to D_A and D_B were 1.5 dB and 1.7 dB, respectively. Figure 3-9 (b) shows the results of the wireless experiments. Only 0.8 dB and 1.1 dB received power penalties were observed as the cost of PNC at the BER level of 10^{-3} . It should be clarified that even we equalize the power of D_A and D_B , the modulation index and characteristics of the two MZMs were not identical, which would lead to the performance differences between D_A and D_B . Nevertheless, the experimental results have shown that the proposed PNC-based VPN structure brought moderate power penalties, yet led to drastic throughput improvement.

3.2.5 Conclusion

In this section, we have proposed and experimentally investigate the PNC-based VPN in a RoF-PON supporting heterogeneous services. The flexible VPN scheme can support wireless VPN and wired VPN simultaneously. The power penalties induced

by the coding process were quite moderate, while the system throughput is largely improved.

3.3 Physical-layer network coding in visible light communication

3.3.1 Introduction

Visible light communication (VLC) is an attractive optical wireless communication technology exploiting the information transmission potential of widely deployed commercial light-emitted diodes (LED), apart from their role of illumination. Benefitting from its high throughput, low cost, ease of integration with existing lighting facilities, and high security, VLC is expected to be a promising complement of wireless access system in future internet of things (IoT).

Unlike FOC, VLC transmits its signal in free space. The practical application and deployment of VLC, however, are limited by two drawbacks. First, as an informative transmitter, an LED's transmission range is short subject to its limited brightness, fast decay, and the divergence of light. Second, VLC largely relies on the accessibility of the line-of-sight (LoS) transmission; without LoS, the light signal that arrives the receiver will be very weak or even be blocked. Likewise, these drawbacks also exist in wireless communication technologies, especially for those whose carrier frequency is high, such as 60 GHz or beyond [95].

One easy but effective solution is relay. With the help of relay nodes, information

can reach farther, and bypass the blockages.

Relaying is a simple but effective solution to overcome the drawbacks. The relay technology can effectively extend the coverage of VLC and bypass the LoS obstacles, thus enables the deployment of large-scale VLC networks. Particularly, in the scenario of IoT, a lot of devices are deployed at different locations and communicate with each other. To communicate users who are out of each other's coverage or whose LoS transmission path is blocked, a relay, or even a set of multi-hop relays, is necessary. Two-way relay network supports bi-directional information exchange via the relay node. For a two-way-relay-assisted connection in VLC, the throughput is bottlenecked at the relay node thus improving the performance of two-way relay is crucial in VLC.

In this section, we present physical-layer network coded visible light communication (PNC-VLC), a visible light communication architecture that adopts physical-layer network coding (PNC) to boost the throughput of VLC networks. The idea of PNC, first proposed in 2006 [58], is to exploit network coding [56] at the physical layer.

As a novel interference-exploited physical layer network coding (PNC) scheme to improve the overall throughput, PNC has been successfully introduced into different scenarios, such as wireless communication [60], direct detected optical communication [64], and coherent optical communication [66]. In the simplest PNC-VLC setup, two nodes (equipped with LED and PD) exchange information via a relay in a two-way relay network (TWRN). The two nodes first transmit their messages

simultaneously to the relay; the relay then maps the overlapped signals to a network-coded message and broadcasts it to the two nodes; and each of the two nodes retrieve the message from the other node based on the network-coded message and the knowledge of its own message.

Our PNC-VLC is the first work that employs physical-layer network coding method to boost the throughput of visible light communication networks. The main contributions of this work includes:

- (a) First, to the best of our current knowledge, this is the first work that introduces PNC into VLC to improve the network throughput. This is also the first work that applies finite-set PNC (PNCF) in optical communications.
- (b) Second, we designed both the MAC and PHY layers of the proposed VL-PNC system. Furthermore, we experimentally demonstrated a quadrature phase-shift keying (QPSK) modulated PNC, which is seldom realized in other PNC studies.
- (c) Third, we designed a phase-aligned method to improve the performance of PNC. Our new method achieved a significant BER performance improvement and makes PNC feasible to use in practical VLC systems.

3.3.2 System model

In this section, we first explain the principle of physical-layer network coding. We then introduce the physical-layer (PHY) design of the PNC-VLC. Finally, we present our

beacon-triggered MAC protocol designed for PNC-VLC system.

3.3.2.1 Physical-Layer Network Coding in Visible Light Communication

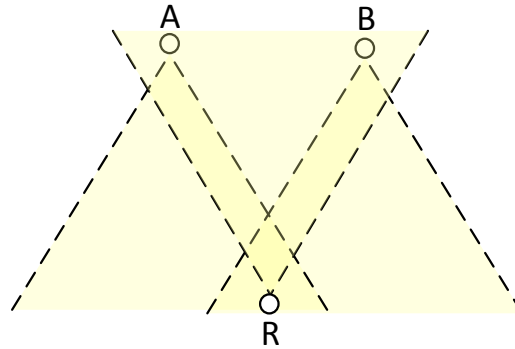
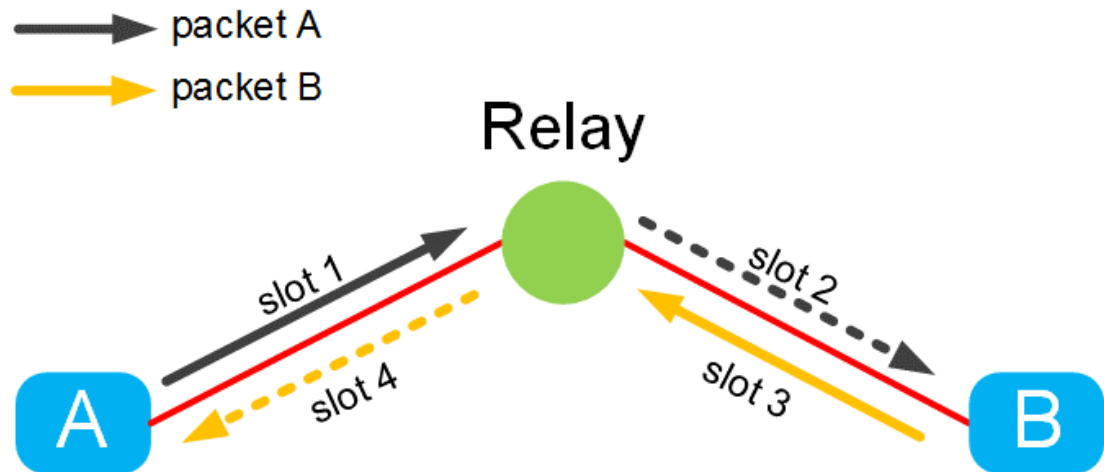


Figure 3-10 A two-way relay VLC network

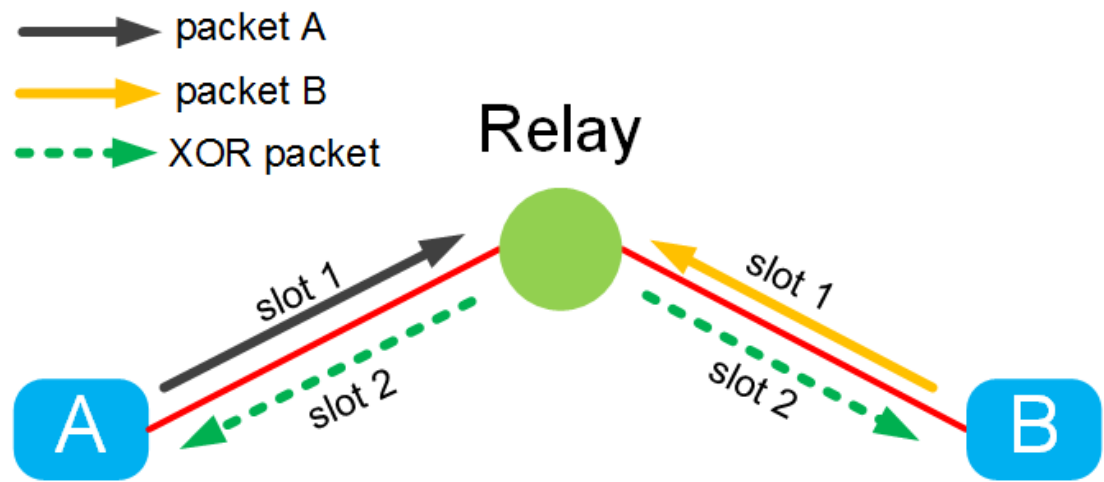
As shown in Figure 3-10, bi-directional information exchange is a common communication pattern in visible light communication which is hindered by short transmission range and LoS transceiving. In this scenario, the main challenge is how to speed up the bi-directional information exchange of the two-way relay. For example, the two end nodes (node A and node B) exchange a pair of packets with each other via a relay node. Nodes A, B, and R are all VLC transceivers, each equipped with an LED as the transmitter and a photodiode (PD) as the receiver. Both node A and node B can communicate with node R, but node A and B cannot communicate with each other directly. Therefore, the communication between A and B must be relayed by R. The system model can be abstracted to a widely recognized PNC model in Figure 3-11(a), where node A and node B exchange a pair of packets P_A and P_B through the relay R.

As shown in Figure 3-11(a), conventional two-way relay method takes four time slots to exchange two packets between nodes A and B, one in each direction.

Conventionally, A and B need four time slots (TS) to exchange their respective packet P_A and P_B via R. As depicted in Figure 3-11(a), in the first TS, A transmits P_A to R; in the second TS, R forwards P_A to B; in the third TS, B transmits P_B to R; in the fourth TS, R forwards P_B to A.



(a) Conventional bi-directional relay



(b) PNC-VLC

Figure 3-11 Two end nodes exchange a pair of packets via the relay node in the visible light communication network: (a) the conventional VLC bi-directional relay takes four time slots; (b) the PNC-VLC only takes two time slots

In our PNC-VLC system shown in Figure 3-11(b), node A and node B transmit their

packets simultaneously to the relay node in the first slot. The relay node receives an overlapped signal of packet A and packet B. The relay node then decodes the overlapped signal into the XOR of packet A and packet B using the PNC decoding algorithm, which will be elaborated in Section 3.3.3. In the second slot, the relay node broadcasts the XOR packet to both the end nodes. Each of the two end nodes then retrieves the packet from the other node based on the XOR packet and the knowledge of its own packet. In all, the VL-PNC system takes only two time slots to exchange a pair of packets, thus improves the net throughput by 100% compared with conventional relay method.

The VLC channel is similar to wireless communication channel that suffers frequency selectivity. To enable reliable communication, we design the physical-layer (PHY) of our PNC-VLC based on the widely used orthogonal frequency division multiplexing (OFDM) modulation technique to counter the frequency-selective channel.

In PNC-VLC, the packet exchange in VL-PNC consists of two phases: multiple access phase and broadcast phase. Each phase takes one time slot. In the first time slot, node A and node B modulate their source packets into OFDM signals. We denote the source packets of node A and node B by two binary sequences

$$U^i = (u_1^i, u_2^i, \dots, u_L^i), \quad i \in \{A, B\}, \quad (3.15)$$

where L is the length of the binary sequence and u_l^i is the l -th input bit of end node i 's source packet.

Next, U^A and U^B are fed into their respective OFDM modulator to produce the

two sequences of baseband complex symbols. We focus on BPSK mapping throughout this paper, but our framework can be easily extended to higher order constellations). Let \mathbf{X}^i denote the node i 's frequency-domain signals after BPSK mapping, and $X_{k,n}^i$ denote the n -th sample of \mathbf{X}^i on the k -th subcarrier. Hence the transmitted frequency-domain signals are

$$\mathbf{X}^i = \begin{bmatrix} X_{1,1}^i & X_{1,2}^i & \cdots & X_{1,N}^i \\ X_{2,1}^i & \ddots & & \\ \vdots & & \ddots & \vdots \\ X_{K,1}^i & & \cdots & X_{K,N}^i \end{bmatrix}, i \in \{A, B\}. \quad (3.16)$$

After the BPSK mapping, we perform IFFT on \mathbf{X}^i to produce the time-domain OFDM symbols and append cyclic prefix (CP) to each OFDM symbol. These symbols are then intensity-modulated and transmitted to the relay via the LEDs.

Upon receiving the time-domain overlapped signal from node A and node B, the relay node removes the CP and performs FFT to obtain the frequency-domain signal \mathbf{Y}^R . The relay node then demaps the frequency-domain signal to produce the XOR source packet U^R that is an estimate of $U^A \oplus U^B$. This demapping process will be elaborated in Section 3.3.3. In the second time slot, the relay node broadcasts U^R to both the end nodes using the conventional VLC transmission.

3.3.2.2 VL-PNC frame format and medium access control method

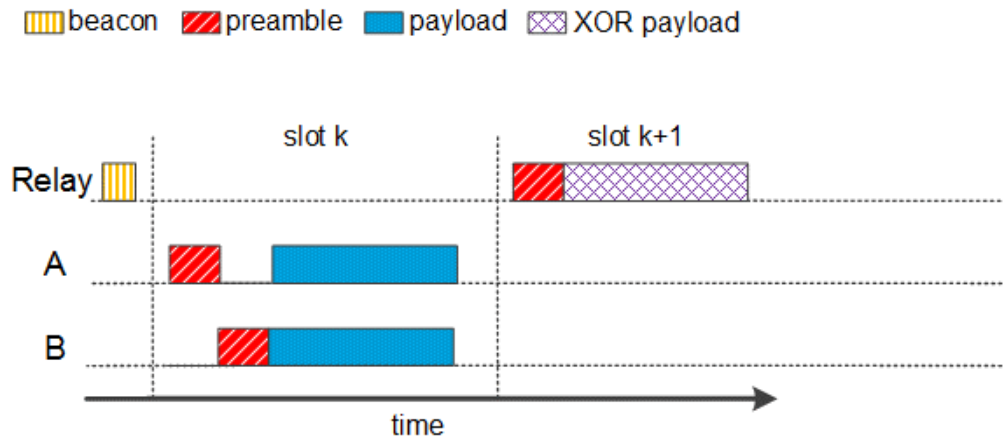


Figure 3-12 The media access control (MAC) procedure of the PNC-VLC

In this work, we focus our medium access control (MAC) design for the two-way relay communication pattern as shown in Figure 3-11(a) and leave the investigation of multiple-node PNC for future work. The PNC-VLC frame includes preamble and payload. The preamble is used by the receiver to estimate the channel state information (CSI) and do packet detection and synchronization.

We let node A and node B employ orthogonal preambles, allowing the relay node to estimate the CSI between itself and node A/B separately. Practically, we can insert a sequence of zeros after node A's preamble and also before node B's preamble, therefore the preambles of node A and node B are non-overlapping (orthogonal).

The MAC protocol design is shown in Figure 3-12. The goal of our MAC protocol design is to enable the two end nodes to transmit simultaneously to the relay node in the first time slot. So we let the relay node broadcast a beacon signal to trigger the simultaneous transmission of the end nodes. In a practical system, the relay node

broadcasts a beacon to all the end nodes to initialize the information interchange. Upon receiving the beacon signal, end nodes A and B transmit their packets simultaneously in the next time slot. Note that in the following time slot, the beacon can be piggy-backed with the broadcasted packet. Also note that the two packets from node A and B may not arrive at the relay node precisely at the same moment, due to imperfect time synchronization (i.e., node A and node B have different processing delay and transmission delay). This time asynchrony, however, can be countered by the OFDM modulation as long as it is less than the CP duration.

Upon receiving the overlapped packet, the relay first estimates the CSIs of node A's and node B's channel using the orthogonal preambles, respectively. Then the relay node decodes the overlapped payload into the XOR payload using PNC decoding explained in the next section. In the second time slot, the relay node broadcasts the XOR payload $U^R = U^A \oplus U^B$ to both the end nodes using conventional VLC transmission. After receiving the broadcasted packet U^R , node A retrieves the source packet U^B from node B by XORing U^R with its own packet U^A . In the same way, node B can also retrieve node A's source packet U^A .

3.3.3 Decoding algorithm of physical-layer network coding

This section explain the PNC demapping algorithm used at the relay node to map the received overlapped packet into the XOR packet. We first show the mathematical representation of the received overlapped signal, and then explain how to map the

overlapped signal into the XOR of source packets.

3.3.3.1 Baseband signal received by the relay node

In this section, we focus on the signal processing at the relay node. First, the overlapped packet is detected and received by the relay node, and the relay down-convert the signal back to basebands. Based on the orthogonal preamble designed described in the previous section, the relay node can estimate the CSI between itself and node A/B, respectively. After removing the CP of each OFDM symbol in the payload part, the relay node performs FFT on the overlapped symbols and obtains the frequency-domain baseband signal \mathbf{Y}^R . Let $Y_{k,n}^R$ denotes the n -th sample on the k -th subcarrier of \mathbf{Y}^R , hence

$$\mathbf{Y}^R = \begin{bmatrix} Y_{1,1}^R & Y_{1,2}^R & \cdots & Y_{1,N}^R \\ Y_{2,1}^R & \ddots & & \\ \vdots & & \ddots & \vdots \\ Y_{K,1}^R & & \cdots & Y_{K,N}^R \end{bmatrix}. \quad (3.17)$$

Specifically, each term in (3.17), the baseband signal received by the relay, is an overlapped signal

$$Y_{k,n}^R = h_k^A X_{k,n}^A + h_k^B X_{k,n}^B + w_{k,n}^R, \quad (3.18)$$

where $X_{k,n}^i$ denotes the n -th sample on the k -th subcarrier of \mathbf{X}^i , the transmitted signal from node I in frequency domain. The channel coefficients of the k -th subcarrier channels from node A and node B to the relay node are represented by h_k^A and h_k^B , respectively. The term $w_{k,n}^R$ is the Gaussian noise on the k -th subcarrier with variance σ^2 .

In the VL-PNC system model, both h_k^A and h_k^B are complex numbers. We denote the relative phase difference between h_k^A and h_k^B by $\phi_k = \angle(h_k^B / h_k^A)$ on the k -th subcarrier. In our system design and experiments, we do not assume perfect channel estimation, since the channel coefficients are obtained by using the orthogonal preamble as described in Section 3.3.2. A further study on the impact of channel estimation errors will be conducted in our future work.

3.3.3.2 XOR mapping of physical-layer network coding

This section explains the XOR mapping algorithm employed by the relay node to decode the overlapped packet. In VL-PNC, the key signal-processing step at the relay is to map the overlapped packet \mathbf{Y}^R into the XOR packet \mathbf{X}^R using the binary XOR rule. Upon receiving the overlapped packet, the XOR mapping module at the relay node first compute the likelihood of the signal $X_{k,n}^A, X_{k,n}^B$

$$\Pr(Y_{k,n}^R | X_{k,n}^A, X_{k,n}^B) = \frac{1}{\sqrt{2\pi\sigma^2}} \exp\left\{-\frac{|Y_{k,n}^R - h_k^A X_{k,n}^A - h_k^B X_{k,n}^B|^2}{2\sigma^2}\right\}. \quad (3.19)$$

The relay then calculates $\Pr(Y_{k,n}^R | X_{k,n}^R)$, the likelihood of the XORed bit $X_{k,n}^R$, based on the probability in Equation (3.19), and decodes the XORed bit by maximizing the likelihood function

$$\begin{aligned} \hat{X}_{k,n}^R &= \max_{X_{k,n}^R} \Pr(Y_{k,n}^R | X_{k,n}^R) \\ &= \max_{X_{k,n}^R} \sum_{X_{k,n}^A, X_{k,n}^B: X_{k,n}^A \oplus X_{k,n}^B = X_{k,n}^R} \Pr(Y_{k,n}^R | X_{k,n}^R). \end{aligned} \quad (3.20)$$

where $\hat{X}_{k,n}^R$ is the decoding output of the XOR mapping algorithm. After the XOR mapping, the relay node obtains $\mathbf{X}^R = \mathbf{X}^A \oplus \mathbf{X}^B$, which is the the bit-by-bit XOR of

packet A and packet B.

In the second time slot of VL-PNC, the relay node broadcasts the XOR packet \mathbf{X}^R to both node A and node B, using the conventional point-to-point VLC transmission. After receiving the XOR packet, node A can simply retrieve node B's packet by XOR \mathbf{X}^R with its own transmitted packet

$$\mathbf{X}^A \oplus \mathbf{X}^R = \mathbf{X}^A \oplus (\mathbf{X}^A \oplus \mathbf{X}^B) = \mathbf{X}^B. \quad (3.21)$$

Similarly, node B can also retrieve node A's packet using the same method.

3.3.4 Phase-aligned physical-layer network coding

In the first time slot of PNC-VLC, the relay's received signal has a singular constellation map which is the overlapping of the constellation of node A and node B. However, the overlapped constellation, due to the phase difference between the channel coefficients of the two end nodes, may not have the optimal constellation point layout and sometimes even causes decoding failure [59]. In this section, we describe our phase pre-distortion method for PNC-VLC to align the constellation of end node A and B so that their overlapped constellation achieves good decoding performance.

In PNC-VLC, we perform per subcarrier PNC decoding and the decoding algorithm is expressed in Equation (3.21). In this decoding method, we classify the points of the overlapped constellation (in total 16 points) into four groups based on their XOR value. Let $X_{k,n}^{XOR}$ denotes the center point of the constellation points group that has the same XOR value, Equation (3.20) can be expressed as

$$\hat{X}_{k,n}^R = \max_{X_{k,n}^{XOR}} \Pr(Y_{k,n}^R | X_{k,n}^{XOR}) = \frac{1}{\sqrt{2\pi\sigma^2}} \exp\left\{-\frac{|Y_{k,n}^R - X_{k,n}^{XOR}|^2}{2\sigma^2}\right\} \quad (3.22)$$

Therefore, the BER of this decoding algorithm is bounded by

$$P_e \leq (M-1)Q\left(\frac{d_{min}}{\sqrt{2N_0}}\right) \quad (3.23)$$

where M is the number of the constellation points of the composite overlapped signal ($M=16$ here), N_0 is the single-sided power spectrum density of the noise; d_{min} is the minimum distance between any pair of constellation points that belongs to different XOR group.

In VL-PNC, in which QPSK is used for both end nodes, the minimum distance is

$$\begin{aligned} d_{min} &= \sqrt{2}|h_k^A - h_k^B| \\ &= \min\left\{1 - \frac{1}{e^{j\varphi}}\right\}, -\pi/4 < \varphi \leq 0 \end{aligned} \quad (3.24)$$

where $\phi_k = \angle(h_k^B / h_k^A)$ is the phase offset between the two end nodes' channel coefficients. As the constellation here is centro-symmetric, we only consider the range $\varphi \in (-\frac{\pi}{4}, 0]$. The maximum of d_{min} is achieved when φ is zeros, meaning that best BER performance is achieved when the constellation of node A and node B are aligned. In the next section, we present our method to align the phase of the two end nodes' constellation using the channel state information measured at the relay node.

3.3.5 Experiments

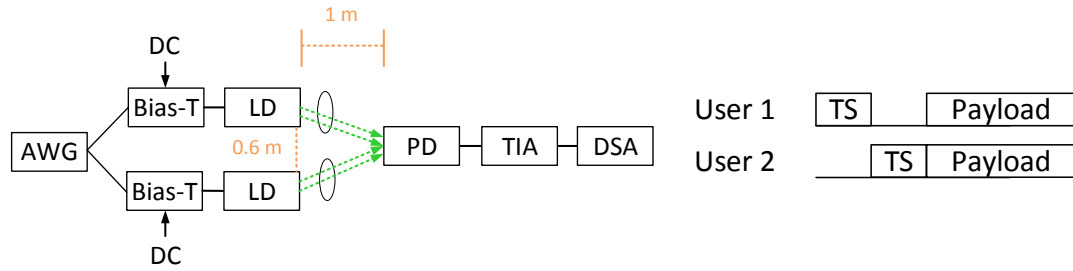


Figure 3-13 (a) Experimental Setup; (b) Frame structure

3.3.5.1 Experimental setup

Figure 3-13(a) depicts our experimental setup. The transmitted data samples were offline generated using MATLAB and then fed to an arbitrary waveform generator (AWG). The two output electrical signals were for A and B. The two signals were discrete current (DC) biased by bias-tees and fed to two laser diodes (LDs) to generate modulated optical signals. Two pairs of lenses were used to focus the light beams to a common PD, which was 1-m away from both LDs. After the optical-to-electrical conversion by the PD, the electrical signal was then amplified by a trans-impedance amplifier (TIA) and captured by a digital storage scope (DSC). The captured samples were then offline processed by MATLAB.

The non-phase-aligned PNC (non-PA-PNC) consists only one transmission. As the channel state information (CSI) of A and B should be estimated individually, the training sequences (TS) of A and B should not be overlapping. Hence, we designed the frame structure shown in Figure 3-13(b).

In phase-matched PNC (PA-PNC), the process was two-step. In the first step, a TS was generated and sent over the whole system to estimate the CSI. The CSI was then used to pre-distort the phase of the payload signals. In the second step, the phase pre-distorted signals were transmitted in the system. The BER was measured by counting error numbers of 200 frames, each composed of 240 payload OFDM symbols.

3.3.5.2 Results and discussions

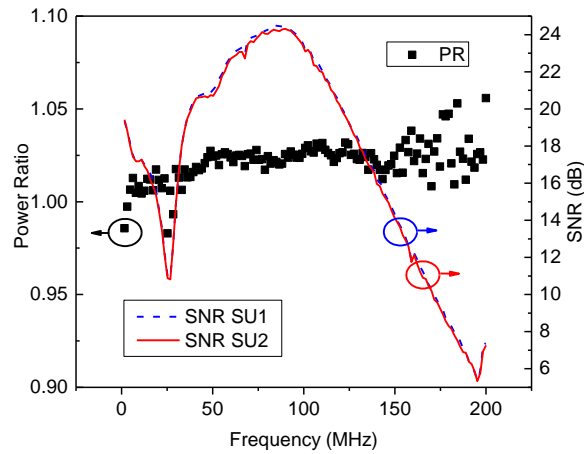


Figure 3-14 SNR and power ratio (PR) of the two users, AWG sampling rate at 400 MSa/s

We first set the power ratio (PR) of the two users to 1, and the sampling rate of AWG to 400 MSa/s. Figure 3-14 shows the SNRs and the PRs of the two users on different subcarriers with different frequencies. It could be observed that as the frequency increased, the SNR firstly dropped to 10 dB at a frequency of about 28 MHz. Then the SNR increased drastically to the peak value of about 24 dB at 100 MHz, and decreased thereafter.

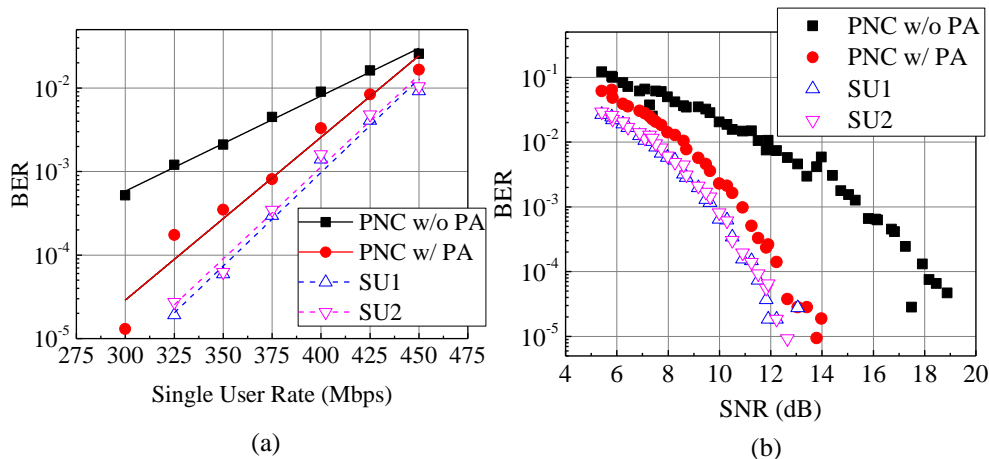


Figure 3-15 Experimental results: (a) BER vs. single user data rate; (b) BER vs. SNR. PA: phase align.

Figure 3-15(a) depicts the measured BER with regard to different single user rate, which was controlled by the sampling rate of AWG. As can be seen from the figure, the PNC scheme with phase alignment reached a BER of 3.8×10^{-3} at 400 Mbps, while the non-PNC scheme could transmit at 425 Mbps with a similar BER. Consider that the transmission time of the PNC scheme is only a half of the non-PNC scheme, the throughput improvement achieved by adopting PNC is about $(400 - 212.5) / 212.5 = 88.23\%$. Besides, the throughput improvement brought by non-PA-PNC was about 71.43%, compared to the non-PNC scheme.

We also compare the BER performance of the PNC scheme to the non-PNC scheme with regard to the SNR. As is shown in Figure 3-15(b), the SNR penalty induced by the adoption of PA-PNC at 3.8×10^{-3} was about 1 dB, which was quite moderate, considering the great improvement achieved by PNC. Besides, the PA-PNC showed a remarkable SNR reduction of 4 dB compared to the non-PA-PNC, at a BER of 3.8×10^{-3} .

3.3.6 Conclusion

We have proposed PNC in VLC as well as a phase-matching method. The feasibility of the proposed scheme is verified by theoretical and experimental studies. An 88.23% improvement in throughput was brought by the adoption of PNC, compared to the non-PNC scheme. What's more, a 4-dB reduction in the required SNR to reach a BER of 3.8×10^{-3} was realized by the adoption of phase alignment. Moreover, the SNR penalty induced by the adoption of PA-PNC was only 1 dB at a BER of 3.8×10^{-3} .

Chapter 4 Non-Orthogonal Multiple Access in Optical Communications

4.1 Introduction

4.1.1 Background

As has been introduced in Section 2.3.4, NOMA has been recently introduced into optical communications, especially in VLC, in [85-87]. Numerical studies have been conducted on the feasibility and some practical issues of NOMA in VLC.

It is claimed in [85] that NOMA was quite suitable for VLC, with the main advantages as below:

- The detection of signals in VLC is related to the receiving power at PD. This is directly related to the concept of power domain multiplexing, or NOMA.
- VLC service is limited to small cells with multiple end users. The transmission loss of VLC is very high due to the nature of illuminative lights from LED. This leads to serious near-far effect, which is exactly the basis of NOMA.
- The decoding of NOMA adopts successive interference (SIC), which relies on the channel state information (CSI) of NOMA end users. Compared to wireless communication, VLC is more stationary and deterministic, thus

being quite suitable for NOMA.

- The receiving powers of different NOMA end users can be changed by the transmission angle of LED as well as the field of view (FOV) of PD. Therefore, the performance of NOMA could be optimized.

In the recent few years, NOMA in wireless communications has drawn great interest, with numerous publications [81-84]. Its counterpart in VLC, however, has just begun drawing researchers' attention.

4.1.2 MUD methods

Appropriate multiuser detection (MUD) method is necessary in NOMA to distinguish and decode multiple signals from the interfered signal.

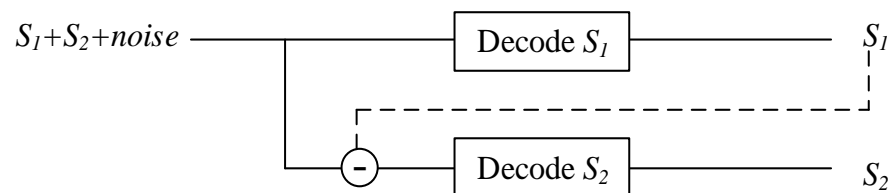


Figure 4-1 Successive interference cancellation process of a two-user NOMA.

Almost all previous NOMA implementations adopt successive interference cancellation (SIC). An illustration of SIC process of a two-user NOMA is depicted in Figure 4-1. In SIC, the signals are detected in the order of descending power. Assume a two-user-system, in which the signal of the 1st user is stronger in power than the signal of the 2nd user. SIC detector firstly detects the symbols for the 1st user, S_1 , treating the signal for the 2nd user as noise. Then, the signal for the 1st user is reconstructed and subtracted from the complex signal, on the basis of the detected S_1 .

Then, the symbols for the 2nd user, S_2 , is detected from the residual signal.

It should be noted that SIC can be applied in an iterative way. As long as there the symbols are channel-coded, the gain brought by channel coding in each iteration can improve the system performance [74,96].

Another well-known MUD method is joint detection (JD). Specially, in a two-user NOMA, joint detection detects the signals of two users jointly in one step, instead of two steps in SIC. The application of JD in NOMA has been reported before [97], with an increase of channel capacity in NOMA, compared to SIC.

4.2 Non-orthogonal multiple access in visible light communication with successive interference cancellation and phase pre-distortion

4.2.1 Introduction

As has been introduced, NOMA is a promising multiple access technology in VLC. Previous studies in [85-87] demonstrated NOMA in VLC theoretically and numerically. So far to the author's knowledge, there has been no experimental study on this topic.

One problem arose in these previous studies that the performance of NOMA largely depends on the power ratio of multiple access users. For instance, it was discovered in [86] that in a two-user NOMA system, the outage probability drastically increased when the power ratio reached a threshold. The stringent power ratio constraint severely limits the practicality of NOMA. How to relieve the required power

ratio, or how to decrease the BER in a poor power ratio, is still unexplored. In this section, we demonstrate a novel phase pre-distortion method for NOMA in VLC. By theoretical and experimental studies, it is unveiled that by pre-distorting the transmitted signals from NOMA users, the BER performance for NOMA under both low and high relative power ratios can be improved. Specifically, at low relative power ratios, the proposed method can eliminate the possible BER floors and alleviate the power ratio requirement by 2 dB at the BER of 3.8×10^{-3} .

4.2.2 System model

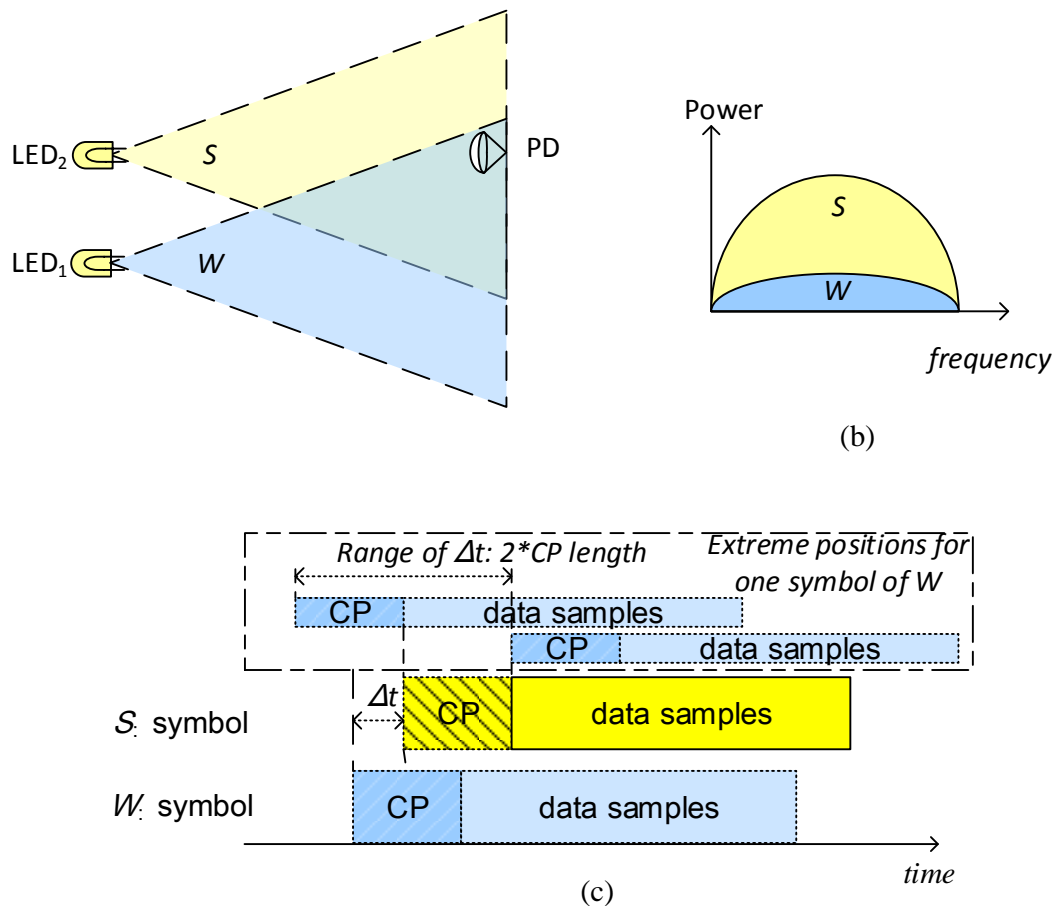


Figure 4-2 (a) System model for the non-orthogonal multiple access in visible light communication;

(b) power levels of S and W; (c) asynchrony in NOMA.

Figure 4-2(a) depicts a typical VLC system supporting NOMA. Two light emitting diodes (LEDs), namely LED₁ and LED₂, are employed as the optical-wireless transmitters for providing VLC services to their illuminated areas, in which there is a slight overlap between them. A photodiode (PD) is placed at the center of the illuminated region of LED₂, but at the edge of the illuminated region of LED₁, and thus it receives a stronger signal S from LED₂ but a weaker signal W from LED₁, simultaneously, forming a composite signal C . The powers of S and W are shown in Figure 4-2(b). For each of the signals S and W , orthogonal frequency division multiplexing (OFDM) signal format is employed, in which its transmission band is divided into N subcarriers. Since the OFDM signal is intensity modulating the LED, the two sidebands of a real-value signal are Hermitian symmetric in frequency-domain. The n^{th} time-domain sample in one OFDM symbol is [37]

$$y(n) = \sum_{k=0}^{N-1} \left(X(k) \cdot e^{j2\pi \frac{kn}{N}} \right), \quad \text{for } 0 \leq n \leq N \quad (4.1)$$

$$X(k) = X^*(N-k)$$

where $X(k)$ is the frequency-domain symbol on the k^{th} subcarrier, and $X^*(k)$ denotes its complex conjugate. Conventionally, OFDM is implemented by *inverse fast Fourier transform* (IFFT) \mathcal{F}^{-1} , which can be expressed as

$$y(n) = \mathcal{F}^{-1} \{ X(k) \} \quad (4.2)$$

In practice, signals S and W may arrive at PD with a time asynchrony. The asynchrony is due to the practical implementation of the VLC system, such as different transmission time, different hardware processing time, different transmission distances,

and multipath effect. Fortunately, this stringent synchrony constraint could be relaxed by appending cyclic prefix (CP) to each OFDM symbol, which is a common practice in OFDMA. As illustrated in Figure 4-2(c), time asynchrony within the CP length can be accommodated.

Assume the misalignment between S and W is m samples (m is not necessarily an integer), the signal C has been synchronized and we cut down CP with respect to the frame duration of signal S . Denote the signals S and W , as well as the composite signal C by subscripts s , w , and c , respectively, the n^{th} sample in one symbol of the signal C received at PD, is given by

$$y_c(n) = y_s(n) * h_s(n) + y_w(n+m) * h_w(n) + w \quad (4.3)$$

where the symbol $*$ stands for convolution operation; $h_s(\cdot)$ and $h_w(\cdot)$ are the time-domain channel impulse responses between LED₁ and PD, as well as that between LED₂ and PD, respectively; w is the additive white Gaussian noise (AWGN). After *fast Fourier transform* (FFT), denoted by \mathcal{F} , on both sides, (3) becomes

$$\begin{aligned} Y_c(k) &= \mathcal{F}\{y_c(n)\} \\ &= X_s(k) \cdot H_s(k) + X_w(k) \cdot H_w(k) \cdot e^{j2\pi\frac{mk}{N}} + w'(k) \end{aligned} \quad (4.4)$$

where $H_s(k)$ and $H_w(k)$ are the respective frequency domain channel responses on the k^{th} subcarrier of S and W ; $w'(k)$ is the noise on the k^{th} subcarrier of the received signal at PD.

Upon receiving the overlapped signal C in time domain y_c , PD estimates the channel coefficients H_s and H_w using the training sequences in the frame. After

recovering Y_c by FFT, successive interference cancellation (SIC) is employed to detect the individual signals sent from LED₁ and LED₂. The SIC process consists of two steps: (1) the strong signal X_s is decoded while treating the weak signal component, $X_w \cdot H_w$, as noise; (2) the term $X_s \cdot H_s$ is reconstructed and subtracted from Y_c before the weak signal X_w is decoded.

4.2.3 SIC-based NOMA with phase pre-distortion in NOMA

Owing to the two-step decoding property of SIC, any decoding error in step (1) inevitably leads to an error in step (2). To improve the overall bit-error-rate (BER) performance of NOMA, reducing the BER in step (1) is essential. The effectiveness of phase pre-distortion relies on a proposition that the BER varies with respect to the relative phase difference between signals S and W , which is induced by the asynchrony between the two signals in the envelop detection, and there exists an optimal relative phase leading to the minimum BER. We have derived the BER with respect to the relative phase in AWGN channel, under two scenarios: (A) both users employ quadrature phase-shift keying (QPSK) modulation; (B) one user employs QPSK modulation and the other one employs binary phase-shift keying (BPSK) modulation.

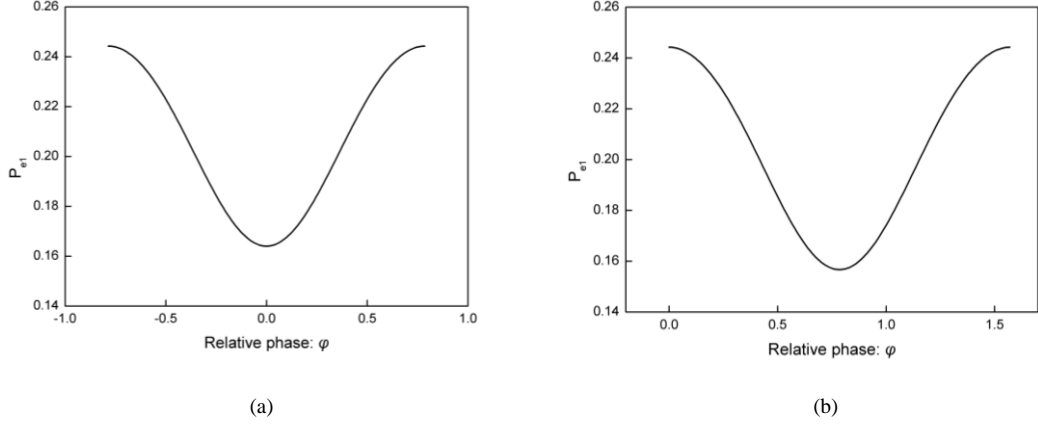


Figure 4-3 The symbol error rate (P_{e1}) in step (1) of successive interference cancellation decoding versus the phase difference φ between the two users. (a) P_{e1} vs S(QPSK)-W(QPSK) relative phase φ ; (b) P_{e1} vs S(QPSK)-W(BPSK) relative phase φ .

4.2.3.1 QPSK-QPSK

Assume that each of the signals S and W is QPSK modulated with four constellation points $\frac{\sqrt{2}}{2}\{1 + i, -1 + i, -1 - i, 1 - i\}$. Without loss of generality, we consider one subcarrier at the receiver. Ignore the index k and absorb the exponential term into H_w , Equation (4.4) can be re-written as

$$Y_c = X_s \cdot H_s + X_w \cdot H_w + w' \quad (4.5)$$

Let

$$\frac{H_w}{H_s} = r e^{j\varphi}, \quad r_{dB} = -20 \cdot \log(r) \quad (4.6)$$

where r denotes the amplitude ratio of the two channel coefficients and r_{dB} is the power ratio in dB; φ denotes the relative phase offset between the channel coefficients H_w and H_s . We model φ as a uniformly distributed random variable over $\varphi \in (0, 2\pi]$.

In a noiseless case, one subcarrier of the received overlapped signal C received

at the PD forms an irregular composite 16-quadrature amplitude modulation (16QAM) constellation. Let P_{e1} and P_{e2} denote the BERs in step (1) and step (2) of SIC, respectively. Also, let P_m denotes the probability that the strong user transmits symbol $m \in \frac{\sqrt{2}}{2}\{1+i, -1+i, -1-i, 1-i\}$, and P_n denotes the probability that the weak user transmits symbol $n \in \frac{\sqrt{2}}{2}\{1+i, -1+i, -1-i, 1-i\}$. In addition, let P_{mn} denotes the probability that S contains message m while W contains message n . The symbol error probability in the SIC step (1) is

$$P_{e1} = \sum_{m=1}^4 P_m \sum_{n=1}^4 P_n P_{e|mn} \quad (4.7)$$

where $P_{e|mn}$ denotes the error probability of the strong user sending message m and the weak user sending message n , while $P_{c|mn}$ as the respective correct decision of m and n . As the in-phase noise and the quadrature-phase noise are orthogonal and independent, the error probability $P_{e|mn}$ can be expressed as

$$\begin{aligned} P_{e|mn} &= 1 - P_{c|mn} = 1 - P_{Ic|mn} \cdot P_{Qc|mn} \\ &= 1 - \left(1 - P_{Ie|mn}\right) \cdot \left(1 - P_{Qe|mn}\right) \\ &= P_{Ie|mn} + P_{Qe|mn} - P_{Ie|mn} \cdot P_{Qe|mn} \end{aligned} \quad (4.8)$$

where $P_{Ie|mn}$ and $P_{Qe|mn}$ are the error probabilities of the in-phase dimension and the quadrature-phase dimension, respectively. For a specific constellation point s_{mn} , its in-phase and quadrature-phase error probabilities are given by [68]

$$P_{Ie|mn} = Q\left(\frac{\text{Re}\{s_{mn}\}}{\sqrt{N_0}/2}\right) ; \quad P_{Qe|mn} = Q\left(\frac{\text{Im}\{s_{mn}\}}{\sqrt{N_0}/2}\right) \quad (4.9)$$

where $Q(\cdot)$ denotes the Q -function. Therefore,

$$\begin{aligned}
P_{e1} &= \sum_{m=1}^4 P_m \sum_{n=1}^4 P_n P_{e|mn} \\
&= \sum_{m=1}^4 P_m \sum_{n=1}^4 P_n \left(P_{Ie|mn} + P_{Qe|mn} - P_{Ie|mn} \cdot P_{Qe|mn} \right) \\
&= \sum_{m=1}^4 P_m \sum_{n=1}^4 P_n \left(Q \left(\frac{\operatorname{Re}\{s_{mn}\}}{\sqrt{N_0/2}} \right) + Q \left(\frac{\operatorname{Im}\{s_{mn}\}}{\sqrt{N_0/2}} \right) \right. \\
&\quad \left. - Q \left(\frac{\operatorname{Re}\{s_{mn}\}}{\sqrt{N_0/2}} \right) \cdot Q \left(\frac{\operatorname{Im}\{s_{mn}\}}{\sqrt{N_0/2}} \right) \right)
\end{aligned} \tag{4.10}$$

Assume that all the messages are equi-probable, that is $P_m = P_n = 1/4$. As the overlapped constellation is centrally symmetric with respect to the origin, we only compute the error probability of the constellation points in the first quadrant. Thus

$$P_{e1} = \frac{1}{4} \sum_{n=1}^4 \left(Q \left(\frac{\frac{\sqrt{2}}{2} + r \cos(\varphi + \frac{n\pi}{2} - \frac{\pi}{4})}{\sqrt{N_0/2}} \right) + Q \left(\frac{\frac{\sqrt{2}}{2} + r \sin(\varphi + \frac{n\pi}{2} - \frac{\pi}{4})}{\sqrt{N_0/2}} \right) \right. \\
\left. - Q \left(\frac{\frac{\sqrt{2}}{2} + r \cos(\varphi + \frac{n\pi}{2} - \frac{\pi}{4})}{\sqrt{N_0/2}} \right) \cdot Q \left(\frac{\frac{\sqrt{2}}{2} + r \sin(\varphi + \frac{n\pi}{2} - \frac{\pi}{4})}{\sqrt{N_0/2}} \right) \right) \tag{4.11}$$

Moreover, as the overlapped constellation is also rotational symmetry, we only consider $-\pi/4 < \varphi \leq 0$. The optimal phase difference φ_{opt} is obtained by

$$\varphi_{opt} = \arg \min_{\varphi} P_{e1}, \quad \varphi \in (-\pi/4, 0] \tag{4.12}$$

Assume r is 0.7. By numerical analysis, we plot the value of P_{e1} with respect to the phase difference φ , as depicted in Figure 4-3(a). Our numerical analysis shows that the optimal phase difference is $\varphi_{opt}=0$.

From the discussion above, it can be seen that P_{e1} does not stay constant with regard to φ . Therefore, it can be deduced that the BER can be reduced by pre-distorting the transmitted signal to the optimal phase difference $\varphi_{opt}=0$.

4.2.3.2 QPSK-BPSK

We next consider the scenario in which two users are in different modulation formats. To ensure successful decoding, the far user employs BPSK modulation with constellation points $n \in \{+1, -1\}$; whereas the near user employs QPSK modulation with constellation points $m \in \frac{\sqrt{2}}{2}\{1 + i, -1 + i, -1 - i, 1 - i\}$. Therefore, the PD receives an overlapped signal of 8-QAM.

Similar to the QPSK-QPSK case, the PD uses SIC to decode both the strong and the weak signals. Following the analysis described in the previous section, the symbol error probability in the step (1) of SIC is given by

$$\begin{aligned}
 P_{e1} &= \sum_{m=1}^4 P_m \sum_{n=1}^2 P_n P_{e|mn} \\
 &= \sum_{m=1}^4 P_m \sum_{n=1}^2 P_n \left(P_{Ie|mn} + P_{Qe|mn} - P_{Ie|mn} \cdot P_{Qe|mn} \right) \\
 &= \sum_{m=1}^4 P_m \sum_{n=1}^2 P_n \left(Q\left(\frac{\text{Re}\{s_{mn}\}}{\sqrt{N_0/2}}\right) + Q\left(\frac{\text{Im}\{s_{mn}\}}{\sqrt{N_0/2}}\right) \right. \\
 &\quad \left. - Q\left(\frac{\text{Re}\{s_{mn}\}}{\sqrt{N_0/2}}\right) \cdot Q\left(\frac{\text{Im}\{s_{mn}\}}{\sqrt{N_0/2}}\right) \right)
 \end{aligned} \tag{4.13}$$

Assume all the transmitted messages are equi-probable, that is, $P_m = 1/4$, $P_n = 1/2$. As the overlapped constellation is centrally symmetric with respect to the origin, we only need to compute the error probability of the constellation points in the first quadrant. Thus,

$$P_{e1} = \frac{1}{2} \sum_{n=1}^2 \left(Q\left(\frac{\frac{\sqrt{2}}{2} + r \cos(\varphi + (n-1)\pi)}{\sqrt{N_0/2}}\right) + Q\left(\frac{\frac{\sqrt{2}}{2} + r \sin(\varphi + (n-1)\pi)}{\sqrt{N_0/2}}\right) \right. \\
 \left. - Q\left(\frac{\frac{\sqrt{2}}{2} + r \cos(\varphi + (n-1)\pi)}{\sqrt{N_0/2}}\right) \cdot Q\left(\frac{\frac{\sqrt{2}}{2} + r \sin(\varphi + (n-1)\pi)}{\sqrt{N_0/2}}\right) \right) \tag{4.14}$$

The optimal phase pre-distortion term is the value of φ that minimizes the probability in Equation (4.14). Figure 4-3(b) shows the numerical results of P_{e1} in the range of $\varphi \in [-\pi/2, \pi/2)$ when r is fixed at 0.7, and the optimal phase pre-distortion term φ_{opt} is shown to be $\pi/4$.

4.2.4 Experiment

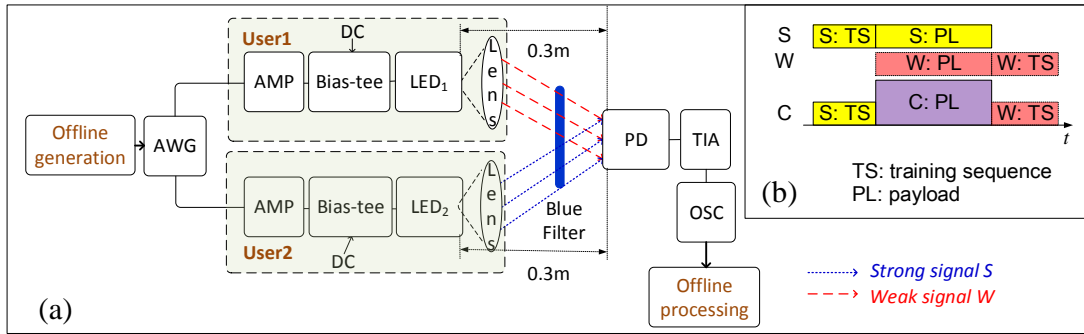


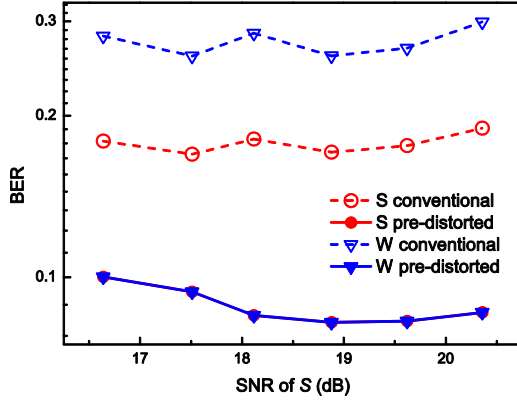
Figure 4-4 (a) Experimental Setup to evaluate the proposed phase pre-distortion method, AWG: arbitrary waveform generator, AMP: amplifier, DC: direct current, LED: lighting emitted diode, PD: photodiode, TIA: trans-impedance amplifier, DSO: digital storage oscilloscope; (b) frame format for the NOMA users.

4.2.4.1 Experimental setup

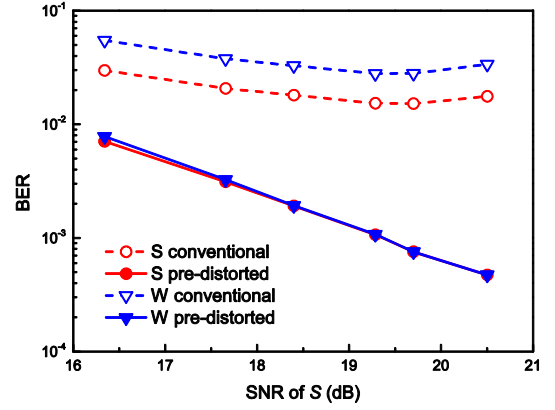
Figure 4-4(a) shows the experimental setup to evaluate the proposed phase pre-distortion method for NOMA in VLC. In conventional NOMA, the signal transmission was in single phase without any prior training sequences. The signals were directly transmitted without any channel state information (CSI) feedback. Two transmitted signals were generated, via an arbitrary waveform generator (AWG), and were amplified by the amplifiers (AMP), before being fed to the LEDs (OSRAM LUW W5AM), via bias-tees, respectively. A lens was mounted in front of each LEDs so as

to focus the respective output light to a common photodiode (HAMAMATU S10784), placed behind a blue filter. The distance between each LED and the PD was fixed to be 0.3 meter. During the experiment, the received signal powers from both LEDs, as well as their relative power ratios were adjusted by tuning the respective driving signal amplitudes of the LEDs. On the receiver side, we first amplified the received signal from the PDs by a trans-impedance amplifier (TIA), and then fed it to an oscilloscope (DSC) for data acquisition and offline processing. Each OFDM frame comprised 10 training symbols for channel estimation and 240 payload symbols for data transmission. For each OFDM symbol, the FFT size was 256, and the cyclic prefix (CP) length was 32. The two subcarriers next to the DC level were nulled, owing to the DC block of the bias-Tee. The sampling rates of the AWG and the OSC were 100 MS/s and 250 MS/s, respectively. To avoid collision of training symbols, the signal frames of S and W were designed, as illustrated in Figure 4-4(b).

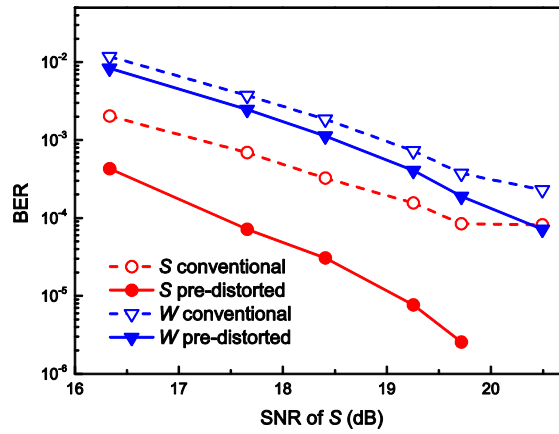
Meanwhile, the proposed phase pre-distorted NOMA case was a two-phase process. In the first phase, each user transmitted a training sequence to the receiver, where the CSI was estimated, based on the training sequence, and fed back to the respective user. In the second phase, each user pre-distorted its payload, based on the



(a) $r_{dB} = 1.2$ dB



(b) $r_{dB} = 4.2$ dB



(c) $r_{dB} = 6.9$ dB

Figure 4-5 Bit error rate (BER) versus the SNR of the strong signal, for strong signal (S) in QPSK and weak signal (W) in QPSK: (a) $r_{dB}=1.2$ dB, (b) $r_{dB}=4.2$ dB, (c) $r_{dB}=6.9$ dB.

CSI acquired in the first phase, before being sent over the VLC system, similar to the conventional NOMA case.

4.2.4.2 Results and discussion

To evaluate our analysis in Section 4.2.3, we consider two scenarios (1) both users employ QPSK modulation and (2) one user employs QPSK modulation and the other one employs BPSK modulation.

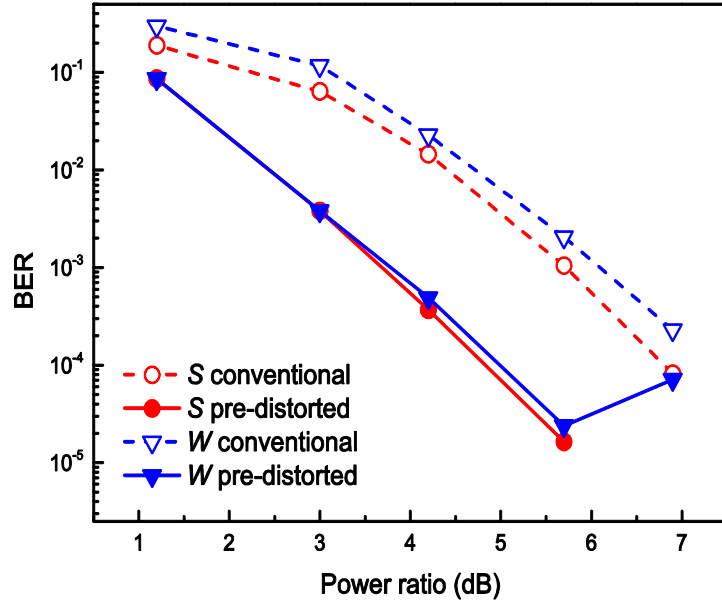


Figure 4-6 Measured BER versus the relative power ratio r_{dB} between the strong signal S (in QPSK) and the weak signal W (in QPSK), with the SNR of S is fixed as 20.5 dB.

Firstly, we investigated the scenario that both users adopted QPSK modulation format.

Figure 4-5 shows the comparisons of the measured BER, as a function of the SNR of the strong signal S , under different power ratios between the signals S and W , for both cases of the conventional NOMA scheme and the proposed pre-distorted NOMA scheme. Assume r_{dB} was the relative power ratio between signals S and W in dB scale. It could be observed that the proposed pre-distorted NOMA scheme substantially reduced the BERs of both signals S and W , compared to the conventional NOMA scheme under all power ratios of both signals S and W . When r_{dB} was 1.2 dB, there was a slight improvement in the system performance, though it was not sufficient to meet forward error correction (FEC) threshold of 3.8×10^{-3} . When r_{dB} was increased to 4.2 dB, with pre-distortion, BERs of S and W could drop below FEC threshold when the SNR of S was greater than 17.2 dB. However, the conventional NOMA still could not meet the required BER for FEC, even when the SNR of S was greater than 20.5

dB. When r_{dB} was further increased to 6.9 dB, the proposed pre-distorted NOMA scheme still exhibited superior improvements, compared to the conventional case. Besides, it could be observed that when the relative power ratios were relatively small, as in the cases of r_{dB} being 1.2 dB or 4.2 dB, the BERs of S and W were always nearly identical. This indicated that the errors in decoding W were mostly attributed to the error propagation from the decoding process of S .

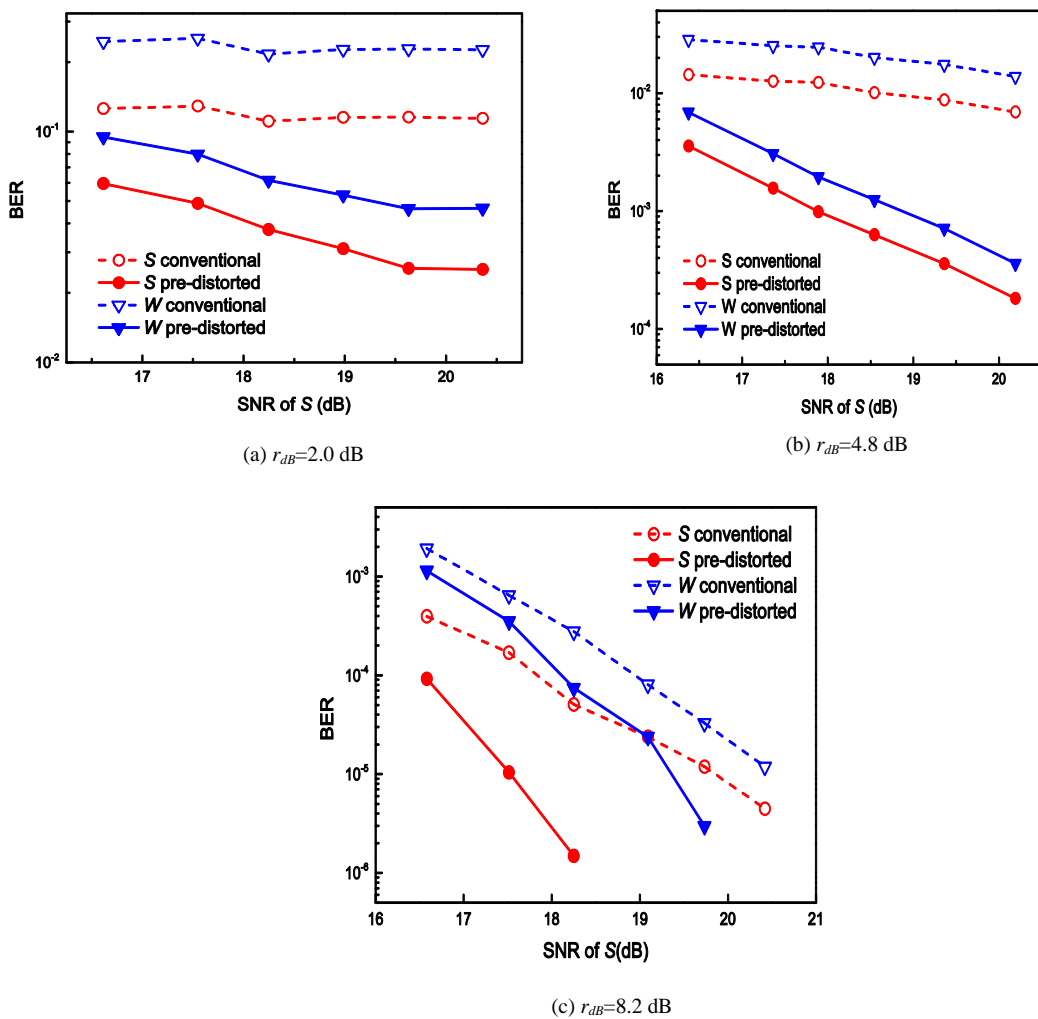


Figure 4-7 Measured BER versus the SNR of the strong signal S , under the scenario of signal S was in QPSK modulation and W was in BPSK modulation, and the relative power ratios r_{dB} were (a) 2.0 dB, (b) 4.8 dB, and (c) 8.2 dB, respectively.

By keeping the SNR of S and changing the relative power ratio between S and W , the BER of S and W along with the variation of the relative power ratio is depicted in Figure 4-6. When the SNR of S was 20.5 dB, with the adoption of phase pre-distortion, the required r_{dB} for individual signal S and W to reach FEC threshold were reduced by 2.1 and 1.9 dB, respectively. The increase in the BER of signal W at high r_{dB} could be attributed to the insufficient SNR of W .

Secondly, we investigated the scenario that signal S employed QPSK modulation while signal W employed BPSK modulation. Figure 4-7 shows the comparisons of the measured BER, as a function of the SNR of the strong signal S , under different r_{dB} . It could be observed that by pre-coding the phase difference to $\varphi_{opt} = \pi/2$, the performances of both signals S and W under different relative power ratios outperformed the conventional NOMA scheme.

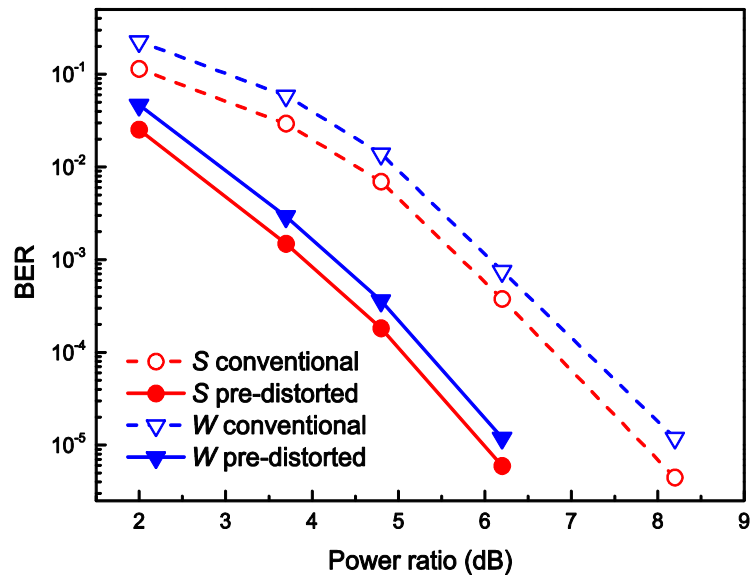


Figure 4-8 Measured BER versus the relative power ratio r_{dB} between the strong signal S (in QPSK) and the weak signal W (in BPSK), with the SNR of S is fixed as 20.5 dB.

Figure 4-8 shows the BER performance versus r_{dB} , while fixing the SNR of S at 20.5 dB. It could be noticed that compared to the required r_{dB} of 5.0 dB and 5.3 dB for S and W to reach below feed-forward correction (FEC) threshold, only r_{dB} of 3.0 dB and 3.4 dB were necessary for the same level of BER performance for S and W , respectively. In other words, the proposed scheme worked well under different modulation formats at multiple access users.

4.2.5 Conclusion

In this section, we have proposed a phase pre-distortion method for NOMA with successive interference cancellation (SIC) decoding in VLC systems. This method improves the BER performance of SIC decoding by maximizing the minimum distance of the received signal constellation under NOMA. With the retrieved channel state information, the users can compute the optimal phase pre-distortion term, which is then used to pre-distort the phases of the individual signals, accordingly, prior to transmission. Experimental results showed that the proposed phase pre-distortion method improved the BER performance under low, medium, and high relative power ratios between both signals, which were in QPSK or BPSK modulations, compared to the conventional NOMA scheme. In particular, the phase pre-distorted NOMA eliminated the BER error floors as in the conventional NOMA case, at low relative power ratios and also alleviated the relative power ratio requirement by around 2 dB, so as to achieve a BER of 3.8×10^{-3} .

4.3 Joint detection of visible light communication signals under non-orthogonal multiple access

4.3.1 Introduction

In the previous section, we have experimentally implemented NOMA in VLC with a newly proposed phase pre-distortion method. The benefit brought by our method is significant. The decoding method adopted in the last section is successive interference cancellation (SIC), a multiuser detection (MUD) method. In SIC, the decoding of multiple signals is in the order of descending power level. The receiver firstly detects and decodes the signal which is strongest in the power treating the interference from weak signals as noise; secondly the strongest signal is reconstructed and subtracted from the composite signal; thereafter, the receiver detects and decodes the second strongest signal in a similar process and so on.

Another MUD method is joint detection (JD) [97]. In JD, multiple signals are decode jointly. Like SIC, JD is also a common decoding algorithm in MA systems, including CDMA and NOMA. The application of JD in NOMA in VLC, to the knowledge of the authors, is still unexplored.

Just like SIC, the performance of JD also depends on the phase relationship of multiple signals. In this section, we present JD into NOMA in VLC. We have also proposed a novel phase pre-distortion method in JD-based NOMA in VLC. Interestingly, we find that the optimal relative phase difference between the multiple users in JD-based NOMA is different from the SIC-based case. It is found that the

optimal relative phase difference depends on the power ratio. Moreover, it is found that the BER can be further decreased by adopting phase pre-distorted JD-based NOMA, compared to its SIC-based counterpart.

4.3.2 System model

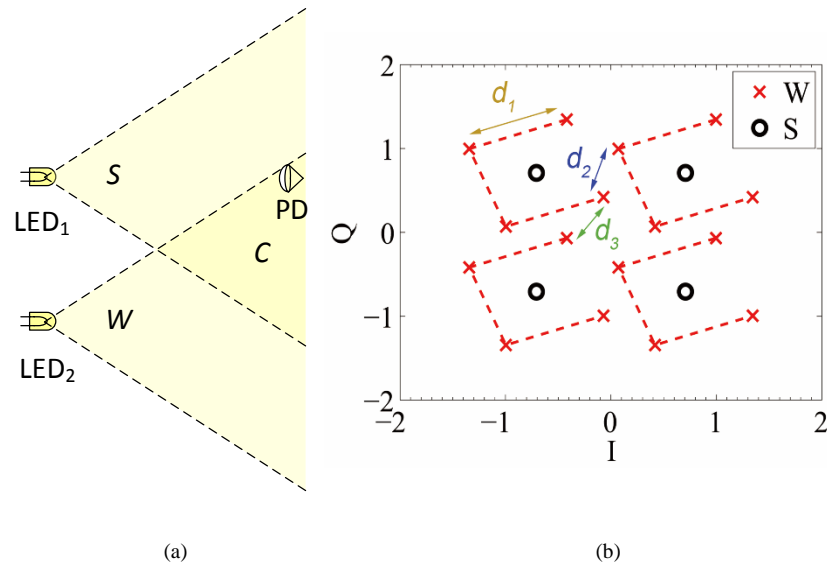


Figure 4-9 System model for the NOMA in visible light communications. LED: lighting emitted diode; PD: photo diode, S and W are the transmitted signals from LED₁ and LED₂, respectively; (b) an example of the three Euclidean distances at $r=1.43$, where $d_1=1/r$; $d_2 = |1-(1+j)/re^{j\varphi}|$; $d_3 = |1-1/re^{j\varphi}|$.

Consider an uplink VLC system, as shown in Figure 4-9(a), it comprises two light-emitting diodes (LEDs), namely LED₁ and LED₂, as transmitters and a photodiode (PD) as the receiver. The PD lies within the overlapping area of the two LEDs' illuminative regions, hence receiving the signals from both LEDs. Suppose the PD is closer to LED₁ than to LED₂, thus receives a stronger signal S from LED₁ but a weaker signal W from LED₂. The signals S and W overlap with each other, forming a composite signal C . Without loss of generality, we assume that S and W are both

4QAM-OFDM modulated, that is, modulated with four constellation points $(\sqrt{2}/2)\{1 + i, -1 + i, -1 - i, 1 - i\}$. Considering one subcarrier retrieved at the PD after OFDM demodulation and matched filtering, the received signal is

$$y_c = h_s x_s + h_w x_w + n \quad (4.15)$$

where x_s and x_w are the modulated data of S and W from LED₁ and LED₂, respectively, h_s and h_w are the respective individual channel responses between the transmitting LEDs and the PD, and n is the complex additive white Gaussian noise (AWGN). Let

$$h_s/h_w = r e^{j\varphi}, r_{dB} = 20 \log r \quad (4.16)$$

where r denotes the amplitude ratio of the channel coefficients of S over W , r_{dB} denotes the power ratio in dB, and $\varphi \in [0, 2\pi)$ denotes the relative phase difference between h_s and h_w . Such relative phase difference is random, depending on multiple factors, such as different transmission distances, different angles of arrival, and multiple paths.

4.3.3 Multiuser detection algorithms for NOMA

At the NOMA receiver, the received symbols from multiple users are detected and retrieved from the received composite overlapped signal. Appropriate techniques are necessary to distinguish and decode the symbols from each transmitter. This necessitates appropriate multi-user detection strategies, such as SIC and JD.

4.3.3.1 SIC-based NOMA

In SIC-based NOMA, upon receiving the composite overlapped signal, the receiver detects and decodes the signal from multiple transmitters in the descending order of

the signal strengths. Specifically, in the given two-user case, the SIC process at the PD consists of two steps: (1) decode the strong signal S while treating the weak signal W as noise; (2) subtract S from C and decode for W . When the decision of S in step (1) is wrong, the decoding output in step (2) would be inevitably erroneous. The key issue in SIC-based NOMA is to decrease the bit-error-rate (BER) in step (1) of SIC. It has been demonstrated in [98] that the performance of SIC-based NOMA could be effectively improved by applying phase pre-distortion.

4.3.3.2 JD-based NOMA

In JD-based NOMA, S and W are detected jointly in one step. In the two-user case, JD algorithm can be expressed by the following equation

$$\begin{aligned}
\{\hat{x}_s, \hat{x}_w\} &= \arg \max_{\{x_s, x_w\}} \Pr \{y_c | x_s, x_w\} \\
&= \arg \max_{\{x_s, x_w\}} \frac{1}{\sqrt{2\pi\sigma^2}} \exp \left\{ -\frac{|y_c - h_s x_s - h_w x_w|^2}{2\sigma^2} \right\} \\
&= \arg \min_{\{x_s, x_w\}} |y_c - h_s x_s - h_w x_w|^2
\end{aligned} \tag{4.17}$$

where $\{\hat{x}_s, \hat{x}_w\}$ is the detected signal pair output by JD algorithm.

Unlike SIC, JD treats both S and W as useful information, thus is maximum-likelihood (ML) optimal. Considering the transmitted data symbols as well as the channel responses of S and W , the received symbol forms an irregular 16-QAM constellation. Figure 4-9(b) illustrates an example. The detection of the signals S and W is to find the constellation point that is the closest to the received signal y_c . Therefore, the performance of JD is dominated by the distribution of the constellation

points. In fact, the symbol error rate (SER) of the decision is bounded by [68],

$$\frac{1}{M} \sum_{\substack{1 \leq m \leq M, \\ \exists m' \neq m: \|s_m - s_{m'}\| = d_{\min}}} Q\left(\frac{d_{\min}}{\sqrt{2N_0}}\right) \leq P_e \leq (M-1)Q\left(\frac{d_{\min}}{\sqrt{2N_0}}\right) \quad (4.18)$$

where M is the number of the constellation points of the composite overlapped signal ($M=16$ here), N_0 is the single-sided power spectrum density of the noise; d_{\min} is the minimum Euclidean distance between any pair of constellation points, and can be expressed, based on the observations from Figure 4-9(b), as,

$$\begin{aligned} d_{\min} &= \min \left\{ \sqrt{2}|h_w|, \sqrt{2}|h_s - h_w|, \sqrt{2}|h_s - (1+j)h_w| \right\} \\ &= \min \left\{ \frac{\sqrt{2}|h_s|}{r}, \sqrt{2} \left| h_s - \frac{h_s}{re^{j\varphi}} \right|, \sqrt{2} \left| h_s - (1+j) \frac{h_s}{re^{j\varphi}} \right| \right\} \\ &= \min \left\{ \frac{1}{r}, \left| 1 - \frac{1}{re^{j\varphi}} \right|, \left| 1 - \frac{1+j}{re^{j\varphi}} \right| \right\}, -\pi/4 < \varphi \leq 0 \end{aligned} \quad (4.19)$$

where r is defined as the signal power ratio (PR) of S to W . As the constellation here is centro-symmetric, we only consider the range $\varphi \in (-\frac{\pi}{4}]$. From Equation (4.19), it is evident that both the upper and the lower bounds of SER largely depends on the value of d_{\min} . A larger value of d_{\min} leads to a smaller SER, thus better BER performance of NOMA.

We propose to maximize d_{\min} by pre-distorting the phase of the signal W with a phase term, which corresponds to the relative phase difference φ in Equation (4.19) and can be computed based on the channel response. To simplify the mathematical notation, we define a new metric function, as

$$\mathcal{M}_r(\varphi) = \min \left\{ \frac{1}{r}, \left| 1 - \frac{1}{re^{j\varphi}} \right|, \left| 1 - \frac{1+j}{re^{j\varphi}} \right| \right\} \quad (4.20)$$

and the optimal phase term φ_{opt} can be determined by

$$\varphi_{opt} = \arg \max_{\varphi} \mathcal{M}_r(\varphi), \quad -\frac{\pi}{4} < \varphi \leq 0 \quad (4.21)$$

In Equation (4.20), the three Euclidean distances (d_1 , d_2 , and d_3) are constant, monotonically decreasing, and monotonically increasing, respectively. Hence, the solution of Equation (4.21) can be divided into four cases, depending on the values of r .

$$a) \quad r \geq 2.41 \quad (r_{dB} \geq 7.7dB)$$

In this case, the following relationships always holds.

$$\mathcal{M}_r(\varphi) = \frac{1}{r}, \quad \varphi \in \left(0, \frac{\pi}{4} \right] \quad (4.22)$$

Thus, the value of d_{min} is determined by the value of r . Since r is constant within the range of φ , the BER performance cannot be improved by changing the phase difference between S and W . Hence, phase pre-distortion is ineffective. Figure 4-10(a) shows the values of the three Euclidean distance terms when $r = 2.5$. As the minimum Euclidean distance is determined by the constant value $1/r$. Hence, phase pre-distortion does not work in this case.

$$b) \quad 2 \leq r < 2.41 \quad (6.0dB \leq r_{dB} < 7.7dB)$$

When r falls in this range, the following expression holds.

$$\mathcal{M}_r(\varphi) = \begin{cases} \frac{1}{r}, & \varphi \in \left(0, \frac{\pi}{4} - \arccos\left(\frac{r^2+1}{2\sqrt{2}r}\right)\right] \\ \left|1 - \frac{1+j}{re^{j\varphi}}\right|, & \varphi \in \left(\frac{\pi}{4} - \arccos\left(\frac{r^2+1}{2\sqrt{2}r}\right), \frac{\pi}{4}\right] \end{cases} \quad (4.23)$$

Considering the monotonicities of the three functions, the value of d_{min} is maximized at $\varphi \in \left[\arccos\left(\frac{1+r^2}{2\sqrt{2}r}\right) - \frac{\pi}{4}, 0\right]$. Thus, the optimal pre-distorted phase is within a range rather than a single value. Figure 4-10(b) shows the values of the three Euclidean distance terms when $r = 2.2$. Obviously, the SER can be minimized by pre-distorting the relative phase difference to this region.

$$c) \quad 1.93 \leq r < 2 \quad (5.7dB \leq r_{dB} < 6dB)$$

In this range of r , the following expression holds.

$$\mathcal{M}_r(\varphi) = \begin{cases} \left|1 - \frac{1}{re^{j\varphi}}\right|, & \varphi \in \left(0, \arccos\left(\frac{r}{2}\right)\right] \\ \frac{1}{r}, & \varphi \in \left(\arccos\left(\frac{r}{2}\right), \frac{\pi}{4} - \arccos\left(\frac{r^2+1}{2\sqrt{2}r}\right)\right] \\ \left|1 - \frac{1+j}{re^{j\varphi}}\right|, & \varphi \in \left(\frac{\pi}{4} - \arccos\left(\frac{r^2+1}{2\sqrt{2}r}\right), \frac{\pi}{4}\right] \end{cases} \quad (4.24)$$

Similar to the previous case, the d_{min} is also maximized in a range of φ , that is, $\arccos\left(\frac{r}{2}\right) < \varphi \leq \arccos\left(\frac{\sqrt{2}}{2}r - \frac{1}{2}\right)$. Therefore, the phase pre-distortion is effective. Figure 4-10(c) shows the values of the three Euclidean distance terms when $r = 2.2$. The minimum Euclidean distance can be maximized by pre-distorting φ to $\arccos\left(\frac{r}{2}\right) < \varphi \leq \arccos\left(\frac{\sqrt{2}}{2}r - \frac{1}{2}\right)$.

$$d) \quad 1 \leq r < 1.93 \quad (0dB \leq r_{dB} < 5.7dB)$$

In this case, the following expression holds.

$$\mathcal{M}_r(\varphi) = \begin{cases} \left| 1 - \frac{1}{re^{j\varphi}} \right|, & \varphi \in \left(0, \arcsin\left(\frac{1}{2r}\right) \right] \\ \left| 1 - \frac{1+j}{re^{j\varphi}} \right|, & \varphi \in \left(\arcsin\left(\frac{1}{2r}\right), \frac{\pi}{4} \right] \end{cases} \quad (4.25)$$

Therefore, the value of d_{min} reaches its maximum value at $\varphi = \arcsin(1/2r)$.

Figure 4-10(d) shows the values of the three Euclidean distance terms when $r = 1.43$.

Apparently, it is beneficial to pre-distort the relative phase difference to the optimal point $\varphi = \arcsin(1/2r)$, which is the intersection point of the blue line and magenta line (in Figure 4-10(d), for better system performance.

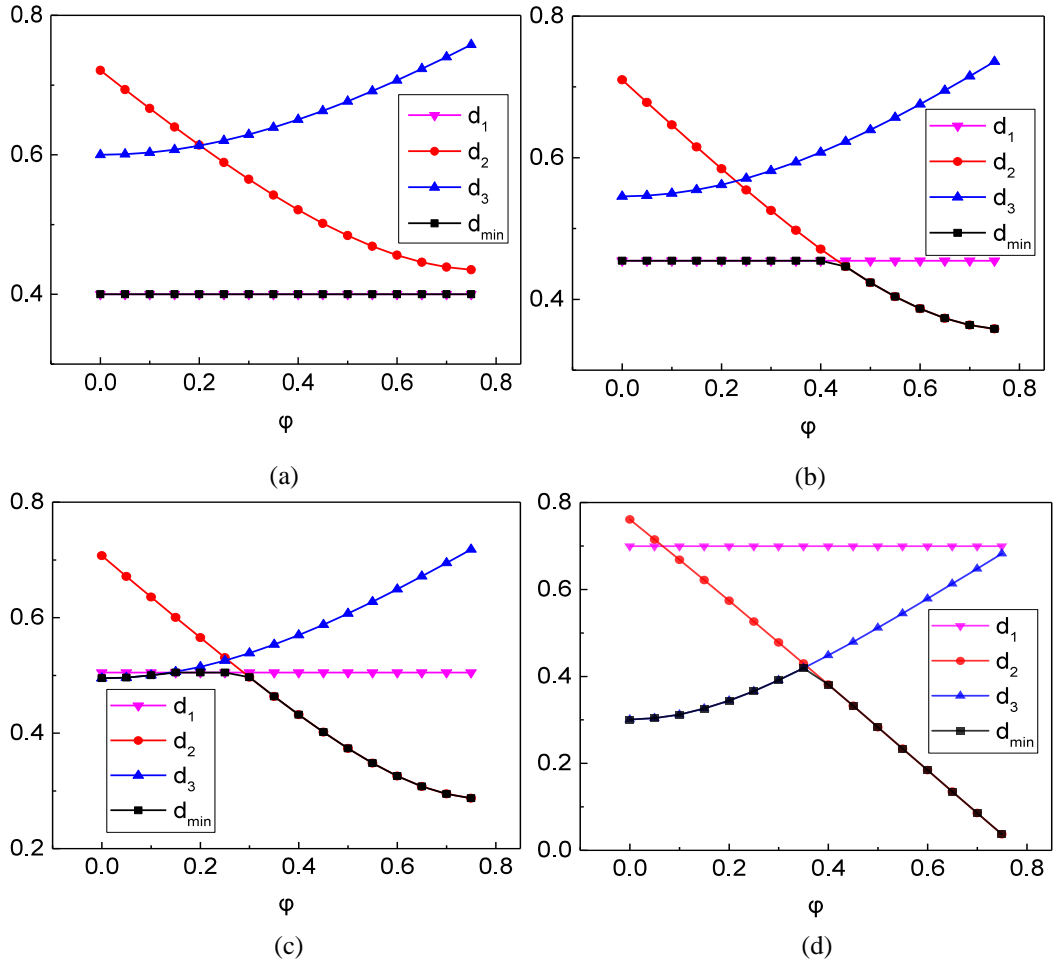


Figure 4-10 Distances comparison of the three terms in four cases: (a) $r=2.5$; (b) $r=2.2$; (c) $r=1.98$; (d) $r=1.43$.

4.3.4 Experiments

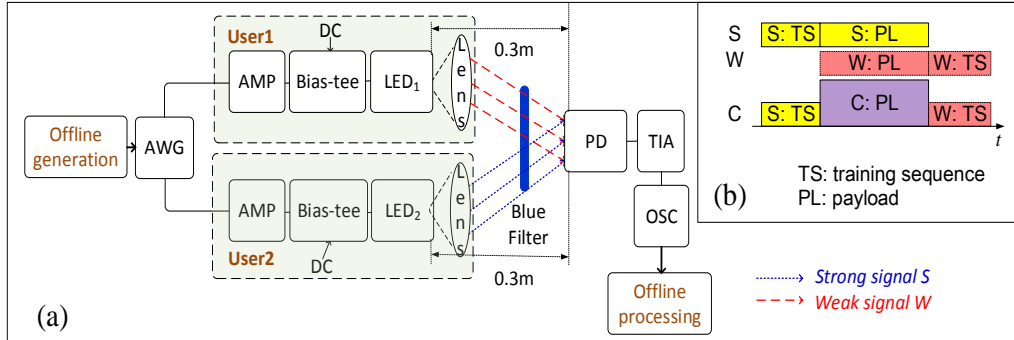


Figure 4-11 (a) Experimental setup to evaluate the proposed joint detection method with phase pre-distortion; (b) frame format for the NOMA users.

Figure 4-11(a) shows the experimental setup. For conventional NOMA, the transmitted data was offline generated and sent to an arbitrary waveform generator (AWG). Each output of AWG was individually amplified by an amplifier (AMP) and biased by a bias-tee before driving a LED (OSRAM LUW W5AM). Two lenses were mounted after the LEDs to direct the light to the same PD (HAMAMATU S10784) after a blue filter. The distances between the LEDs and the PD were both fixed at 0.3 m. The receiving powers and the power ratios r_{dB} were tuned by changing the LED driving signals. The received signal was then amplified by a trans-impedance amplifier (TIA), sampled by a digital storage oscilloscope (DSC) and offline processed using MATLAB. The fast Fourier transform (FFT) size of OFDM was 256 and the cyclic prefix (CP) length was 32. Due to the DC block property of the bias-tees, the two subcarriers next to the DC term were set to null. Therefore, the effective number of subcarriers in each symbol was 124 out of 256. Each frame consisted of 10 OFDM training symbols (TS) and 240 payload symbols. As shown in Figure 4-11(b), we deliberately designed the frames of S and W to make their TS non-overlapped. The

sampling rates of AWG and DSC were 100 MS/s and 250 MS/s, respectively. On the other hand, the proposed JD-based phase pre-distorted NOMA, similar to its SIC counterpart reported in [98], comprised two steps. In the first step, a training sequence was offline generated and transmitted, as in the conventional NOMA. Upon receiving the composite overlapped signal, the PD estimated the channel state information (CSI) using the TS and fed the CSI back to the transmitters. In the second step, the transmitters pre-distorted the phase of the payload symbols based on the obtained CSI before transmitting the signals.

Figure 4-12 shows the measured BER performances of both the strong signal (S) and the weak signal (W) using our proposed JD method and the conventional SIC methods with or without phase pre-distortion. From the results, the method of JD with phase pre-distortion achieved the best BER performance, and outperformed the others under all three cases of signal power ratios. The performance improvement was the most significant when the power ratio was low. In the case of low signal power ratio, such as $r_{dB} = 1.2$ dB as shown in Figure 4-12(a), the performance of SIC showed error floors for both S and W at BER of about 10^{-1} , while JD was not bounded by any error floor. In the case of medium signal power ratio, such as $r_{dB} = 4.2$ dB as in Figure 4-12(b), the performances of JD for both users were about 1-dB better than that of SIC at BER of 10^{-3} . In the case of high signal power ratio such as $r_{dB} = 6.9$ dB as shown in Figure 4-12(c), the performance of JD was only slightly better than that of SIC. Thus, SIC required a higher signal power ratio to obtain good performance, while JD alleviates the signal power ratio requirement. Hence, our proposed phase pre-distorted

joint detection based NOMA shows the best performance over other schemes, especially when the signal power ratio is low.

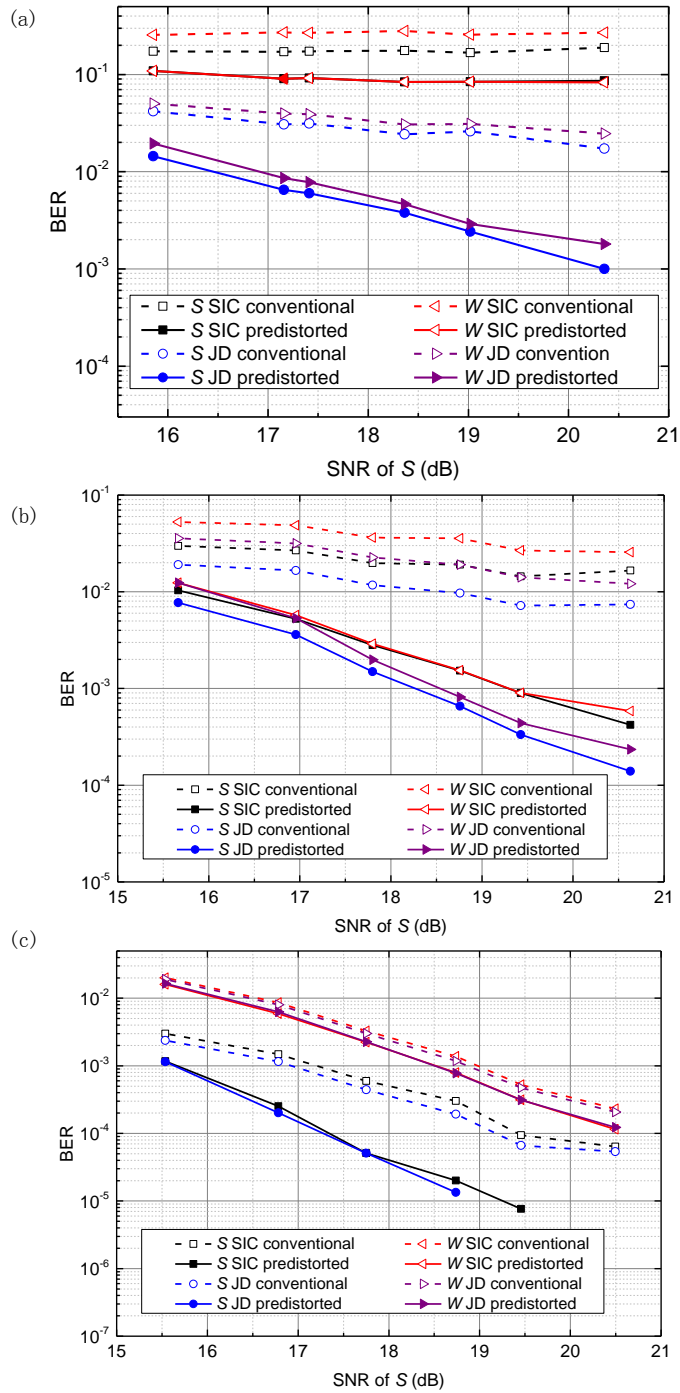


Figure 4-12 Bit error rate (BER) versus the SNR of the strong signal: (a) $r_{dB}=1.2$ dB, (b) $r_{dB}=4.2$ dB, (c) $r_{dB}=6.9$ dB.

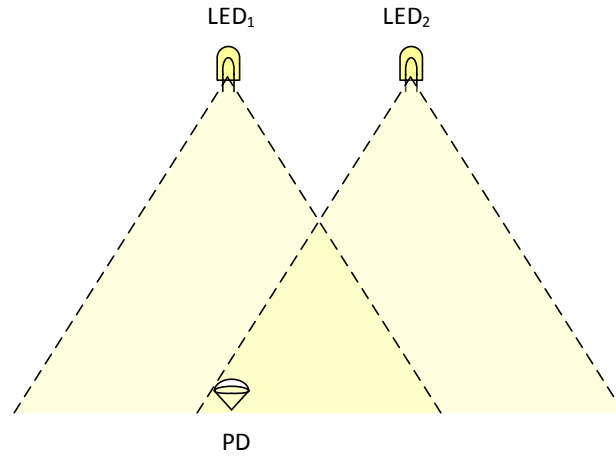
4.3.5 Conclusion

We have proposed a phase pre-distorted joint detection method for uplink non-orthogonal multiple access (NOMA) in visible light communication systems. It achieves superior BER performance, compared to other previously reported schemes, such as SIC-based ones. Experimental results show that it works well under different power ratios of the signals from multiple users. In particular, when the signal power ratio is low, the proposed scheme eliminates the error floor that exists for the case of SIC-based NOMA.

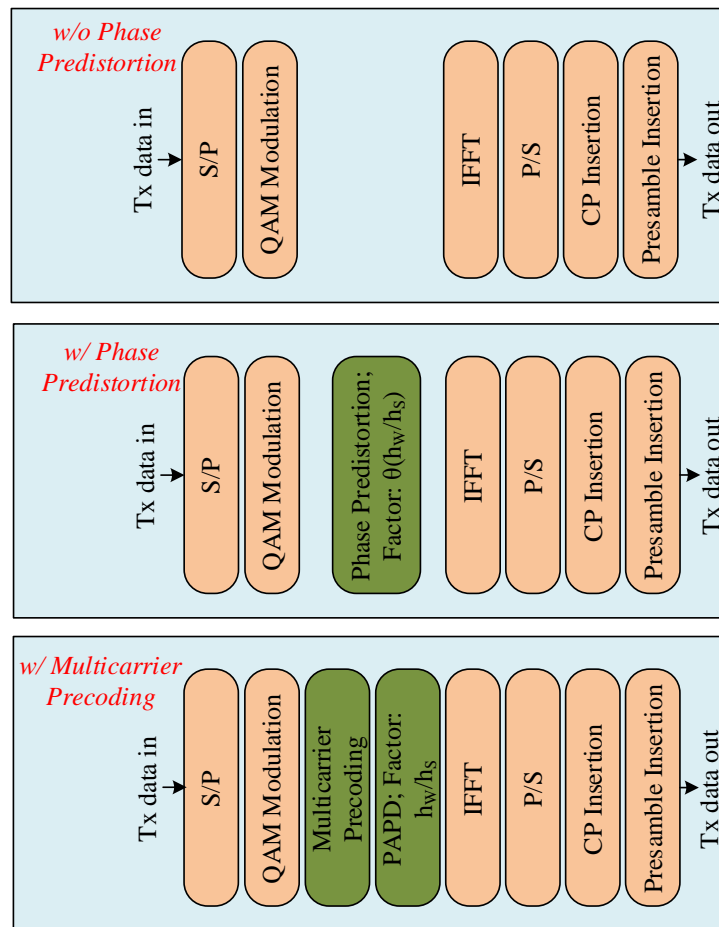
4.4 Non-orthogonal multiple access with multicarrier precoding in visible light communications

4.4.1 Introduction

Nowadays, visible light communication (VLC) is attracting wide attention among researchers as a potential key technology in the future communication systems, benefitting from its high volume, low-cost, reliability, and license-free [32]. Resembling other wireless communication technologies, appropriate multiple access strategies are indispensable for VLC to support multiple connections in one system. Recently in [98], we have proposed a novel scheme that can solve the dilemma between throughput and fairness, which is a main drawback of conventional multiple



(a)



(b)

Figure 4-13 (a) System Model (b) DSP of W in three cases.

access technologies. In non-orthogonal multiple access (NOMA), the multiple access is granted according to different power levels of different users, particularly in every subcarrier of orthogonal frequency division multiplexing (OFDM) signal. We have

also proposed a phase pre-distortion (PP) method to improve the system performance. However, the response across the whole OFDM spectrum is non-uniform. To accommodate different signal-to-noise ratios (SNR) on different subcarriers, adaptive modulation formats are adopted on different subcarriers, thus largely complicates the NOMA process.

Recently, a multicarrier precoding (MP) method based on orthogonal circulant matrix transform (OCT) was proposed in [99] to flatten the SNR of all the subcarriers in an OFDM system. In this paper, we apply the MP method in NOMA to avoid the adoption of higher order modulation formats. A novel phase and amplitude pre-distortion (PAP) process is further proposed to enable the MP method under NOMA.

4.4.2 Principles

The system model of NOMA is depicted in Figure 4-14(a), which is the same to that in [98]. The photo diode (PD), acting as the NOMA receiver, lies near to LED₁ but far from LED₂. The signal PD received from LED₁ (denoted as S) is stronger than the weaker signal from LED₂ (denoted as W). S and W are combined into a composite signal, which is denoted as C . Both S and W are in DC-biased optical OFDM (DCO-OFDM), which means only half of the whole OFDM subcarriers are used.

In MP process proposed in [99], an orthogonal circulant matrix, Q , is multiplexed to H_S and H_W before modulation onto the subcarriers, where $Q = (1/\sqrt{N}) \times [c_1, c_2, \dots, c_N; c_N, c_1, \dots, c_{N-1}; \dots; c_2, c_3, \dots, c_1]$, and each entry c_i corresponds to the element of the Zadoff-Chu (ZC) sequence in index of 1 and length of N . Unlike

conventional NOMA, the introduction of MP interferes the decision of S in the first step of successive interference cancellation (SIC). As a solution, a PAP matrix, $H_W^{-1}H_S$, is multiplexed to W at the transmitter after the MP step. 4-14(b) shows the DSP process of the three cases: (1) NOMA without PAP/MP, or conventional NOMA, (2) NOMA with PAP, as in [99], (3) NOMA with MP and PAP.

4.4.3 Numerical simulations

4.4.3.1 Simulation setup

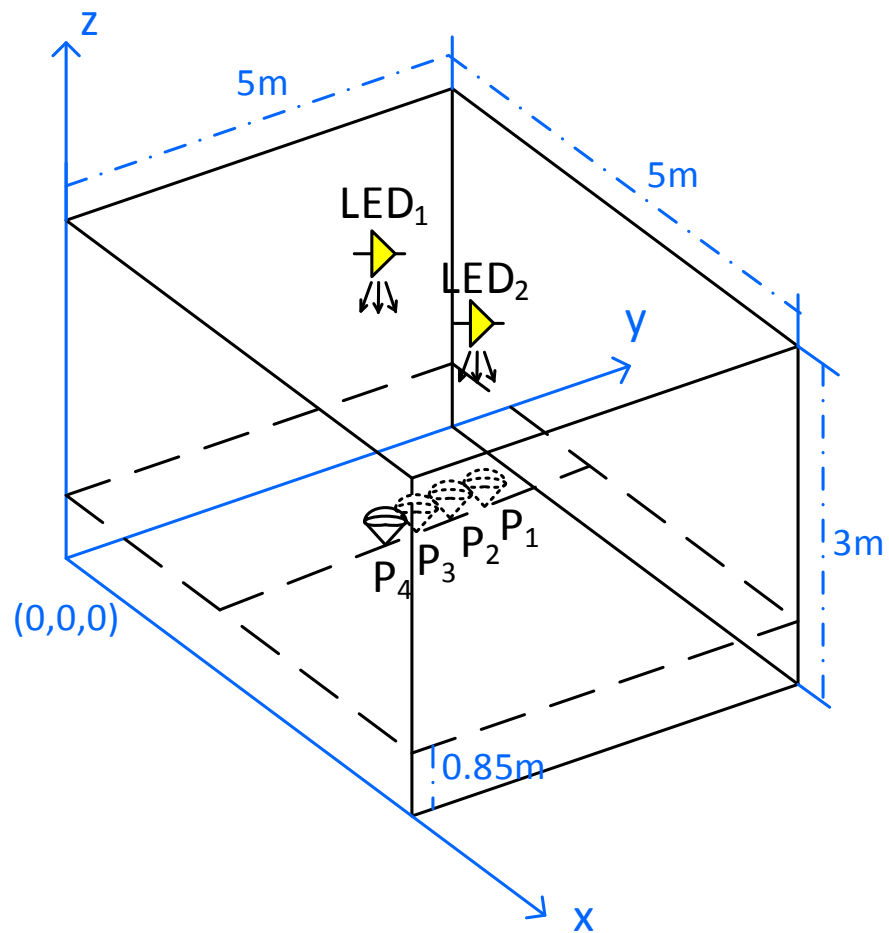


Figure 4-14 Simulation setup.

Table 4-1 Simulation Parameters

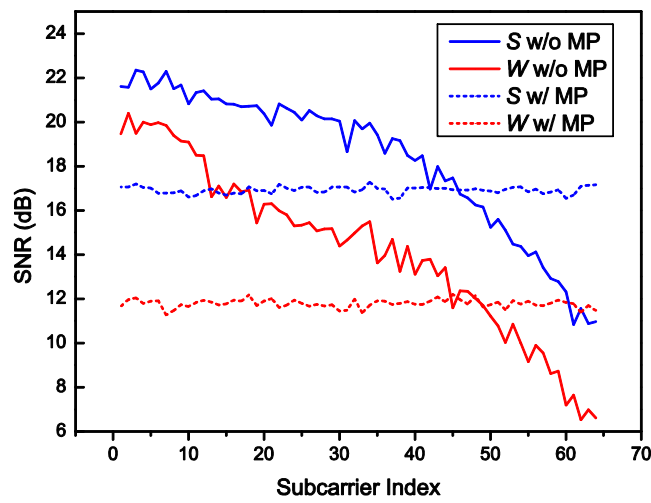
Parameter	Value
LED location	LED ₁ : (1.5,2.5,3); LED ₂ : (3.5,2.5,3)
PD location	P ₁ : (2,4,0.85); P ₂ : (2,3.5,0.85); P ₃ : (2,3,0.85); P ₄ : (2,2.5,0.85)
Detection area of PD	1 cm ²
Number of Rays	50000
Reflection coefficient (walls/floor/ceiling)	0.83/0.63/0.4
Max. reflection order	5
Receiver field of view	60°
System sample rate	200MSa/s
DCO-OFDM bandwidth	100MHz
FFT size	256
CP length	32

Figure 4-14 shows the simulation setup of an indoor VLC system. Two LEDs are mounted on the ceiling for illumination and communication, while a PD is positioned on a plane with 0.85 m in height to simulate the height of desk surface. Four PD positions are considered to simulate different receiving signal qualities. The simulation parameters are summarized in Table 4-1. The three DSP processes mentioned in the last section are studied in comparison. Two factors are controlled in the simulation: the location of PD, and the power of both two LEDs.

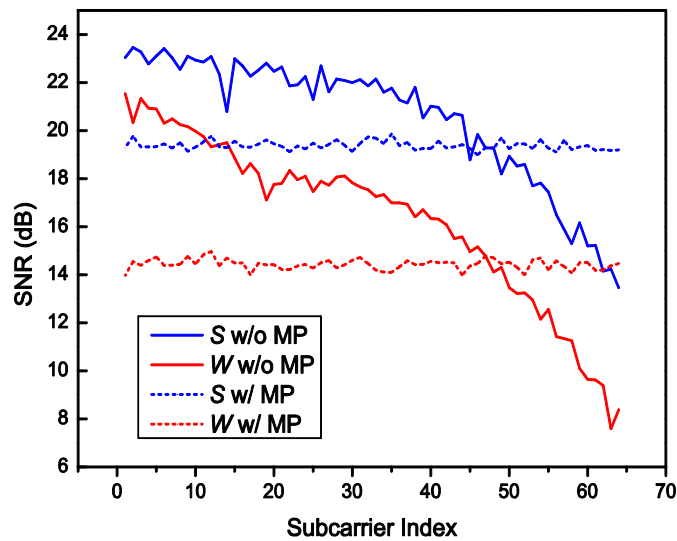
4.4.3.2 Simulation results

We first investigate the effect MP brought to the SNR performance of the whole spectrum of OFDM. Figure 4-15 shows the SNR comparisons of all the OFDM subcarriers, with and without the MP. Solid lines represent the case without MP, while dashed lines are the multicarrier-precoded SNRs. It could be observed that the SNRs of all the subcarriers in one OFDM transmitter could be equalized by MP. On the other

hand, PD at P_4 enjoys higher SNRs as well as larger SNR differences between S and W over the whole band, while the SNRs and SNR differences at P_1 are smaller. Figure 4-16 shows the BER performance when PD is placed at different positions in the simulation setup. Although different PD positions lead to different SNRs as well as different power ratios between S and W , in most cases the adoption of MP decreases the BER of S and W compared to those without PP/MP and without MP. Specifically,



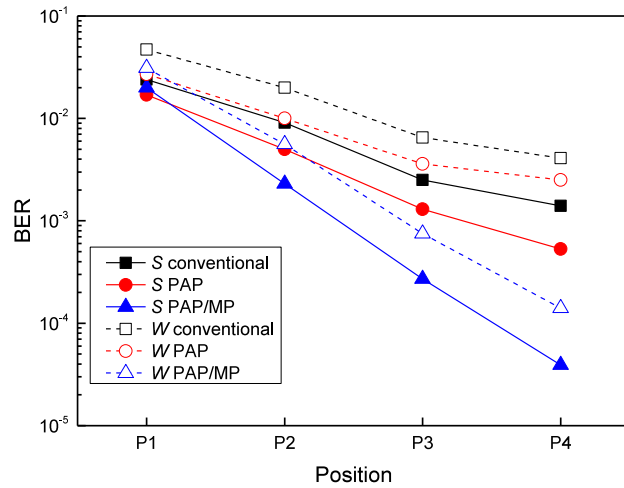
(a)



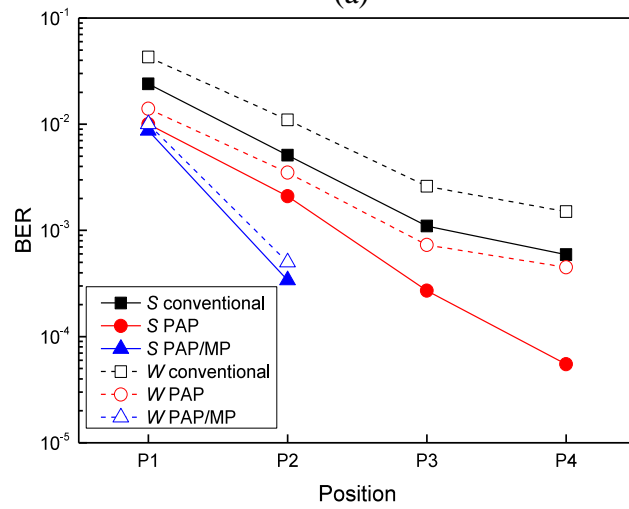
(b)

Figure 4-15 SNR of OFDM data subcarriers: (a) LED power=2W, PD at P_2 , (b) LED power=2W, PD at P_4 .

we compare the case with PP to that with MP. When PD is located at P₂ and the LED power is 1.5W, the BER of *S* drops from 5×10^{-3} to 2.5×10^{-3} while the BER of *W* drops from 1×10^{-2} to 6×10^{-3} , indicating minor improvements. When the LED power increases to 2 W, the BER of *S* changes from 2×10^{-3} to 2×10^{-4} , while the BER of *W* decreases from 4×10^{-3} to 4×10^{-4} . This conclusion is further verified by simulating the BER performance in regard to the LED power. Figure 4-17 shows the BER comparisons by fixing the PD at P₂ or P₄ and changing the power of LEDs. In both



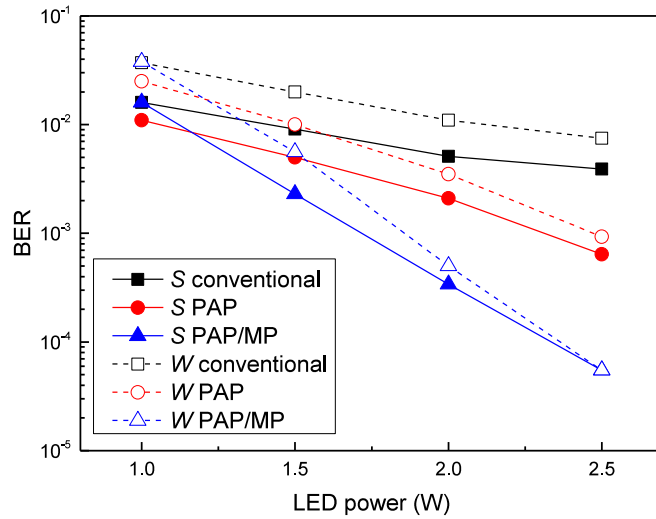
(a)



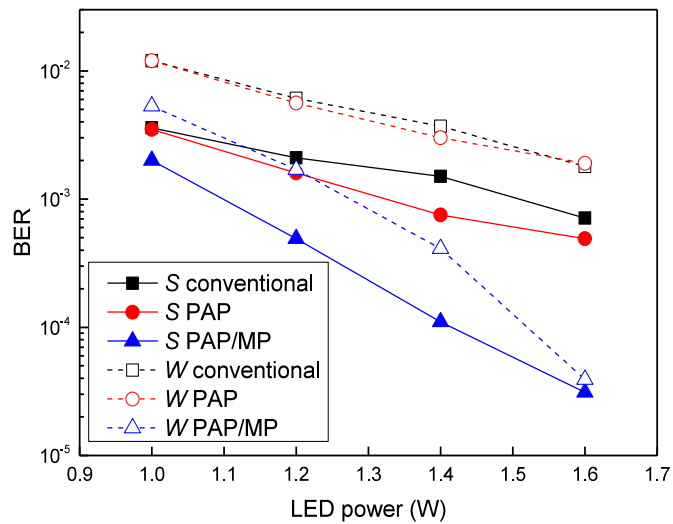
(b)

Figure 4-16 BER comparisons: (a) LED power=1.5W, (b) LED power=2W

cases, the BER drops faster in MP case than PP case. It could be found that the improvement brought by MP is more significant under an appropriately better signal quality.



(a)



(b)

Figure 4-17 BER comparisons: (a) PD at P_2 , (b) PD at P_4 .

4.4.4 Summary

We have proposed a multicarrier precoding scheme for NOMA in VLC. The proposed scheme combats the low-pass nature of VLC systems by keeping low BER, high throughput without introducing adaptive modulation formats. Simulation studies have proved the effectiveness of the proposed scheme.

Chapter 5 Summary and Future work

5.1 Summary

In this thesis, we have summarized our work in the past a few years in turning the detrimental interference in communication systems into benefit. The main contribution include two aspects, namely, physical-layer network coding in optical communication and non-orthogonal multiple access in optical communication. The optical communication here includes fiber optics communication (FOC) and optical wireless communication (OWC).

The first interference-assisted technology discussed in this thesis is physical-layer network coding (PNC), which is a very promising technology in optical communication. We have conducted several projects on applying PNC in optical communication.

On one hand, PNC can be introduced into FOC to improve the throughput. We have verified this issue by experimentally demonstrating a physical-layer network coding scenario in a coherent optical orthogonal frequency division multiplexing system. It has been shown that the throughput of a multicast network can be doubled with an acceptable optical signal to noise ratio (OSNR) penalty. We have carried out a group of experiments to verify the feasibility of the proposed scheme.

On the other hand, we have proposed a novel virtual private network (VPN) structure in passive optical networks (PON). In this structure, VPN supporting both

wired PON services and VPN supporting fiber-wireless (FiWi) services in a carrier frequency of about 2.5 GHz are realized. Similarly, the proposed VPN enjoys a throughput gain of about 100% percent compared to conventional VPNs, with low receiving power penalties.

Besides, we have proposed a novel relay scheme in visible light communication, a special form of OWC. This scheme extends the reach distance of VLC services and solves the non-line-of-sight problem. To improve the system throughput, physical-layer network coding is adopted to enable a full-duplex two-way relay channel. Meanwhile, finite-set PNC (PNCF) is adopted in the proposed scheme to eliminate the degradations in the connections between the source nodes and the relay node, such as noise, nonlinearity, and so on. Furthermore, we have proposed a novel phase-matching method in VLC PNC, which is prohibited in wireless PNC due to the arbitrary phase induced by CFO and PN. It has been theoretically and experimentally demonstrated that our newly proposed phase-matching method outperforms the conventional PNC scheme, with a newly 5-dB improvement at a BER of 10^{-3} in the experiments.

The second interference-assisted technology that has been introduced in this thesis is non-orthogonal multiple access (NOMA).

Firstly, we have investigated NOMA in the uplink of a VLC uplink. In this case, NOMA can take advantage of the near-far effect and turn the detrimental power imbalance into benefit. Specially, we design two pre-distortion method to improve the system performance. One of them is based on a multiuser detection (MUD) algorithm

in successive interference cancellation (SIC), the other is based on another MUD algorithm, joint detection (JD). It has been demonstrated that SIC and JD-based NOMA with pre-distortion can both decrease the bit error rate (BER), while JD outperforms SIC in the given scenario.

Secondly, we have proposed a novel NOMA uplink system with multicarrier precoding. The multicarrier precoding (MP) based on orthogonal circular transform can equalize the SNR over the whole spectrum of OFDM. By combining NOMA and MP, the whole OFDM spectrum can accommodate NOMA with high throughput while the necessity of complicated adaptive bit loading is eliminated.

5.2 Future work

Despite the diverse applications of PNC and NOMA proposed in this thesis, it should be noted that the potential of these two technologies are not limited to these schemes. Much more innovations and applications are still to be investigated.

The research of the application of PNC in optical communication is just beginning, expecting great potential and numerous opportunities. For example, current studies of PNC are limited to TWRC, however, PNC can work in topologies beyond TWRC [63]. The future work of PNC firstly comes in finding more application topologies in fiber optics communication, or more specifically, in scenarios with more than two users.

Meanwhile, it is also of great importance to find specific application scenarios for PNC. For instance, in a recent work by us, it has been discovered recently that PNC

can reduce the intra-rack transmission latency in an optical data center when the intra-rack packet exchange requests exceeds the system design capacity. This provides a new clue for applying PNC in a practical system.

As has been pointed out, visible light communication is a very suitable scenario for PNC. The limited service coverage of VLC necessitates the help of relays, and the absence of CFO enables the optimum phase pre-distortion of PNC. The work demonstrated in this thesis is just a preliminary result, with only physical-layer demonstration. On one hand, a more systematic study is still needed. On the other hand, it is also necessary to discuss the networking of VLC, involving PNC-assisted multi-hop connection. We are expecting more future works to dig deeper in this field.

NOMA has recently aroused great research enthusiasm in many research fields, while its application in VLC is just beginning to draw attention. Though at early stage of study, NOMA in VLC is widely recognized as a key technology in light fidelity (Li-Fi), as has been pointed out in [100]. It's imperative to experimentally demonstrate NOMA and its variations in VLC. Thanks to the inspiring works of NOMA in information theory and wireless communication researchers, a lot of novel NOMA concepts are being proposed, such as cooperative NOMA [84], user pairing in NOMA [101], and MIMO in NOMA [83]. Therefore, it is reasonable to expect more applications of NOMA in VLC.

Meanwhile, it is also researchers' task to well address the special characteristics of VLC when introducing NOMA in Section 4.4 serves as a preliminary work in this

aspect, while further works are still needed.

Apart from VLC, NOMA can also be applied in fiber optics communication. In [102], researchers have realized a fiber optical communication system based on NOMA. However, the limited number of publications on this topic also elicit more future works.

List of publications

Journals

[1] X. Guan, and C. K. Chan, “Physical-layer network coding in coherent optical OFDM”, *OSA Optics Express*, vol. 23, no. 8, pp. 10057-10063, April, 2015.

[2] X. Guan, Q. Yang, Y. Hong, and C. K. Chan, “Non-orthogonal multiple access with phase pre-distortion in visible light communication systems”, *OSA Optics Express*, vol. 24, no. 22, pp. 25816-25823, 2016.

[3] X. Guan, Q. Yang, and C. K. Chan, “Joint detection of visible light communication signals under non-orthogonal multiple access”, *IEEE Photonics Technology Letters*, accepted.

[4] X. Guan, Q. Yang, Y. Hong, and C. K. Chan, “Phase-aligned physical-layer network coding in visible light communications”, *IEEE Photonics Technology Letters*, in preparation.

Conferences

[1] X. Guan, T. Bo, and C. K. Chan, “Virtual private networks in OFDM-PON supporting radio-over-fiber based on physical-layer network coding”, *PS 2015*, Florence, Italy, September, 2015.

[2] X. Guan, T. Bo, and C. K. Chan, “Mitigation of inter-carrier interference induced by phase noise and residual carrier frequency offset in CO-OFDM systems”, *PS 2015*,

Florence, Italy, September, 2015.

[3] X. Guan, Y. Hong, Q. Yang, and C. K. Chan, "Phase pre-distortion for non-orthogonal multiple access in visible light communications", *OFC 2016*, Anaheim, USA, March, 2016.

[4] Y. Hong, X. Guan, L. K. Chen, and J. Zhao, "Experimental demonstration of an OCT-based precoding scheme for visible light communications", *OFC 2016*, Anaheim, USA, March, 2016.

[5] X. Guan, Y. Hong, and C. K. Chan, "Non-Orthogonal multiple access with multicarrier precoding in visible light communications", *OECC/PS 2016*, Niigata, Japan, July, 2016.

[6] Z. Feng, M. Tang, X. Guan, C. K. Chan, Q. Wu, R. Wang, R. Lin, S. Fu, L. Deng, and D. Liu, "Digital domain power division multiplexing DDO-OFDM transmission with successive interference cancellation", *CLEO 2016*, San Jose, USA, May, 2016.

[7] Z. Feng, M. Tang, X. Guan, C. K. Chan, Q. Wu, X. Chen, R. Wang, R. Lin, S. Fu, L. Deng, D. Liu "Spectrally overlaid DDO-OFDM transmission enabled by optical power division multiplexing", *ICOON 2016*, Hangzhou, Zhejiang, China, September, 2016.

List of abbreviations

16QAM: 16 quadrature amplitude modulation

AF: amplify and forward

ANC: analog network coding

AON: active optical network

AWG: arbitrary waveform generator

AWGN: additive white Gaussian noise

BS: base station

CCI: co-channel interference

CD: chromatic dispersion

CDMA: code division multiple access

CMA: constant modulus algorithm

CO-OFDM: coherent optical orthogonal frequency division multiplexing

CP: cyclic prefix

CPE: common phase error

CSI: channel state information

DAC: digital to analog converter

DC: data center

DCO-OFDM: direct-current-biased optical orthogonal frequency division multiplexing

DF: decode and forward

DFT: discrete Fourier transform

DSA: digital sampling analyzer

DSL: digital subscriber line

ECL: external cavity laser

EDFA: erbium doped fiber amplifier

EM: electromagnetic

EPON: ethernet passive optical network

FDMA: frequency division multiple access

FFT: fast Fourier transform

Fi-Wi: fiber wireless

FOC: fiber optical communication

FPNC: frequency physical-layer network coding

FTTH: fiber to the home

GRPA: gain ration power allocation

ICI: inter-carrier interference

IDFT: inverse discrete Fourier transform

IFFT: inverse fast Fourier transform

IoT: internet of things

ISI: inter-symbol interference

ITU-T: International Telegraph Union Telecommunication Standardization Sector

GPON: gigabit passive optical network

LDPC: low density parity check

LED: light-emitted diode

Li-Fi: light fidelity

LLCD: lunar laser communication demonstration

LNA: linear amplifier

LoS: line of sight

LTE: long-term evolution

MA: multiple access

MAI: multiple access interference

MP: multicarrier precoding

MUD: multiuser detection

MZM: Mach-Zehnder modulator

NASA: National Aeronautics and Space Administration

NC: network coding

NOMA: non-orthogonal multiple access

oAN: optical access network

OBI: optical beating interference

oBN: optical beating noise

OCT: orthogonal circular transform

OFDM: orthogonal frequency division multiplexing

OFDMA: orthogonal frequency division multiple access

OFDM-PON: orthogonal frequency division multiplexing passive optical network

OLT: optical line terminal

ONU: optical network user

OPNC: optical physical-layer network coding

OSA: optical spectrum analyzer

OSNR: optical signal to noise ratio

OWC: optical wireless communication

P2P: peer to peer

PAM4: pulse amplitude modulation 4

PAP: phase and amplitude pre-distortion

PC: polarization controller

PD: photodiode

PMD: polarization mode dispersion

PN: phase noise

PNC: physical-layer network coding

PON: passive optical network

RN: remote node

RoF-PON: radio over fiber passive optical network

RPO: residual phase offset

SDN: software defined network

SFO: sampling frequency offset

SIC: successive interference cancellation

SMF: single mode fiber

TDMA: time division multiple access

TDM-PON: time domain multiplexing passive optical network

ToR: top of rack

TS: training sequence

TWRC: two-way relay channel

USRP: Universal Software Radio Peripheral

VCSEL: vertical-cavity surface-emitting laser

VOA: variable optical attenuator

VPN: virtual private network

WDM: wavelength division multiplexing

Wi-Fi: wireless fidelity

XOR: exclusive or

ZC: Zadoff-Chu

Bibliography

- [1] C. K. Kao, and G. A. Hockham, “Dielectric-fibre surface waveguides for optical frequencies,” in *Proceedings of the Institution of Electrical Engineers*, vol. 113, no. 7, pp. 1151-1158, July 1966.
- [2] E. Agrell, M. Karlsson, A. R. Chraplyvy, *et al.*, “Roadmap of optical communications,” *Journal of Optics*, vol. 18, no. 6, pp. 063002, May 2016.
- [3] F. Mitschke, *Fiber optics: physics and technology*, Springer Science & Business Media, 2010.
- [4] M. Channegowda, R. Nejabati, and D. Simeonidou, “Software-defined optical networks technology and infrastructure: Enabling software-defined optical network operations,” *Journal of Optical Communications and Networking*, vol. 5, no. 10 pp. A274-A282, October 2013.
- [5] P. Winzer, and R. J. Essiambre, “Advanced Optical Modulation Formats,” *Proceedings of the IEEE*, vol. 94, no. 5, pp. 952-985, May 2006.
- [6] N. Sambo, P. Castoldi, A. D'Errico, *et al.*, “Next generation sliceable bandwidth variable transponders,” *IEEE Communications Magazine*, vol. 53, no. 2, pp. 163–171, February 2015.
- [7] S. Frisken, G. Baxter, D. Abakoumov, *et al.*, “Flexible and grid-less wavelength selective switch using LCOS technology,” in *Optical Fiber Communication*

Conference, Paper OTuM3, March 2011.

- [8] O. Gerstel, M. Jinno, A. Lord, *et al.*, “Elastic optical networking: A new dawn for the optical layer,” *IEEE Communications Magazine*, vol. 50, no. 2, pp. s12-s20, February 2012.
- [9] C. Lin, *Broadband optical access networks and fiber-to-the-home: systems technologies and deployment strategies*, John Wiley & Sons, 2006.
- [10] K. S. Kim, “On the evolution of PON-based FTTH solutions,” *Information Sciences*, vol. 149, no. 1, pp. 21-30, January 2003.
- [11] T. Mukojima, “Next generation optical access trends and OKI's activities,” *OKI Technical Review*, issue 221, vol. 80, no. 1, May 2013.
- [12] M. Mahloo, J. Chen, and L. Wosinska, “PON versus AON: Which is the best solution to offload core network by peer-to-peer traffic localization,” *Optical Switching and Networking*, vol. 15, pp. 1-9, January 2015.
- [13] I. Cale, A. Salihovic, and M. Ivekovic, “Gigabit passive optical network-GPON,” in *29th International Conference on Information Technology Interfaces*, pp. 679-684, June 2007.
- [14] G. Kramer, and G. Pesavento, “Ethernet passive optical network (EPON): building a next-generation optical access network,” *IEEE Communications Magazine*, vol. 40, no. 2, pp. 66-73, February 2002.

- [15] T. Muciaccia, G. Fabio, and P. Vittorio, "Passive optical access networks: State of the art and future evolution," *Photonics*, vol. 1, no. 4, pp. 323-346, October 2014.
- [16] Q. Deniel, F. Saliou, P. Chanclou, *et al.*, "Self-seeded RSOA based WDM-PON transmission capacities," in *Optical Fiber Communication Conference*, Paper OW4D. 3, March 2013.
- [17] C. W. Chow, C. H. Yeh, Y. F. Wu, *et al.*, "13 Gbit/s WDM-OFDM PON using RSOA-based colourless ONU with seeding light source in local exchange," *Electronics Letters*, vol. 47, no. 22, pp. 1235-1236, October 2011.
- [18] M. Omella, V. Polo, J. Lazaro, *et al.*, "10 Gb/s RSOA transmission by direct duobinary modulation," in *ECOC*, Paper Tu.3.E.4, September 2008.
- [19] H. K. Shim, H. Kim, and Y. C. Chung, "Practical 12.5-Gb/s, 12.5-GHz spaced ultra-dense WDM PON," *Optics Express*, vol. 22, no. 23, pp. 29037-29047, November 2014.
- [20] T. Benson, A. Akella, and D. A. Maltz, "Network traffic characteristics of data centers in the wild," in *Proceedings of the 10th ACM SIGCOMM Conference on Internet Measurement*, pp. 267-280, November 2010.
- [21] D. Sadot, G. Dorman, A. Gorshtein, *et al.*, "Single channel 112Gbit/sec PAM4 at 56Gbaud with digital signal processing for data centers applications," *Optics Express*, vol. 23, no. 2, pp. 991-997, January 2015.

- [22] Y. Benlachtar, R. Bouziane, R. I. Killey, *et al.*, “Optical OFDM for the data center,” in *12th IEEE International Conference on Transparent Optical Networks*, pp. 1-4, June 2010.
- [23] F. Karinou, C. Prodaniuc, N. Stojanovic, *et al.*, “Directly PAM-4 modulated 1530-nm VCSEL enabling 56 Gb/s data-center interconnects,” *IEEE Photonics Technology Letters*, vol. 27, no. 17, pp. 1872-1875, June 2015.
- [24] N. Farrington, E. Rubow, and A. Vahdat, “Data center switch architecture in the age of merchant silicon,” in *17th IEEE Symposium on High Performance Interconnects*, pp. 93-102, August 2009.
- [25] C. S. Tainter, and A. G. Bell, “Selenium and the photophone,” *Nature*, vol. 22, pp. 500-503, September 1880.
- [26] A. G. Alkholidi, and K. S. Altowij, “Free space optical communications — theory and practices,” in *Contemporary Issues in Wireless Communications*, Rijeka, Croatia, Intech, 2014, ch. 5, pp. 159-212.
- [27] D. M. Boroson, B. S. Robinson, D. V. Murphy, *et al.*, “Overview and results of the lunar laser communication demonstration,” *SPIE LASE. International Society for Optics and Photonics*, vol. 8971, pp. 89710S-1-11, March 2014.
- [28] K. Toshihiko, and M. Nakagawa, “Fundamental analysis for visible-light communication system using LED lights,” *IEEE Transactions on Consumer Electronics*, vol. 50, no. 1, pp. 100-107, February 2004.

- [29] A. Jovicic, J. Li, and T. Richardson, "Visible light communication: opportunities, challenges and the path to market," *IEEE Communications Magazine*, vol. 51, no. 12, pp. 26-32, December 2013.
- [30] S. Shao, A. Khreishah, M. B. Rahaim, *et al.*, "An indoor hybrid WiFi-VLC internet access system," in *IEEE 11th International Conference on Mobile Ad Hoc and Sensor Systems*, pp. 569-574, October 2014.
- [31] A. Moussa, H. Elgala, A. Khreishah, *et al.*, "Coexistence of WiFi and LiFi toward 5G: concepts, opportunities, and challenges," *IEEE Communications Magazine*, vol. 54, no. 2, pp. 64-71, February 2016.
- [32] S. B. Weinstein, and P. M. Ebert, "Data transmission by frequency division multiplexing using the discrete Fourier transform," *IEEE Transactions on Communications*, vol. 19, no. 10, pp. 628-634, October 1971.
- [33] J. Cooley, and J. Tukey, "An algorithm for the machine calculation of complex Fourier series," *Mathematics of computation*, vol. 19, no. 90, pp. 297-301, April 1965.
- [34] Y. G. Li, and G. L. Stuber, *Orthogonal frequency division multiplexing for wireless communications*, Springer Science & Business Media, 2006.
- [35] W. Shieh, and I. Djordjevic, *OFDM for optical communications*, Academic Press, 2009.

- [36]S. Hara, and R. Prasad, *Multicarrier techniques for 4G*, Artech House, 2003.
- [37]Q. Pan, and R. J. Green, “Bit error rate performance of lightwave hybrid AM/OFDM systems with comparison with AM/QAM systems in the presence of clipping impulse noise,” *IEEE Photonics Technology Letters*, vol. 8, no. 2, pp. 278-280, February 1996.
- [38]J. Tang, P. M. Lane, and K. A. Shore, “High-speed transmission of adaptively modulated optical OFDM signals over multimode fibers using directly modulated DFBS,” *Journal of Lightwave Technology*, vol. 24, no. 1, pp. 429-441, January 2006.
- [39]A. J. Lowery, and J. Armstrong, “10Gbit/s multimode fiber link using power-efficient orthogonal-frequency-division multiplexing,” *Optics Express*, vol. 13, no. 25, pp. 10003–10009, December 2005.
- [40]A. J. Lowery, L. Du, and J. Armstrong, “Orthogonal frequency division multiplexing for adaptive dispersion compensation in long haul WDM systems,” in *Optical Fiber Communications Conference*, paper PDP 39, Anaheim, CA, March 2006.
- [41]J. Yu, X. Zhou, M. Huang, *et al.*, “21.7 Tb/s (161×114Gb/s) polmux-RZ-8PSK transmission over 662 km of ultra-low loss fiber using C-band EDFA amplification and digital coherent detection,” in *European Conference and Exhibition on Optical Communication*, paper Th.3.E.2, Brussels, Belgium,

September 2008.

- [42] A. N. Barreto, and S. Furrer, "Adaptive bit loading for wireless OFDM systems," in *IEEE International Symposium on Personal, Indoor and Mobile Radio Communications*, vol. 2, pp. G88-G92, October 2001.
- [43] G. Bansal, J. Hossain, and V. K. Bhargava, "Adaptive power loading for OFDM-based cognitive radio systems," in *2007 IEEE International Conference on Communications*, pp. 5137-5142, June 2007.
- [44] M. Z. Afgani, H. Haas, H. Elgala, *et al.*, "Visible light communication using OFDM," in *International Conference on Testbeds and Research Infrastructures for the Development of Networks and Communities (TRIDENTCOM)*, Barcelona, Spain, March 2006.
- [45] Y. Zhao, and S. G. Haggman, "Intercarrier interference self-cancellation scheme for OFDM mobile communication systems," *IEEE Transactions on Communications*, vol. 49, no. 7, pp. 1185-1191, July 2001.
- [46] J. Armstrong, "Analysis of new and existing methods of reducing intercarrier interference due to carrier frequency offset in OFDM," *IEEE Transactions on Communications*, vol. 47, no. 3, pp. 365-369, March 1999.
- [47] G. Liu, and W. Zhu, "Compensation of phase noise in OFDM systems using an ICI reduction scheme," *IEEE Transactions on Broadcasting*, vol. 50, no. 4, pp. 399-407, December 2004.

- [48]C. R. N. Athaudage, “BER sensitivity of OFDM systems to time synchronization error,” in *The 8th International Conference on Communication Systems*, vol. 1, pp. 42-46, November 2002.
- [49]J. G. Proakis, “Intersymbol interference in digital communication systems,” in *Encyclopedia of Telecommunications*, 2003.
- [50]R. H. Mahadevappa, and J. G. Proakis, “Mitigating multiple access interference and intersymbol interference in uncoded CDMA systems with chip-level interleaving,” *IEEE Transactions on Wireless Communications*, vol. 1, no. 4, pp. 781-792, October 2002.
- [51]X. Yang, and P. P. Athina, “Co-channel interference modeling and analysis in a Poisson field of interferers in wireless communications,” *IEEE Transactions on Signal Processing*, vol. 51, no. 1, pp. 64-76, January 2003.
- [52]J. Y. Yu, M. F. Sun, T. Y. Hsu, *et al.*, “A novel technique for I/Q imbalance and CFO compensation in OFDM systems” in *IEEE International Symposium on Circuits and Systems*, pp. 6030-6033, May 2005.
- [53]C. Rose, “CDMA codeword optimization: Interference avoidance and convergence via class warfare,” *IEEE Transactions on Information Theory*, vol. 47, no. 6, pp. 2368-2382, September 2001.
- [54]S. Y. R. Li, R. W. Yeung, and N. Cai, “Linear network coding,” *IEEE Transactions on Information Theory*, vol. 49, no. 2, pp. 371–387, February 2003.

- [55]S. Katti, S. S. Gollakota, and D. Katabi, “Embracing wireless interference: analog network coding,” in *ACM SIGCOMM*, pp. 397–408, August 2007.
- [56]S. Zhang, S. C. Liew, and P. P. Lam, “Hot topic: physical-layer network coding,” in *ACM Proceedings of the 12th annual international conference on Mobile computing and networking*, September 2006.
- [57]S. Katti, H. Rahul, W. Hu, *et al.*, “XORs in the air: practical wireless network coding,” in *ACM SIGCOMM computer communication review*, vol. 36, no. 4, pp. 243-254, September 2006.
- [58]L. Lu, and S. C. Liew, “Asynchronous physical-layer network coding,” *IEEE Transactions on Wireless Communications*, vol. 11, no. 2, pp. 819-831, February 2012.
- [59]L. Lu, T. Wang, S. C. Liew, *et al.*, “Implementation of physical-layer network coding,” *Physical Communication*, vol. 6, pp. 74-87, March 2013.
- [60]D. Wang, S. Fu, and K. Lu, “Channel coding design to support asynchronous physical layer network coding,” in *IEEE Global Telecommunications Conference*, 2009, pp. 1-6, November 2009.
- [61]S. Zhang, and S. C. Liew, “Channel coding and decoding in a relay system operated with physical-layer network coding,” *IEEE Journal on Selected Areas in Communications*, vol. 27, no. 5, pp. 788-796, June 2009.

- [62] Q. Yang, and S. C. Liew, "Asynchronous convolutional-coded physical-layer network coding," *IEEE Trans. Wireless Commun.*, vol. 14, no. 3, pp. 1380–1395, October 2014.
- [63] J. He, and S. C. Liew, "Building blocks of physical-layer network coding," *IEEE Transactions on Wireless Communications*, vol. 14, no. 5, pp. 2711–2728, May 2015.
- [64] Q. Wang, K. H. Tse, L. K. Chen, *et al.*, "Physical-layer network coding for VPN in TDM-PON," *IEEE Photonics Technology Letters*, vol. 24 no. 23, pp. 2166–2168, December 2012.
- [65] Z. Liu, M. Li, L. Lu, *et al.*, "Optical physical-layer network coding," *IEEE Photon. Technol. Lett.*, vol. 24, no. 16, pp. 1424–1427, August 2012.
- [66] M. Li, Y. Wu, L. K. Chen, *et al.*, "Common-channel optical physical-layer network coding," *IEEE Photon. Technol. Lett.*, vol. 26, no. 13, pp. 1340–1342, July 2014.
- [67] Z. Liu, L. Lu, L. You, *et al.* "Optical physical-layer network coding for fiber-wireless," in *European Conference on Optical Communications (ECOC)*, London, UK, Paper Mo.3.F.3, September 2013.
- [68] J. G. Proakis, *Digital Communications*, McGraw-Hill, New York, 1995.
- [69] A. Jamalipour, T. Wada, and T. Yamazato, "A tutorial on multiple access technologies for beyond 3G mobile networks," *IEEE Communications Magazine*,

vol. 43, no. 2, pp. 110-117, February 2005.

[70]J. Lee, and L. E. Miller, *CDMA Systems Engineering Handbook*, Artech House, Inc., 1998.

[71]A. J. Viterbi, *CDMA: Principles of Spread Spectrum Communication*, Addison Wesley Longman Publishing Co., Inc., 1995.

[72]Y. Saito, Y. Kishiyama, A. Benjebbour, *et al.*, “Non-orthogonal multiple access (NOMA) for cellular future radio access,” in *IEEE 77th Vehicular Technology Conference (VTC Spring)*, June 2013.

[73]A. Ruegg, and A. Tarable, “Iterative SIC receiver scheme for non-orthogonally superimposed signals on top of OFDMA,” in *21st Annual IEEE International Symposium on Personal, Indoor and Mobile Radio Communications*, pp.156-161, September 2010.

[74]H. Haci, “Non-orthogonal multiple access (NOMA) with asynchronous interference cancellation,” Ph.D. dissertation, University of Kent, U.K., 2015.

[75]J. Schaepperle, and A. Ruegg, “Enhancement of throughput and fairness in 4G wireless access systems by non-orthogonal signaling,” *Bell Labs Technical Journal*, vol. 13, no. 4, pp. 59-77, December 2009.

[76]R. Jain, D. M. Chiu, and W. R. Hawe, “A quantitative measure of fairness and discrimination for resource allocation in shared computer system,” *Eastern*

Research Laboratory, Digital Equipment Corporation, September 1984.

- [77]K. Higuchi, and A. Benjebbour, “Non-orthogonal multiple access (NOMA) with successive interference cancellation for future radio access,” *IEICE Transactions on Communications*, vol. 98, no. 3, pp. 403-414, March 2015.
- [78]D. Tse, and P. Viswanath, *Fundamentals of Wireless Communication*, Cambridge university press, 2005.
- [79]NTT Docomo, “5G concept and technologies,” in *IEEE GLOBECOM Industry Workshop*, December 2014.
- [80]NTT Docomo, “DOCOMO 5G white paper,” July, 2014.
- [81]K. Higuchi, and Y. Kishiyama, “Non-orthogonal access with random beamforming and intra-beam SIC for cellular MIMO downlink,” in *IEEE 78th Vehicular Technology Conference (VTC Fall)*, pp. 1-5, September 2013.
- [82]H. Huseyin, and H. Zhu, “Performance of non-orthogonal multiple access with a novel interference cancellation method,” in *Proc. IEEE International Conference on Communications (ICC)*, pp. 2912-2917, June 2015.
- [83]Z. Ding, R. Schober, and H. V. Poor, “A general MIMO framework for noma downlink and uplink transmission based on signal alignment,” *IEEE Transactions on Wireless Communications*, vol. 15, no. 6, June 2016.
- [84]Z. Ding, M. Peng, and H. V. Poor, “Cooperative non-orthogonal multiple access

- in 5G systems,” *IEEE Communications Letters*, vol. 19, no.8, pp. 1462-1465, August 2015.
- [85]H. Marshoud, V. M. Kapinas, G. K. Karagiannidis, *et al.*, “Non-orthogonal multiple access for visible light communications,” *IEEE Photonics Technology Letters*, vol. 28, no. 1, pp. 51-54, January 2016.
- [86]L. Yin, X. Wu, and H. Haas, “On the performance of non-orthogonal multiple access in visible light communication,” in *Proc. IEEE 26th Annual International Symposium on Personal, Indoor, and Mobile Radio Communications (PIMRC)*, pp. 1354-1359, August 2015.
- [87]R. C. Kizilirmak, C. R. Rowell, and M. Uysal, “Non-orthogonal multiple access (NOMA) for indoor visible light communications,” in *Proc. 4th International Workshop on Optical Wireless Communications (IWOW)*, pp. 98-101, September 2015.
- [88]W. Shieh, H. Bao, and Y. Tang, “Coherent optical OFDM: theory and design,” *Opt. Express*, vol. 16, no. 2, pp. 841–859, January 2008.
- [89]X. Yi, W. Shieh, and Y. Tang, “Phase estimation for coherent optical OFDM,” *IEEE Photon. Technol. Lett.*, vol. 19, no. 12, pp. 919–921, June 2007.
- [90]Y. Su, Y. Tian, E. Wong, *et al.*, “All-optical virtual private network in passive optical networks,” *Laser & Photon. Reviews*, vol. 2, no. 6, pp. 460-479, December 2008.

- [91]N. Ghazisaidi, M. Maier, and C. M. Assi, "Fiber-Wireless (FiWi) access networks: a survey," *IEEE Communications Magazine*, vol. 47, no. 2, pp. 160-167, February 2009.
- [92]D. Qian, J. Hu, P. Ji, *et al.*, "10-Gb/s OFDMA-PON for delivery of heterogeneous services", in *Optical Fiber Communication Conference*, March, 2008.
- [93]Y. M. Lin, and P. L. Tien, "Next-generation OFDMA-based passive optical network architecture supporting radio-over-fiber," *IEEE Journal on Selected Areas in Communications*, vol. 28, no. 6, pp. 791-799, August 2010.
- [94]K. Miller, T. Biermann, and H. Woesner, "Network coding in passive optical networks", in *IEEE International Symposium on Network Coding*, June 2010.
- [95]Z. Lan, C. S. Sum, H. Wang, *et al.*, "Relay with deflection routing for effective throughput improvement in Gbps millimeter-wave WPAN systems," *IEEE Journal on Selected Areas in Communications*, vol. 27, no. 8, pp. 1453-1465, October 2009.
- [96]H. Haci, H. Zhu, and J. Wang, "A novel interference cancellation technique for non-orthogonal multiple access (NOMA)," in *Proc. IEEE Global Communications Conference (GLOBECOM)*, pp. 1-6, December 2015.
- [97]T. Yazaki, and Y. Sanada, "Effect of joint detection and decoding in non-orthogonal multiple access," in *Proc. IEEE International Symposium on Intelligent Signal Processing and Communication Systems (ISPACS)*, pp. 245-250,

December 2014.

- [98] X. Guan, Y. Hong, Q. Yang, *et al.*, “Phase pre-distortion for non-orthogonal multiple access in visible light communications,” in *Optical Fiber Communication Conference*, March 2016.
- [99] Y. Hong, X. Guan, L. K. Chen, *et al.*, “Experimental demonstration of an oct-based precoding scheme for visible light communications,” in *Optical Fiber Communication Conference*, March 2016.
- [100] H. Haas, L. Yin, Y. Wang, *et al.*, “What is LiFi?” *Journal of Lightwave Technology*, vol. 34, no. 6, pp. 1533-1544, March 2016.
- [101] Z. Ding, P. Fan, and V. Poor, “Impact of user pairing on 5G non-orthogonal multiple access downlink transmissions,” *IEEE Transactions on Vehicle Technology*, vol. 65, no. 8, pp.6010-6023, August 2016.
- [102] Z. Feng, M. Tang, X. Guan, *et al.*, “Digital Domain Power Division Multiplexing DDO-OFDM Transmission with Successive Interference Cancellation,” in *CLEO: Science and Innovations*, paper SF2F. 6, June 2016.